# THE UNIVERSITY OF MICHIGAN

## COLLEGE OF ENGINEERING
### Department of Electrical Engineering
### Space Physics Research Laboratory

Scientific Report

# VOLT-AMPERE CHARACTERISTICS OF CYLINDRICAL AND SPHERICAL LANGMUIR PROBES FOR VARIOUS POTENTIAL MODELS

M. Kanal
W.G. Dow
E.G. Fontheim

ORA Project 06106

# ACKNOWLEDGMENTS

# PROLOGUE

In the early stages of the research presented here, the only intention of the authors was to find an analytic expression for the volt-ampere characteristics of spherical and cylindrical probes for sufficiently general types of potential functions and to check our calculations for the Maxwell-Boltzmann distribution against the self-consistent numerical calculations of Laframboise. In the course of this investigation the classic works of Mott-Smith and Langmuir were subjected to a critical analysis, in terms of the boundary conditions encountered in ionospheric experiments. This analysis revealed serious defects in Langmuir's finite sheath model and put certain limitations on their orbital-motion-limited theory. Furthermore, there seemed to be no agreement among the existing theories as to the mathematical definition of the "sheath" which is the central part of any theory describing the plasma-probe interactions. It was therefore felt that it would be of general benefit to examine in some detail the basic physics of the interaction between the probe and the surrounding plasma. The first two chapters and the beginning of the third chapter of this report, thus, are in the nature of a textbook discussion and should be read in this spirit.

TABLE OF CONTENTS

# LIST OF TABLES

# LIST OF FIGURES

# I. INTRODUCTION

The collisionless theory of electrostatic probes immersed in a
plasma involves the two following basic physical concepts:

(a) The concept of a "sheath" surrounding the probe, in which
the potential change from that of the plasma to that of the
probe occurs, as propounded by Langmuir,[1] and

(b) The existence of distinct velocity distributions of the
electrons and positive ions within the region of interest,
the sheath.

The sheath is fully described when one knows both velocity distributions
and the potential distribution in the sheath.

These two properties of the sheath are, of course, intimately inter-
related. In principle, therefore, the problem of deriving the volt-
ampere relations of an electrostatic plasma probe becomes one of a
simultaneous self-consistent solution of the Poisson and Vlasov equations
and to give the potential and velocity distributions, subject to appropri-
ate boundary conditions in the plasma and at the probe surface. The
collected current is then obtained from the current density at the col-
lector surface which can be calculated from the electron and ion velocity
distributions at the probe radius.

The self-consistent approach to the problem is very complicated,
besides being usually obtained for a relatively narrow range of boundary
conditions. Consequently, for a physically meaningful, tractable, and

1

reasonable widely useful solution, certain simplifying assumptions become necessary.

This paper will present certain such assumptions, and compare some of the results with those obtained by Laframboise[2] who used a numerical approach. But before going into the details of our assumptions, we will give a review of the relationship of our work to the most important existing literature on electrostatic probe theory.

For the past several decades, a considerable amount of effort has been devoted to plasma research by means of electrostatic probes. The most important contributions are those by Mott-Smith and Langmuir,[1] Langmuir and Compton,[3] Bernstein and Rabinowitz,[4] and Gurevitch.[5] The first unified treatment of electrostatic probe theory as a whole, was that by Hok,[6] in a report which has been a valuable resource in much of the work on rocket investigation of the ionosphere by The University of Michigan. Hok discusses the concept of a "potential well" or transition region, important to bipolar electrostatic probes.

The classic works of Mott-Smith and Langmuir[1] and of Langmuir and Compton, have been extensively used in laboratory plasma and ionosphere research, and for this reason part of this paper is devoted to giving a criticial review of certain aspects of their theory, particularly in regard to details of their assumed sheath model and its physical significance. Our early discussion of the "Sheath and Sheath Edge" introduces an examination of the classical theory as to the self-consistency of the sheath model from the standpoint of potential theory. This is then

extended into a discussion of the continuity of the potential across

the plasma-sheath boundary, and then to a study of some general proper-

ties of potential functions for the infinite sheath model.

The "Orbital Analysis" portion of this study employs throughout the con-

cept of the "effective potential." This is defined so that, by incorporating

the effect of angular momentum, it becomes a function which produces a fic-

titious force field governing the radial motion of the charged particles.

By systematically examining the mathematical properties of the effective po-

tential, the treatment then derives the Langmuir criteria for collection of

particles by the probe and in particular demonstrates that the discontinuity

of the electric field at the sheath edge is a necessary condition for Lang-

muir's theory to hold. Finally the infinite sheath limit in Langmuir's the-

ory is discussed.

A two-variable, separable, mathematical form for the maxima of the

effective potential is then introduced which relates in conceptually use-

ful ways to the "admissible space" (Langmuir's term). The admissible

space is defined by the limits of integration employed in obtaining the

probe volt-ampere characteristic. This separable expression is then used

to investigate the volt-ampere characteristics for a general inverse-

power-law potential function.

The underlying conceptual basis of the orbital analysis is similar

to that used by Bernstein and Rabinowitz,[4] and Gurevitch,[5] in that it

neglects collisions in the sheath, and provides a framework for determi-

3

ning current collection by treating the whole region from the collector surface to the undisturbed plasma by means of probability distribution functions.

Following the orbital analysis, the probe volt-ampere relations are derived in analytic form, for cylindrical and spherical probe geometries. Among the assumptions that the whole procedure employs in arriving at the volt ampere relationships, the following two are especially basic:

(a) The probability distribution of the particles is Maxwellian in the undisturbed plasma.

(b) It is reasonable to approximate a part or the whole of the potential distribution by a suitable inverse power law potential.

To check the feasibility and utility of our second assumption, we will compare our volt-ampere characteristics with those obtained by Laframboise.[2] The treatment of Bernstein and Rabinowitz[4] is restricted to monoenergetic distributions and to probes of large radius. Gurevitch[5] and Laframboise[2] have extended the theory to Maxwell-Boltzmann distributions and to probes of arbitrary radius: but only Laframboise had carried out the calculations of the volt-ampere characteristics by solving the whole problem, including the effects due to space charge, in a numerically self-consistent way. His results are, therefore, a logical source for the comparison.

To summarize the purposes of this study, we shall attempt to:

(a) Give a critical review of the classical probe theory of Mott-Smith and Langmuir, examining their sheath model in detail,

especially in regard to discontinuities of the field at the plasma-sheath boundary.

(b) Review the properties of approximations to the potential function. Then, by means of a suitable inverse-power-law potential function, derive the probe volt-ampere relations in analytic form, and compare the results with those obtained numerically by Laframboise.

The first phase of the analysis will deal with a few classical definitions in electrostatic probe theory and their employment in dealing with certain rather general aspects of sheath potential distributions and of the merging of the sheath into the undisturbed plasma.

## II. THE POTENTIAL INSIDE THE SHEATH AND ITS CONTINUITY
## AT THE PLASMA-SHEATH BOUNDARY

2.1 THE SHEATH RADIUS AND "SHEATH EDGES"

Mott-Smith and Langmuir define the sheath and the sheath edge

in the following way.

Let $r_c$ be the radius of the probe (cylindrical or spherical) and

$r_s$ that of the sheath. Further let $\Phi(r)/q$ be the electric potential

of a particle of charge q at a radius r in the field of an accelerating

probe, $\Phi(r_c)/q = \Phi_c/q$ the electric potential at the probe and let $\Phi(r_s)/q =$

$\Phi_s/q = 0$ be the plasma potential. We now quote Mott-Smith and Langmuir,[1]

who define the sheath edge in the following way:

"If we assume any distribution of potential between $r_s$ and $r_c$,

we can always find a cylinder (or sphere) of radius r' intermediate

between $r_s$ and $r_c$ such that, for this cylinder (sphere) or any other

of smaller radius, the condition

$$|\Phi| \geq \frac{r'^2 - r^2}{r'^2 - r_c^2} \frac{r_c^2}{r^2} \tag{1}$$

is satisfied. In other words, such a surface can be taken to be

the edge of the sheath if the distribution for the velocities of

the ions crossing it is known. As far as the equations of orbital

motion determine it, the sheath edge is therefore, simply a surface

on which we know the velocities of the ions and within which the

above condition is satisfied."

6

Note that this does not compel the potential gradient to be zero at, or just beyond, a "sheath edge" where the velocities are known.

Figure 1 illustrates the physical meaning of Eq. (1), and the relationship of a particular "sheath edge" $r' = r_e$ to the sheath radius $r_s$. To aid in constructing Fig. 1, Eq. (1) has been rearranged into the following form:

$$|\Phi| \geq \left[ \frac{\dfrac{r_e^2}{r^2} - 1}{\dfrac{r_e^2}{r_c^2} - 1} \right] |\Phi_c| = f_e |\Phi_c|. \tag{2}$$

When the sheath edge becomes the sheath radius, $r_e = r_s$, the equation changes to

$$|\Phi| \geq \left[ \frac{\dfrac{r_s^2}{r^2} - 1}{\dfrac{r_s^2}{r_c^2} - 1} \right] |\Phi_c| = f_s |\Phi_c|. \tag{3}$$

The definitions of the functions $f_s$ and $f_e$ are contained in these equations.

Note in particular that the slope of the factor $f_s$ goes to zero only as $r \to \infty$, and that, therefore, the slope of the curve is nonzero at $r=r_s$. Thus, as illustrated in Fig. 1, $\Phi(r)$ must also have a nonzero slope as it approaches $r=r_s$ if it is to remain below $f_s \Phi_c$, as Eq. (3) requires (for $\Phi_c < 0$, i.e., attractive potentials).

7
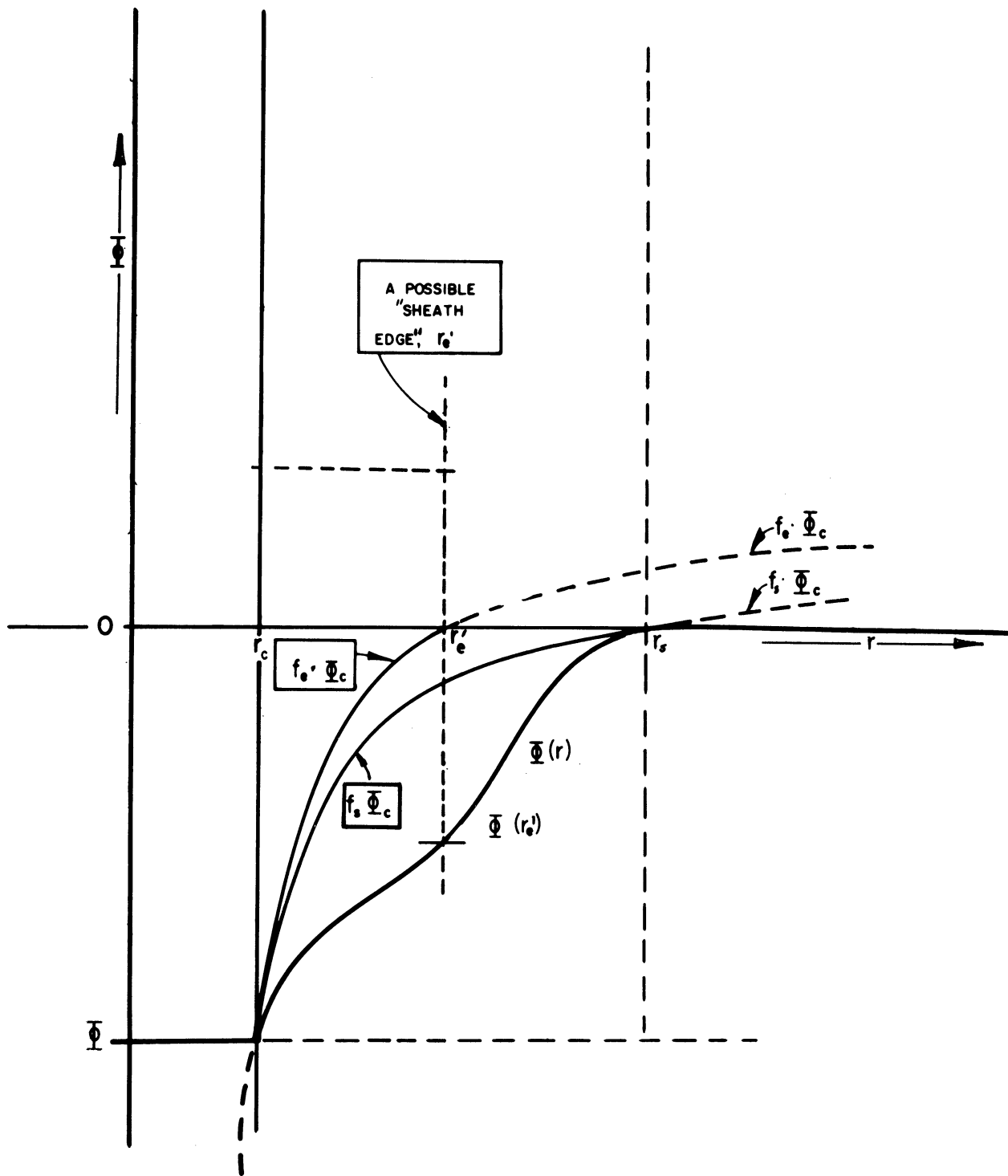
Fig. 1. Illustrates the meaning of Eqs. (1) and (2).

$$f_s = \frac{(r_s^2/r^2)-1}{(r_s^2/r_c^2)-1}, \quad f_e = \frac{(r_e^2/r^2)-1}{(r_e^2/r_c^2)-1}$$

To obtain Eq. (2) which applies when $r_e < r_s$ it is necessary to observe only that:

$$f_e < f_s, \text{ for } r < r_e, \text{ if } r_e < r_s, \text{ because } r_c < r. \tag{4}$$

This is illustrated in Fig. 1 where the $f_e \Phi_c$ curve lies everywhere above the $f_s \Phi_c$ curve. Here $f_e$ and $f_s$ are the bracketed factors multiplying $|\Phi_c|$ in Eqs. (2) and (3), respectively.

One can note, immediately, the following serious weakness in the reasoning underlying Eqs. (2) and (3):

In the case where $r_e = r_s$, Eq. (3), and therefore Eq. (1) with $r' = r_s$, describes a model in which there must be a discontinuity in the potential gradient at $r = r_s$ in order to have $\Phi = 0$ beyond $r_s$. Such a discontinuity is physically nonrealizable, as discussed later in detail. This weakness does not appear when $r'$ is given a value $r_e$ that is significantly less than $r_s$, because at such an $r_e$, the potential is still rising, and the gradient is not compelled by the boundaries of the model to have any particular value at and beyond the selected $r_e$.

Subsequent sections deal with various methods of probe model analysis chosen to avoid this weakness.

The above quotation from Mott-Smith and Langmuir,[1] as illustrated by Fig. 1 and discussions thereof, leads one to conclude that, in general, what Mott-Smith and Langmuir call "sheath edge" need not coincide with the sheath radius $r_s$ at which the potential becomes

9

equal to that of the undisturbed plasma. Furthermore, one concludes

that Mott-Smith and Langmuir considered that it is only _inside_ any "sheath

edge" that the behavior is dominated by the dynamics, thus making the velo-

city distribution different from Maxwellian. Outside the sheath edge,

presumably, the analysis would be that applying to a plasma region in

which there is a gentle potential gradient and a moderate-to-small flux

density of particles. It is therefore reasonable, for analytical purposes,

to place a sheath edge as close to the probe as one may reasonably expect

the velocity distribution to be Maxwellian, with relatively little refer-

ence to where this may lie with respect to the potential distribution.

The right-hand side of the inequality (1), and its equivalent (2),

changes sign when $r' < r < r_s$, and the inequality is reversed when

$|\Phi(r)| < |f_e \Phi_c|$ for $r < r_s$ (see Fig. 1). However, these two aspects

are of little concern, since in the region beyond the sheath edge (i.e.,

$r > r'$) one presumably expects to carry out the analysis not in terms

of particle trajectories in a sheath, but rather in terms of particle behav-

ior in a plasma with a gentle inward gradient insufficient to cause signifi-

cant departure of the velocity distribution from that in the undisturbed

plasma (although it may affect the particle density significantly).

Still more generally, in view of the Mott-Smith and Langmuir

distinction between sheath edge and sheath radius, one may well ask

these two questions as to placement of an $r' < r_s$:

> (a) Can in any realistic model such a sheath edge surface r exist
>
> and be usefully placed, within which the Mott-Smith and Langmuir

condition (1) [also Eq. (2)] is satisfied for all values of

r < r'?  It has already been pointed out earlier that potential

distributions can exist that do not satisfy Eqs. (1) and (2) for

all values of r', particularly if r' is close to or at $r_s$.

(b) If such a surface does exist, what would be the velocity distri-

bution at r=r'?  Presumably, with r=r' properly chosen, this

would be a Maxwellian distribution having parameters governed

by the plasma in which the probe is immersed but this merely changes

the question of properly locating a sheath edge r' within the

sheath model.

In the strict sense, answers to these two questions cannot be given prior

to solving the whole problem of the potential distribution in the self-

consistent way.  Supposing that the self-consistent method gave rise to a

potential function which did not satisfy the inequality (1) for the entire

range $r_c < r < r_s$, one would then expect the corresponding volt-ampere

characteristics not to coincide with those of Mott-Smith and Langmuir.

It is worth while to note that the Mott-Smith and Langmuir "sheath

edge" may well be interpreted as the boundary between the two regions

which Hok[6] calls, respectively, the sheath and the potential well.  The

latter is a transition region exhibiting some slow radial flux of parti-

cles and a gentle potential gradient toward the bipolar probe electrode

system.  He envisions this region as having properties similar to those

in laboratory plasmas exhibiting what Tonks[7] and others[8,9] have called

ambipolar diffusion.  In such plasma regions the ion and electron densi-

ties are very nearly equal, and both are, among themeselves, in thermal

equilibrium, but at different temperatures.  Thus, at Hok's boundary be-

11

tween his sheath and the potential well, he is able to postulate Maxwellian velocity distributions of the particles. Yet he need not postulate the potential to be that of the plasma, nor that there be a zero potential gradient, nor a discontinuity of the gradient at this boundary. These are just the attributes of a Mott-Smith and Langmuir sheath edge, distinct from their sheath radius, and well within the sheath radius.

All contributors, including Mott-Smith and Langmuir, Langmuir and Compton,[3] and Hok,[6] give essentially their whole attention to studying what happens inside what is really a "sheath edge." Yet it is frequently unclear just where this sheath edge is relative to the sheath radius, and still more often the sheath edge is identified with the sheath radius, with various illogical consequences.

It should be clear that, in general, the defining of a sheath edge is justified only if it serves to simplify the problem of determining the volt-ampere relations. The remarkable simplicity of the classical Langmuir probe theory[1,3] lies precisely in the fact that, by setting $r' = r_s$, one is able to bypass the problem of solving for the potential function. Thus, by Langmuir's sheath model, we mean the sheath region described by a potential function $\Phi$ such that

$$|\Phi| = \begin{cases} |\Phi| \geq |\Phi_c| \dfrac{r_s^2 - r^2}{r_s^2 - r_c^2} \dfrac{r_c^2}{r^2} = f_s |\Phi_c|, & \text{for } r \leq r_s \\[2ex] 0, & \text{for } r > r_s \end{cases} \qquad (5)$$

This is consistent with the inequality (2), if the inequality (4) is satisfied.

In general, Langmuir's sheath model will be shown not to be adequate for most plasma probe experiments. Particularly in ionospheric measurements, a potential function describing a finite sheath region and satisfying Eq. (5) cannot exist, unless one assumes the presence of a charge shell at $r = r_s$. Thus, the curve of $\Phi(r)$ in Fig. 1 exhibits a discontinuity in its derivative at $r = r_s$, which could only exist if there were a shell of surface charge to terminate the flux due to the potential gradient just within $r_s$. No such shell can realistically be assumed.

## 2.2 GENERAL PROBLEM OF THE POTENTIAL DISTRIBUTION IN A FINITE SHEATH, AND ELECTRIC FIELD CONTINUITY AT THE PLASMA-SHEATH BOUNDARY

Let us define the electric potential function for a finite sheath by:

$$\Lambda(r) = \frac{1}{q} \Phi(r) \, \Theta(r-r_c) \, \Theta(r_s-r) \tag{6}$$

where q is the electric charge per particle, taken to be positive in this discussion. $\Phi(r)$ is, as heretofore, the potential energy and $\Theta(x)$ is the unit step function:

$$\Theta(x) = \begin{cases} 1 & \text{if } x > 0 \\ 0 & \text{if } x < 0 \end{cases} \tag{7}$$

with

$$\frac{d\Theta(x)}{dx} = \delta(x), \quad \frac{d}{dx} \Theta(-x) = -\delta(x) \tag{8}$$

where $\delta(x)$ is Dirac's delta function. In the above we have considered

only the radial variable, because of the symmetry of the field for both cylindrical and spherical probes. $\Phi(r)$ is considered to be a function that is continuous from $r = 0$ to $r = \infty$.

If Eq. (6) is inserted into Poisson's equation,

$$\nabla^2 \Lambda = -\frac{\rho}{\epsilon_0} \tag{9}$$

one obtains

$$-\frac{\rho}{\epsilon_0} = \nabla^2 \Lambda = \frac{1}{q}\left[ \nabla^2 \Phi\, \Theta(r-r_c)\Theta(r_s-r) + \Phi'\delta(r-r_c)\Theta(r_s-r) \right.$$
$$\left. -\Phi'\delta(r_s-r)\Theta(r-r_c) \right] \tag{10}$$

where $\rho$ is interpreted to include both space-charge density and surface charge density, $\rho$ becoming infinite for the latter. The prime on $\Phi$ represents the derivative with respect to $r$.

Now the surface charge density $\sigma_r$ on any arbitrary surface or set of surfaces S enclosing a region outside of which the electric potential gradient is zero is given by

$$\sigma_r = -\epsilon_0\, \hat{n} \cdot \nabla \chi \Big|_{\text{evaluated on S.}} \tag{11}$$

Here $\chi$ is the electric potential function in the region enclosed by S, and n is the unit normal vector pointing into the region where the electric field exists. $\nabla\chi$ is, of course, to be identified with $\Phi'/q$ in Eq. (10). At $r = r_c$, the unit vector points radially outward, so that $\hat{n} = +1$, whereas at $r = r_s$ it points radially inward, so that $\hat{n} = -1$. Thus Eq. (11) becomes

$$\frac{\Phi'(r_c)}{q} = -\frac{\sigma_r}{\epsilon_o} \quad \text{at } r = r_c \qquad (12)$$

$$\frac{\Phi'(r_s)}{q} = \frac{\sigma_r}{\epsilon_\circ} \quad \text{at } r = r_s \qquad (13)$$

Hence, the expressions for the surface charge densities $\sigma_{rc}$ and $\sigma_{rs}$ at $r = r_c$ and $r = r_s$ respectively, are,

$$\sigma_{rc} = -\frac{\epsilon_o \Phi'_c}{q} \qquad (14\text{-}1)$$

$$\sigma_{rs} = \frac{\epsilon_o \Phi'_c}{q} \qquad (14\text{-}2)$$

where $\Phi'_c = \Phi'(r)|_{r = r_c}$ and $\Phi'_s = \Phi'(r)|_{r = r_s}$. These algebraic signs are consistent with Fig. 1 as long as q is positive, for in that case the $\Phi(r)$ curve in Fig. 1 can equally well represent potential energy per particle and electric potential. If it represents electric potential, the surface charge at $r_c$ is clearly negative, and at $r_s$ positive, from the construction of the figure.

Now let $\rho_v$ denote the volume charge density. Then we may write

$$\nabla^2 \Phi = -\frac{q \rho_v}{\epsilon_o} \qquad (15)$$

It is now instructive to obtain an overall expression for the charge density by inserting Eqs. (14-1), (14-2), and (15) into Eq. (10) to obtain

$$\rho = \rho_v \Theta(r-r_c) \Theta(r_s-r) - \sigma_{rc} \delta(r-r_c) \Theta(r_s-r) - \sigma_{rs} \delta(r_s-r) \Theta(r-r_c) \qquad (16)$$

This is consistent with Eqs. (12) and (13). The delta functions identify the fact that the charge density becomes infinite for a surface charge.

Of course in an integration to obtain total volume charge and total surface charges, the delta-function terms make finite contributions.

From Eq. (14-1) it is seen that $\sigma_{rs} = 0$ only if $\Phi'_s = 0$; i.e., at the sheath outer bound, the electric field must vanish in addition to the vanishing of the potential provided by Eq. (6). If only $\Phi$ vanishes at $r_s$ but not $\Phi'_s$, then there would exist a surface charge layer of strength given by Eq. (14-2). In the interior of a plasma, remote from physical boundaries, the existence of such a shell is obviously unphysical, because it implies a discontinuity in the electric field. We have already seen in the previous section that a nonvanishing $\Phi'$ at $r_s$, approaching from the left in Fig. 1, is required by the Mott-Smith and Langmuir model in which $r' = r_s$ in Eq. (1). Therefore, as discussed in more detail later, this nonvanishing of $\Phi'$ at $r_s$ is a necessary requirement in deriving their volt-ampere relations for a finite sheath in which their "sheath edge" coincides with the sheath outer bound.

In other words, those current expressions will be strictly valid only under the unrealizable condition in which this sheath edge, placed at sheath radius, is replaced by a zero-potential conductor of the same type of geometry as the probe. Presumably Mott-Smith and Langmuir[1] were aware of this, but felt their model, even though containing this element of unrealizability, was an adequate first approximation, and so it has been for very many years.

## 2.3 NEED FOR, AND CONSEQUENCES OF, ABANDONMENT OF THE CONCEPT OF A WELL-DEFINED SHEATH BOUNDARY BY MAKING THE SHEATH RADIUS FORMALLY INFINITE

The finite sheath model has weaknesses that go considerably beyond that of the potential gradient discontinuity at the sheath outer bound, discussed in the previous section. That particular weakness could be formally overcome by employing for $\Phi(r)$ some simple function that monotonically rises from the probe to sheath radius, but whose slope becomes monotonically less steep, finally reaching zero at sheath radius. Or, one could employ one kind of potential function within a sheath edge, and another between sheath edge and sheath radius, with potential gradients forced to be equal at the sheath edge, and that at sheath radius forced to be zero. But in all such highly artificial potential models, the second and perhaps higher derivatives would have discontinuities at these boundaries. The second derivative is intimately related to space-charge density, and it is almost as unrealistic to presume an abrupt discontinuity in space-charge density at a sheath edge or sheath radius as it is to presume a discontinuity in the potential gradient.

In any realistic model, not only the potential but also all of its radial derivatives must be presumed to be continuous through the sheath into the plasma. This type of continuity demands that the sheath potential approach the plasma potential asymptotically with increasing radius; thus, in reality, there can be no well defined sheath radius.

There can of course be described a general range of values of the radius within which the sheath region with its steep gradients merges

into the plasma with its zero gradient. Any plasma will have random potential variations, and the sheath may be considered to have merged into the plasma within any range of values of the radius for which the difference between the sheath potential and that of the undisturbed plasma is of the order of the random variations in plasma potential. In terms of experimental systems, this may occur at relatively small distances from the probe surface.

Mathematically, the merging of the sheath into the plasma is provided for by letting the sheath radius become infinite ($r_s \to \infty$) and requiring that both the potential and the potential gradient be zero at an infinite radius. That is, $\Phi(r)=0$, and $\Phi'(r) = 0$ at $r = r_s = \infty$.

Of course this makes the sheath include the two regions discussed earlier in Section 2.1, namely the steep gradient sheath region proper, and the gentle gradient plasma-like transition region. It also makes the sheath include what Hok[6] has called the potential well that exists around a bipolar probe, which represents a reasonably good conceptual approach to reality.

Thus when we later, for purposes of analysis, extend the sheath radius to infinity, we must recognize that we are including in the sheath two types of regions having wholly different properties. In the region close to the probe, the potential gradient is steep and particles of one or the other polarity dominate so that space charge has a major effect on the potential distribution. In the outer or transition region, the positive ion and electron densities are nearly, but not quite, equal. Particles

of each polarity are in thermal equilibrium, but maybe at different temperatures. There may exist a close parallel to Tonks' ambipolar diffusion region.[7,8,9] The potential gradient and flux of particles to the probe are not zero. The flow of heavy particles (ions) to the probe may be governed by mobilities affected by collisions, or they might pursue orbits with negligibly few collisions. Any self-consistent analysis of the sheath should, to be complete, be equipped to treat both regions, as for example by using what has been called the "combined plasma-sheath equation."

## 2.4 POTENTIAL FUNCTION MODELS AND CHARGE DENSITIES FOR THE INFINITE SHEATH

It is clear from earlier discussions, that the general problem of actually determining the true potential function for a physically realistic model is very complicated, for in Poisson's Eq. (15) the density function $\rho_v$ will, in general, involve $\Phi$ implicitly. Instead of solving this self-consistent problem we shall examine the properties of various potential models and their corresponding volt-ampere characteristics. Each potential model of course implies a certain charge distribution in the sheath. Our investigation will be restricted to potential models having the common property that $\Phi$ and $\Phi'$ approach zero as $r \to \infty$. An illustrative choice of a class of potential models, to be discussed below, is the function

$$\Phi = \Phi_c \left(\frac{r_c}{r}\right)^\alpha , \qquad (17)$$

where $\Phi_c$ is the potential energy per particle at the probe or collector,

and $\alpha$ is a positive number. For an accelerating potential, $(-\Phi_c)$ is numerically positive. The potential energy gradient is

$$\Phi' = (-\Phi_c) \frac{\alpha r_c^{\alpha}}{r^{\alpha+1}} \qquad (18)$$

Clearly, both the potential and its gradient vanish as $r \to \infty$.

The exponent $\alpha$ has a very simple physical interpretation. Using Eq. (14-1) in Eq. (18) when $r = r_c$, we get

$$\alpha = \frac{r_c}{\epsilon_c} \frac{(-\sigma_{rc}q)}{(-\Phi_c)} \qquad (19)$$

in which, for an accelerating potential, both $(-\sigma_{rc}q)$ and $(-\Phi_c)$ are positive quantities. That is, $\alpha$ is proportional to the ratio of the collector surface charge density to the collector potential.

In any realistic model, to which Eq. (17) can of course only be an approximation, one can consider $\sigma_{rc}$ to be the sum of the charge density on the probe that would exist if it were at the potential $\Phi_c$ in a space-charge-free environment, and the induced charge on it due to the space charge in the sheath region. Before criticizing this concept, let us state the charge density distribution called for by Eq. (17). By using it in Eq. (10), the result is

$$\rho = \frac{\epsilon_0(-\Phi_c)}{q} \frac{\alpha(\alpha-\xi)r_c^{\alpha}}{r^{\alpha+2}} + \sigma_{rc}\delta(r-r_c) , \qquad (20)$$

where $\xi = 0$ for the infinite cylinder and $\xi = 1$ for the sphere and $\sigma_{rc}$ is given by Eq. (14-1). Equation (20) applies only if $\alpha > 1$, as will be explained below. In that case no third term appears on the right-

hand side because, as r→∞, the surface charge density at the sheath

boundary goes to zero faster than the surface area of the sheath boundary

increases.

For the spherical geometry, we use $\xi = 1$ in Eq. (20). This means

that if $\xi = 1$ in spherical geometry, Eq. (17) describes a space-charge-

free "sheath" potential (there will generally be substantial space charge

in the sheath of a useful electrostatic probe in a plasma if the probe

potential differs appreciably from the plasma potential ). For the case

where $\alpha = 1$ in spherical geometry, there is a well-defined $\sigma_{rc}$ on the

probe surface, found by using Eq. (18) with $\alpha = 1$ in Eq. (14-1). Since

there is no volume space charge, the electric flux that originates at $\sigma_{rc}$

must terminate at infinite radius. Thus, in this case there would be a

well-defined charge $4\pi r_c^2 \sigma_{rc}$ on the probe, and an equal and opposite charge

at infinite radius where $\Phi = 0$, with $\Phi = \Phi_c$ on the probe. But since this

finite charge is distributed over a spherical shell of infinite radius,

the charge density $\sigma_{rc}$ goes to zero in such a way that the total charge

remains constant, as r→∞. This also corresponds to the result of Eq. (18)

that with $\alpha = 1$, $\lim_{r\to\infty} \Phi' = 0$. Of course in the integration over all volume

elements from $r = r_c$ to r=∞, Eq. (20) must in principle integrate to

zero; for $\alpha = 1$ in spherical geometry, this can be accomplished only by

adding another term $\lim_{r_s\to\infty} \sigma_{rs} \delta(r_s - r)$ whose contribution to the charge

integral is equal in magnitude, and opposite in sign, to the total charge

on the spherical probe.

If, for spherical geometry ($\xi=1$), we use $\alpha > 1$ in Eqs. (18) and

(19) the situation is straightforward, in that the volume integral of

charge is found to equal the area integral of $\sigma_{rc}$; in this case Eq. (20)

includes all electric charges. All electric flux lines then originate

at the probe surface and terminate in the volume charge in the sheath.

The result of the integration is:

$$\text{Total Volume Charge} = \left(\frac{4\pi\epsilon_0}{q}\right) \alpha r_c(-\Phi_c) \text{ Coulombs} \qquad (21)$$

and $\sigma_{rc}$ has an equal but negative value.

But if $0 < \alpha < 1$ for spherical geometry ($\xi = 1$), Eq. (20) predicts a

volume charge of the same sign as the surface charge on the probe. Such a

model obviously is physically unrealistic and will, therefore, not be

discussed in this treatment.

Thus, in summary, for spherical geometry, only the range $\alpha > 1$ in

Eq. (17) has any real interest. But the above comments do suggest the

possible utility of a model in which $\Phi$ is the sum of two terms like Eq.

(17), in one of which $\alpha > 1$ and in the other $\alpha = 1$. In fact such a model

probably closely describes the real potential which can be constructed as

the sum of: (a) a contribution due to the space charge and its induced

charge on the probe, and (b) that for a space-charge-free structure. This

two-term potential model will not be dealt with in the present paper.

For the infinite-cylinder geometry we use $\xi = 0$ in Eq. (20). This

means that no expression of the form of Eq. (17) can describe the space-

charge-free potential structure which is, of course, logarithmic in form.

Furthermore, that logarithmic form is uninteresting because it becomes infi-

nite as r→∞ (with, however, a zero-value Φ' at r = ∞). With the logarithmic potential used in Poisson's equation, the space-charge density term in the new Eq. (20) vanishes and, to make the charge integral balance, we would have to add a term $\lim_{r \to \infty} \sigma_{rs} \delta(r_s - r)$ which would make a finite contribution to the charge integral.

Of course, any cylindrical electrostatic probe used in the ionosphere is not an infinite cylinder. Even if completely isolated from any other conductor, the field of a charged cylinder of finite length would, at a sufficiently large radius, become essentially the same as that for a charged sphere. So there is always, in fact, a finite space-charge-free potential for such a body carrying a finite charge. But our infinite-cylinder analysis is not adequate for studying that aspect of the problem.

If, for the infinite cylinder geometry ($\xi = 0$), we use $\alpha > 0$ in Eqs. (18) and (19) the volume integral of the charge equals the area integral of $\sigma_{rc}$, and Eq. (20) identifies all the charges. The result of the integration of Eq. (20) is:

$$\begin{bmatrix} \text{Total volume charge, per} \\ \text{unit length of cylinder} \end{bmatrix} = \left( \frac{4\pi\epsilon_0}{q} \right) \frac{\alpha}{2} (-\Phi_c), \qquad (22)$$

and $\sigma_{rc}$ has an equal, but negative, value.

In summary, we can say that by postulating a relatively simple potential function (e.g., Eq. (17)), we have obviously no a priori assurance that the charge density implied by such a potential is physically realistic. However, it will be shown later that in the range

$r_c/\lambda_D \leq 5$ the volt-ampere relations obtained from the potential (17) for certain values of $\alpha$ agree very well with those obtained by the self-consistent calculations of Laframboise.[2]   Here $\lambda_D$ is the Debye length.

We shall now proceed to the orbit analysis, which includes a detailed discussion of the behavior of the particles in the sheath region and the selection of those trajectories, which intersect the probe.

# III. ORBIT ANALYSIS

## 3.1 THE "EFFECTIVE POTENTIAL" FOR ACCELERATED TRAJECTORIES

The solution of the equations of motion of a particle approaching

a cylindrical or spherical electrostatic probe (Fig. 2), leads to two
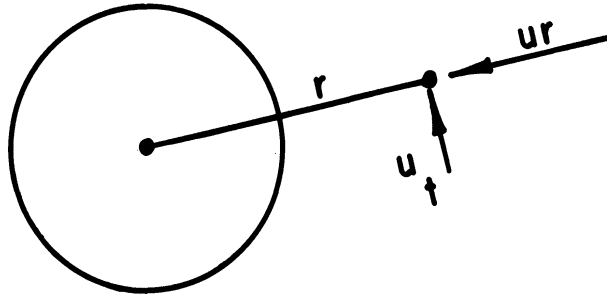


Fig. 2. Radial and tangential velocity components $u_r$ and $u_t$ for
an approaching charged particle at a distance r from the center
of a cylindrical or spherical electrostatic probe.

constants of motion; viz., E, the total energy, and M, the angular momen-

tum. These are given by:

$$E = \frac{1}{2} m \left( u_r^2 + u_t^2 \right) + \Phi, \tag{23}$$

$$M = mru_t, \tag{24}$$

where m is the mass of the particle and $u_r$ and $u_t$ are the components

of the particle velocity in the radial and tangential directions,

respectively, at some point in space located a distance r from the

center; $\Phi$ is the potential energy. In the cylindrical geometry, $u_r$

and $u_t$ are in a plane perpendicular to the axis of the cylinder (taken

25

along the z axis of a right-handed coordinate system) so that E is the total energy due to motion in that plane and M is the component of angular momentum in the z direction. Since the cylinder is considered to be infinite in length, the velocity component $u_z$ in the z direction remains constant and does not play a role in the classification of the orbits. In the spherical geometry, $u_r$ is the radial component and $u_t$ is the total tangential component of the particle velocity. Thus, in this case, E is the total energy and M is the total angular momentum. For both geometries, $\Phi$ is the potential energy at r, relative to a zero value in the plasma. Since we will be dealing exclusively with the situation in which the particles are accelerated toward the collector, we will have $\Phi < 0$ and $\Phi' > 0$, where the prime on $\Phi$ denotes differentiation with respect to r. The classification of the orbits will now be carried out without reference to whether the geometry is cylindrical or spherical.

Now let us introduce the concept of the so-called "effective potential energy" by substituting $u_t$ from Eq. (24) into Eq. (23) to get

$$E = \frac{1}{2}mu_r^2 + \Phi \tag{25}$$

where

$$\Phi_e \equiv \frac{M^2}{2mr^2} + \Phi. \tag{26}$$

The effective potential energy $\Phi_e$ governs the radial motion of the particles. The points, where $u_r = 0$ are the turning points of the orbits. At these points the effective potential energy $\Phi_e$ equals the total energy E.

In principle, the mathematics describes two such points, the apogees

and the perigees of quasi-elliptical orbits. However, the present physical

model deals only with the perigees, as the apogees would be beyond the

sheath region, or more generally beyond the region of interest for the

present study.

## 3.2 RELATIONSHIP OF THE OCCURRENCE OF MAXIMA AND MINIMA OF THE EFFECTIVE POTENTIAL $\Phi_e$ TO THE POTENTIAL STRUCTURE

In order to investigate the qualitative behavior of particle tra-

jectories, we need to examine the behavior of the effective potential $\Phi_e$

as a function of r for various values of the angluar momentum M. In

particular we must study the extrema of $\Phi_e$. On equating to zero the

derivative of $\Phi_e$ with respect to r, keeping $M^2$ constant, in Eq. (26),

we obtain

$$M^2 = mr^3 \Phi', \quad \text{when } \Phi'_e = 0, \tag{27-1}$$

that is,

$$\psi(r) = M^2, \quad \text{when } \Phi'_e = 0, \tag{27-2}$$

where, for convenience, we use a function $\psi(r)$ defined as follows:

$$\psi(r) \equiv mr^3 \Phi'. \tag{28}$$

$\psi(r)$ is a function of the field structure, that has the unique value $M^2$

at values of the radius for which the effective potential $\Phi_e$ has a maxi-

mum or minimum. Of course, the solution of Eq. (27-2) for r is dependent

on the form of $\psi(r)$. If $\psi(r)$ is a monotonically increasing function of $r$, as illustrated in Fig. 3, then for every given value of $M^2$ there exists one and only one value of $r$ for which Eq. (27-2) is satisfied: therefore, there exists only one value of $r$ at which $\Phi_e$ has an extreme value, and this extreme value can only be a minimum.

A sufficient condition for $\psi(r)$ to increase monotonically would be for $\Phi(r)$ to obey an inverse power law varying less steeply than $1/r^2$, for all values of $r$ within the region of interest. Therefore $\psi(r)$ would increase monotonically, as shown in Fig. 3, if $\Phi(r)$ were to vary as $C_1/r$.

In contrast, if $\Phi(r)$ were to vary as $C_1/r^3$, then $\psi(r)$ would be a monotonically decreasing function of $r$. In such a case there would be one and only one value of $r$ at which $\Phi_e(r)$ would have an extreme value; but this would be a _maximum_, resulting in a potential barrier inside the sheath.

The steepness of the potential gradient $\Phi(r)$ is partly determined by the geometry of the probe (i.e., whether it is spherical or cylindrical). In addition the radial dependence of $\Phi(r)$ is governed by the extent to which space charge is present in the region of interest. The potential $\Phi(r)$ is, in general, describable as the sum of a space-charge free term of positive gradient (for example varying as $1/r$ or as $\ln r$) and a space-charge dependent term. This relates to the discussion below Eq. (20), for the condition $\xi = 1$ and $\alpha > 1$ (for spherical geometry), and $\xi = 0$ and $\alpha > 0$ (for cylindrical). The usual physical model for accelerated particles is that of a negative potential probe drawing a current of positive

28
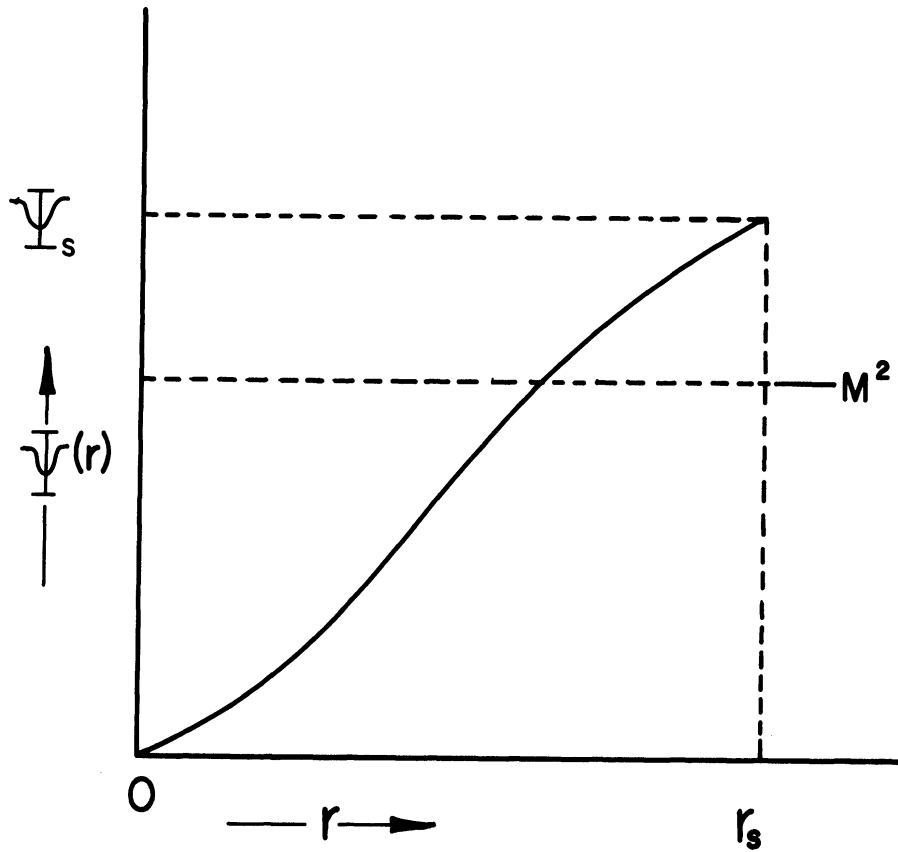
Fig. 3. Graph of the function $\psi(r)$, Eq. (28), for a form of this function that increases monotonically up to the sheath radius $r_S$ and has the value $\psi_S$ at $r_S$. An illustrative value of $M^2$ is shown corresponding to a trajectory for which the angular momentum is $\pm M$ (determined at entry into the sheath).

ions through the sheath. For this model, the space-charge density is positive throughout the sheath. For a potential model that incorporates a space-charge free potential plus a potential due to space-charge content the space-charge free potential term by itself gives rise to a monotonically increasing $\psi(r)$, for either the spherical or the cylindrical geometry. Thus, departure from such a monotonicity comes only when the rate of change of the space charge term in $\psi(r)$ is dominant in a region where this rate of change is negative. As discussed later in connection with Fig. 15, wherever the space-charge density locally declines as $1/r^n$ with $n<4$, it contributes to the monotonic increase of the function $\psi(r)$. But if $\psi(r)$ will increase monotonically only because of the dominance of the space-charge free term over that due to space charge, in the range of radii of interest.

Thus it appears that a sufficient, but not always necessary, condition for $\psi(r)$ to increase monotonically is an adequate domination of the space-charge free effect on the potential distribution over the space-charge effects.

3.3 PROPERTIES OF THE EFFECTIVE POTENTIAL OF LANGMUIR'S FINITE SHEATH MODEL; THE "ADMISSIBLE SPACE" DIAGRAM FOR PARTICLES REACHING THE PROBE

We will first examine $\Phi_e$ in the light of Langmuir's finite sheath model, that is

$$\Phi(r) = \begin{cases} \Phi(r) & \text{when } r \leq r_s; \\ 0 & \text{when } r > r_s; \end{cases} \qquad (29)$$

with $\Phi$ satisfying the inequality (3) for $r_c \leq r \leq r_s$, where $r_c$ and $r_s$ are the radius of the probe and the radius of the sheath, respectively. An illustrative plot of $\psi(r)$ is shown in Fig. 3. We will show that Langmuir's expression for the accelerated current to the probe, for either cylindrical or spherical geometry, can be derived only when it is assumed that

$$\lim_{r \to r_s^-} \Phi'(r) \neq 0, \tag{30}$$

that is, if it is assumed that the potential gradient does not vanish as $r$ approaches $r_s$ from within the sheath.

Let $\psi_s$ denote the value of $\psi(r)$ as $r \to r_s^-$. Then, for $M^2 > \psi_s$, there exist no solutions of Eqs. (27-1) and (27-2) in the range $r < r_s$. In the range $0 \leq M^2 \leq \psi_s$, one value of $r$ is obtained for each given $M^2$ from Eq. (27-2), and at this value of $r$, $\Phi_e$ has a minimum. At $r = r_s$, the value of $\Phi_e$ is, from Eq. (26) given by

$$\Phi_e(r_s) = \frac{M^2}{2mr_s^2} \tag{31}$$

because $\Phi$ is defined to be zero at and beyond $r = r_s$. This expression tells us that, for nonzero $M^2$, $\Phi_e(r_s)$ is always positive. The derivative of $\Phi_e$ at $r_s$ is

$$\Phi_e'(r_s) = \frac{1}{mr_s^3}(\psi_s - M^2) \tag{32}$$

where $\psi_s = \psi(r_s)$. It will be recalled from Eq. (28) that the meaning of this is:

31

$$\Phi'_e(r_s) \;=\; \frac{1}{mr_s^3}\left(mr_s^3\Phi'(r_s) - M^2\right). \tag{33}$$

From Eq. (32) it is clear that from $\Phi'_e(r_s) > 0$ follows

$$M^2 < \psi_s, \tag{34}$$

whereas for other values of $M^2$, $\Phi'_e(r_s) \leq 0$. Plots of $\Phi_e(r)$ are shown in Fig. 4. Now, there exists a value of $M^2 = M_s^2$ such that $\Phi_e(r_c) = \Phi_e(r_s)$. For any potential which satisfies the boundary condition $\Phi(r_s) = 0$, Eq. (26) can be used to show that

$$M_s^2 \;=\; \frac{2mr_s^2 r_c^2}{r_s^2 - r_c^2}\,(-\Phi_c). \tag{35-1}$$

Note that for a very large sheath, when $r_s^2 \gg r_c^2$, this reduces to:

$$M_s^2 \;=\; 2mr_c^2\,(-\Phi_c). \tag{35-2}$$

In reference to Fig. 4, it is seen from Eq. (26) that the $M^2 = 0$ curve describes equally well:

(a) The potential distribution in the sheath:

(b) The energy of a particle that is wholly radially directed and

has zero velocity at $r = r_s$; such a particle falls freely from

rest at $r = r_s$ into the probe; it must begin this fall, because

in the Langmuir model now being described, $\Phi'(r)$ is positive at

$r = r_s$.

In accordance with the discussion following Eqs. (27) and (28) we now

consider a potential that is qualitatively like the $M^2 = 0$ curve in Fig.
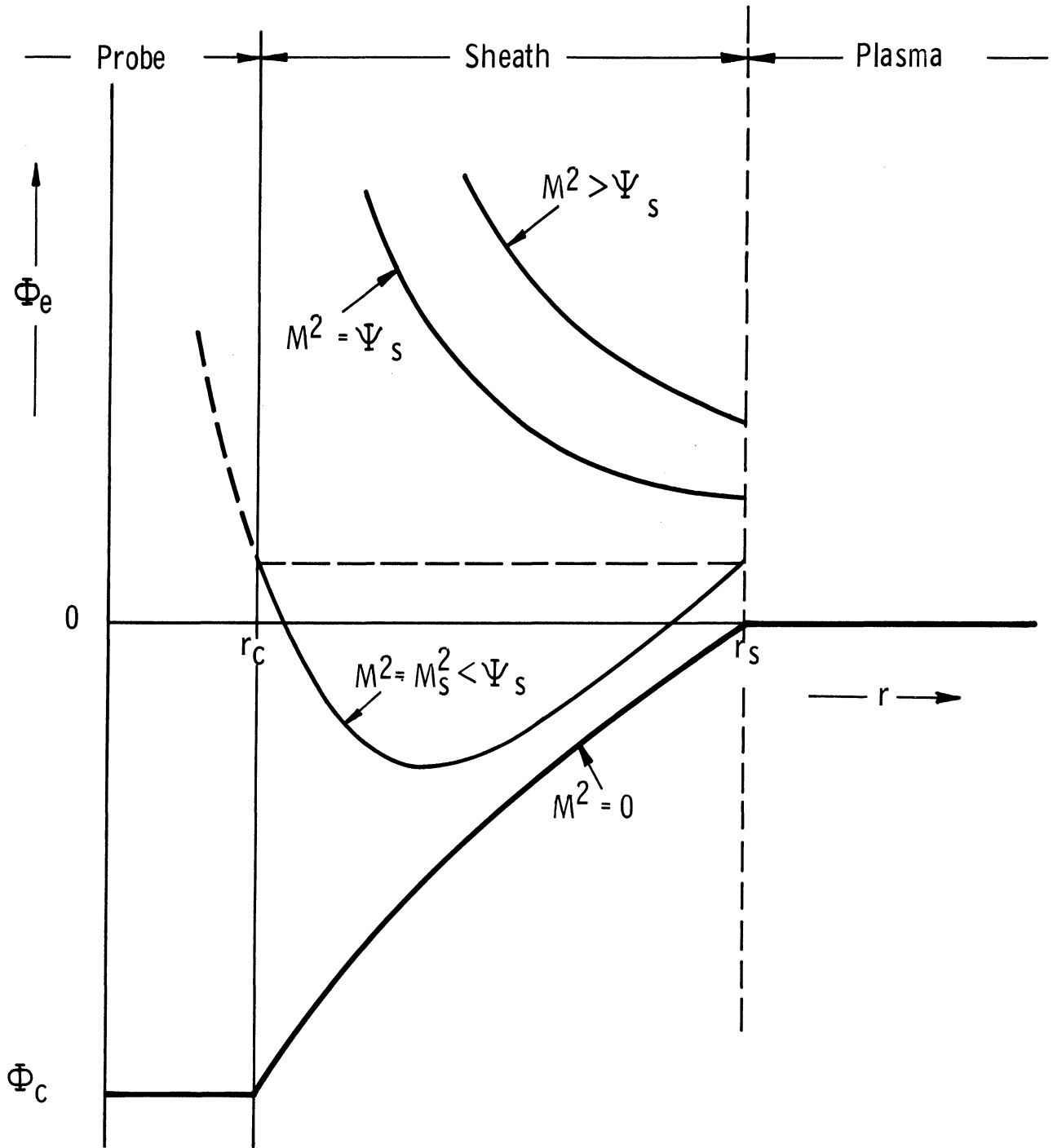
Fig. 4. Plots of the effective potential energy $\Phi_e(r)$, for various values of $M^2$. $M_s^2$ is defined as the value of $M^2$ for which $\Phi_e$ is the same at the probe surface as at the sheath radius. $\psi_s$ is the value of $M^2$ for which the minimum in $\Phi_e$ occurs at sheath radius (see Fig. 3).

4 and has a monotonically increasing $\psi$ function as shown in Fig. 3. Then

each effective potential $\Phi_e(r)$ has one and only one minimum in the range

$r \leq r_s$ as shown in Fig. 4. If $M^2$ is nonzero but very small, the minimum

occurs for $r < r_c$, and so has no physical significance for the present

study. As $M^2$ increases, the minimum moves across $r = r_c$. We are inter-

ested in two particular values of $M^2$.

One of these is of course $M^2 = M_s^2$, for which a particle with zero

initial radial velocity grazes the probe at perigee. If $M_s^2 < \psi_s < M^2$,

a particle with zero initial velocity will not start inward, because

$\Phi_e' < 0$. An illustrative example for such a $\Phi$ curve is shown in Fig. 4.

The second unique value of $M^2$ occurs at $M^2 = \psi_s$, for which, from

Eq. (32), the minimum of $\Phi_e$ occurs just at $r = r_s$. A particle with this

value of $M^2$ and zero initial radial velocity will not move inward from

$r = r_s$ even though $\Phi'(r_s)$ is positive, because the gradient $\Phi_e'(r_s)$ of the

effective potential is zero at $r_s$ and negative for $r < r_s$.

From the above comments it is clear that $M_s^2 \leq \psi_s$, as long as the

potential is such that $\psi(r)$ increases monotonically as illustrated in

Fig. 2.

The relationship of particle trajectories to effective potentials

of the type shown in Fig. 4 will be discussed with reference to Figs. 5a

and 5b. Figure 5a shows, a typical effective potential $\Phi_e(r)$ for a case

in which $M^2 < M_s^2$ and the total energy E is sufficiently large so that

the trajectory will intersect the probe, i.e., a particle along such a

trajectory will be collected. If $M^2 < M_s^2$, the requirement for collection (see Fig. 5a) is that $E \geq \Phi_e(r_s)$ since then also $E > \Phi_e(r_c)$ because of the way in which $M_s^2$ is defined.

Figure 5b shows, a typical $\Phi_e(r)$ for the case in which $M^2 > M_s^2$, with the total energy E larger than $\Phi_e(r_c)$. Thus the trajectory for this E and this M will also intersect the probe, and collection will occur. Note that in this case particles with energy less than $\Phi_e(r_c)$ could exist inside the sheath. But in such a case the perigee $(E = \Phi_e)$ would be at a larger radius than $r_c$ implying that collection would not occur.

In Fig. 5a $(M^2 < M_s^2)$ the requirement that $\frac{1}{2}mu_r2$ cannot be negative, limits the possible values of E to the range $E \geq \Phi_e(r_s)$ and since $\Phi_e(r_s) > \Phi_e(r_c)$ in Fig. 5a, any energy that exceeds $\Phi_e(r_s)$ will give rise to a trajectory reaching the probe. In contrast to this, if $M^2 > M_s^2$ (Fig. 5b), the particle reaches the probe only if $\frac{1}{2}mu_r^2 > 0$ at $r = r_c$ which limits the possible values of E to the range $E \geq \Phi_e(r_c)$. Therefore, we can now define a so-called "admissible space." Each particle can be represented by a point in the $(E, M^2)$ space, since both E and $M^2$ are constants of the motion. Then the admissible space is that subspace of $(E, M^2)$ space which contains the representative points of the collected particles. Based on the above discussion the admissible space is defined by the following relations:

$$E \geq \Phi_e(r_s) = \frac{M^2}{2mr_s^2} \text{ if } 0 \leq M^2 \leq M_s^2 \qquad (36\text{-}1)$$
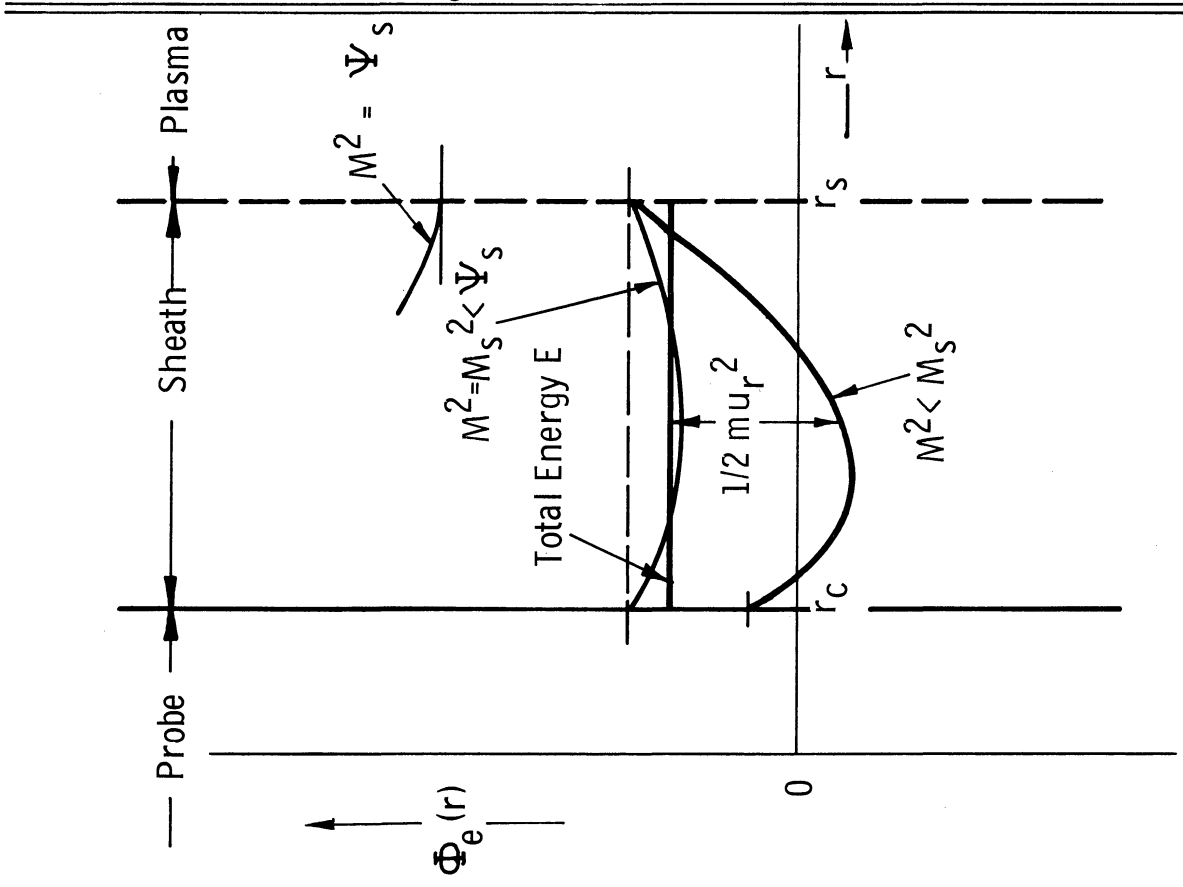
$M^2 = \Psi_s$

Total Energy E

$\Phi_e(r_c)$

$1/2\,mu_r^2$

$M^2 < M^2_s$

$M_s^2 / 2mr_s^2$

$M^2 = M_s^2 < \Psi_s$

$r_s$

$r_c$

$r$

Plasma

Sheath

Probe

0

$\Phi_e(r)$

Fig. 5b. $\Phi_e(r)$ for $M^2 > M_s^2$ and total energy E for which collection occurs.

$M^2 = \Psi_s$

Plasma

Sheath

$M^2 = M_s^2 < \Psi_s$

Total Energy E

$1/2\,mu_r^2$

$M^2 < M_s^2$

$r_s$

$r_c$

$r$

Probe

0

$\Phi_e(r)$
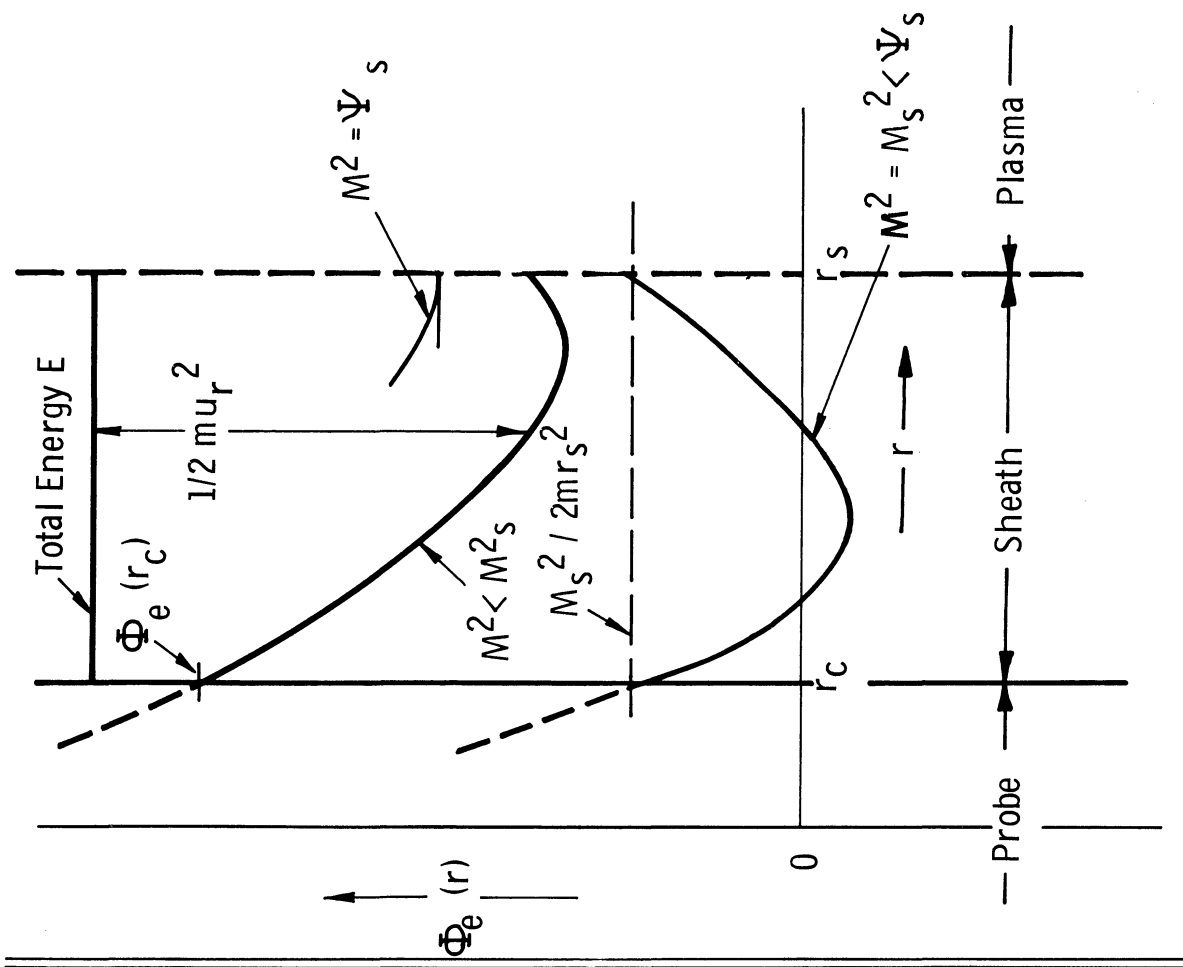
Fig. 5a. $\Phi_e(r)$ for $M^2 < M_s^2$ and total energy E for which collection occurs.

$$E \geq \Phi_e(r_s) = \frac{M^2}{2mr_c^2} + \Phi_c \quad \text{if} \quad M^2 \geq M_s^2 \qquad (36\text{-}2)$$

The shaded area in Fig. 6 illustrates this admissible space.

## 3.4 UTILITY OF THE $\psi$-FUNCTION IN DETERMINING APPLICABILITY OF THE LANGMUIR VOLT-AMPERE RELATIONS

The $\psi$-function (28) plays a very important role in deriving criteria for the validity of Langmuir's theory. We have seen that, if $\psi(r)$ is a monotonically increasing function of r, then for each given $M^2$, $\Phi_e(r)$ has a minimum. For a finite sheath each $\Phi_e$ has a minimum provided $M^2 < \psi_s$, where $\psi_s = \psi(r_s)$.

We wish to show in a slightly different way from the treatment of Mott-Smith and Langmuir that there indeed exists a limiting potential function $\Phi_L(r)$, with the property that any other potential function that varies less steeply than $\Phi_L$, for all values of r, will give rise to Langmuir's current expressions, while any potential function varying more steeply than $\Phi_L$ will give rise to current expressions different from those of Langmuir. First, we note that if $\Phi_e$ has a maximum (for a given $M^2 < M_s^2$) which lies to the left of $r_s$ (see Fig. 4), the condition for collecting the particle corresponding to that $M^2$ will not be determined at $r_s$, but at a smaller distance than $r_s$. This is contrary to Langmuir's requirement that all trajectories intersecting the probe must be determined by initial conditions at $r_s$. Hence the class of potential functions which satisfy this requirement must be such that they produce no maxima in $\Phi_e$ in the region $r_c \leq r < r_s$. As discussed earlier, $\Phi_e$ has minima when $\psi(r)$ has a positive slope and maxima when it has a negative slope. The necessary condition
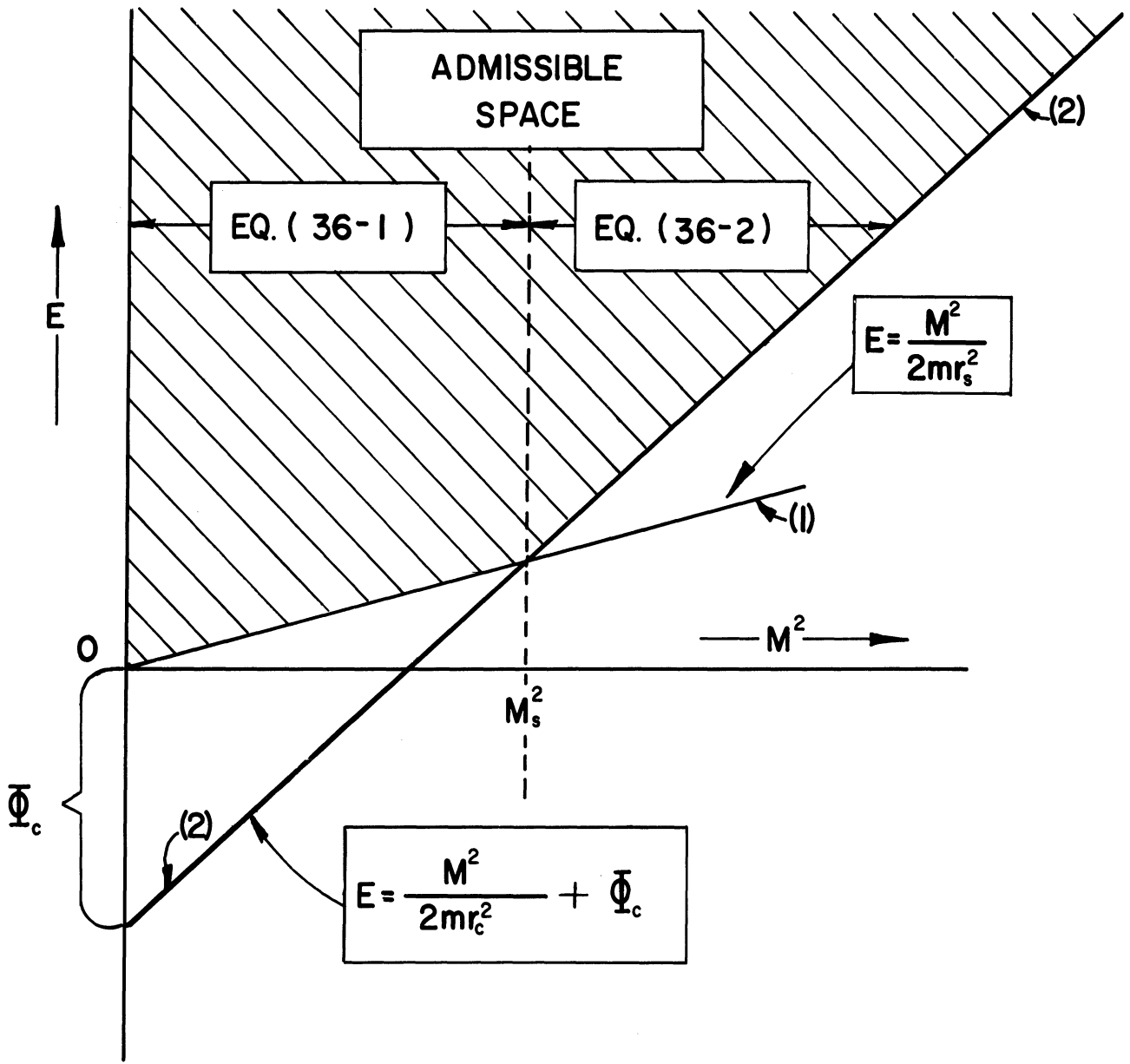
Fig. 6. The shaded area is the "admissible space" in the $(E, M^2)$ plane for Langmuir's finite sheath model. To the left of $M_s^2$ , Eq. (36-1) applies, conditions as illustrated in Fig. 5a. To the right of $M_s^2$ , Eq. (36-2) applies, conditions as in Fig. 5b.

for the applicability of Langmuir's theory can, therefore, be restated by saying that the $\psi$-function cannot have a negative slope. Therefore, $\psi$ (r) can, at most, be a constant in this range of r, in order for Langmuir's volt-ampere equations to be valid. Thus, by setting $\psi(r) = mC_a$, introducing the potential given in Eq. (6), and employing Eq. (28), we have

$$\frac{d\Phi_L}{dr} \; \Theta \; (r-r_c) \; \Theta \; (r_s-r) + \Phi_L \; \delta \; (r-r_c) \; \Theta \; (r_s-r)$$

$$-\Phi_L \; \delta(r_s-r) \; \Theta \; (r-r_c) \; = \; \frac{C_a}{r^3} \tag{37}$$

Upon integrating this, we get

$$\Phi_L(r) + \Phi_c \; = \; C_b - \frac{C_a}{2r^2} \tag{38}$$

On employing the boundary conditions

$$\Phi_L(r) \; = \; \Phi_c \; \text{at} \; r \; = \; r_c,$$
$$\Phi_L(r) \; = \; 0 \quad \text{at} \; r \; = \; r_s, \tag{39}$$

we obtain

$$C_b - \frac{C_a}{2r_c^2} \; = \; 2\Phi_c, \tag{40-1}$$

$$C_b - \frac{C_a}{2r_s^2} \; = \; \Phi_c, \tag{40-2}$$

and therefore

$$C_a \; =- \frac{2(-\Phi_c) \; r_s^2 r_c^2}{r_s^2 - r_c^2} \; , \tag{41-1}$$

$$C_b = \frac{C_a}{2r_c^2} - 2(-\Phi_c). \tag{41-2}$$

Now inserting these values of $C_a$ and $C_b$ into Eq. (38) we get

$$\Phi_L(r) = \Phi_c \frac{r_s^2 - r^2}{r_s^2 - r_c^2} \frac{r_c^2}{r^2} \Theta (r_s - r). \tag{42}$$

Equation (42) defines the desired limiting potential function. It is seen to be of the same form as the potential defined by Eq. (5) which had been employed in an earlier section to identify Langmuir's sheath model. $\Phi_L$ is graphically represented by the $f_s \cdot \Phi_c$ curve in Fig. 1. The corresponding $\psi(r)$ is obtained by using the radial derivative of Eq. (42) for $\Phi'$ in Eq. (28), which yields

$$\psi(r) = (-\Phi_c) \frac{2mr_s^2}{\frac{r_s^2}{r_c^2} - 1} \Theta(r_s - r) \tag{43}$$

As shown in Fig. 7, this is a horizontal straight line for $r \leq r_s$ where it has a step function drop to zero.

The conclusion is that for a finite sheath radius and given boundary value $\Phi'(r_s)$ any monotonically increasing function $\psi(r)$ (corresponding to some potential function) which lies in the rectangle, illustrated in Fig. 7, will give rise to Langmuir's volt-ampere relations. The dashed curves in the figure represent two such possible $\psi(r)$ functions.

For the infinite-sheath case $(r_s \to \infty)$ the right-hand side of Eq. (42) reduces to the inverse square law. Thus for an infinite sheath the limiting potential function (corresponding to the limit of the range for the orbital-motion-limited mode of collection) is simply

40
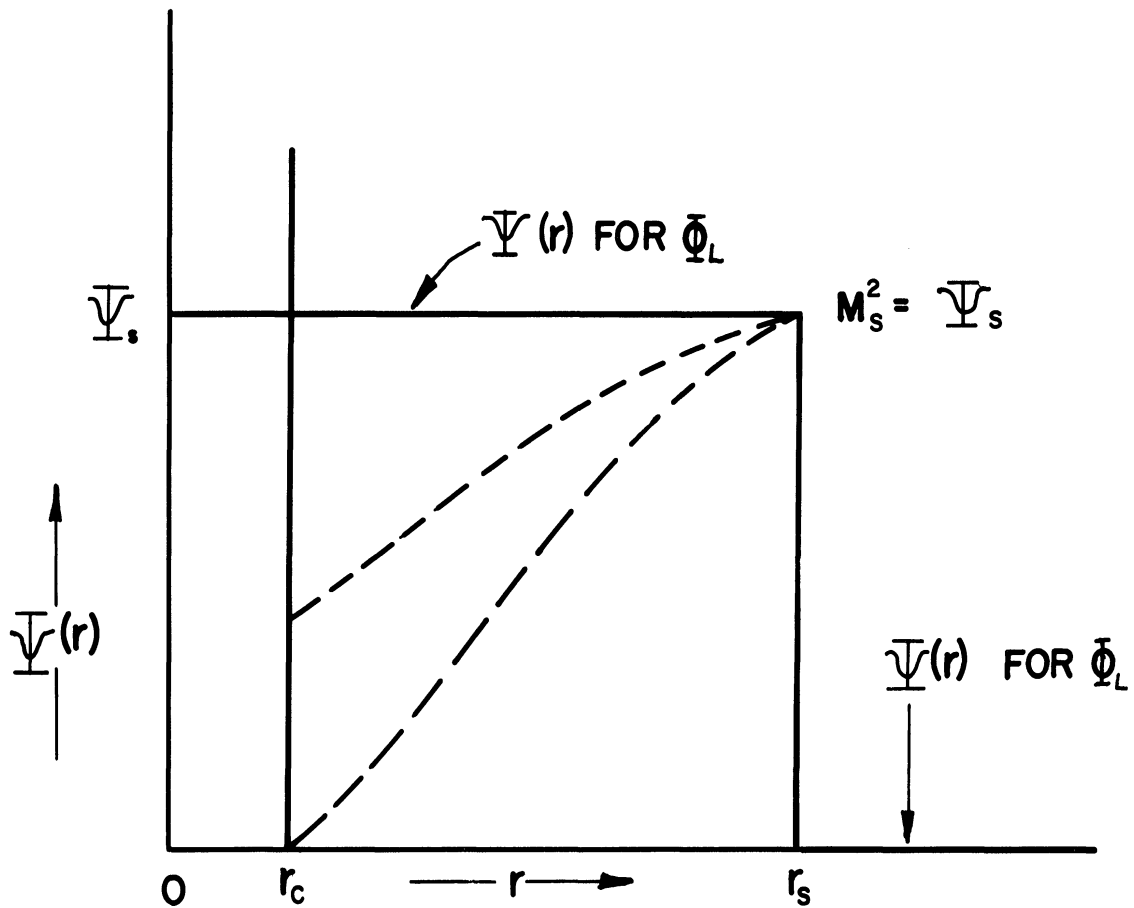
Fig. 7. Graph of the singular $\psi$-function (43) corresponding to the Eq. (42) form of $\Phi_L$, which is the limiting form for validity of the volt-ampere equations of the Langmuir finite sheath model. $\Phi_L$ is the $f_s \cdot \Phi_c$ curve in Fig. 1, for $r < r_s$, and of course $\Phi_L = 0$ for $r > r_s$.

$$\Phi = \Phi_c \left(\frac{r_c}{r}\right)^2 \tag{44}$$

3.5 DEPENDENCE OF THE MOTT-SMITH AND LANGMUIR CURRENT-COLLECTION
EQUATIONS ON THE PRESENCE OF A DISCONTINUITY IN THE POTENTIAL
GRADIENT AT THE SHEATH EDGE

When one employs the domain of integration given by Eqs. (36-1) and

(36-2) as illustrated by Fig. 6, the resulting expressions for the acceler-

ated currents to the cylindrical and the spherical probes are the ones ob-

tained by Mott-Smith and Langmuir[1] (see the Appendix for the derivations).

It is important to note here that it was necessary to assume a discontinuity

in $\Phi'$ across $r_s$ (indicated at $r = r_s$ by the $M^2 = 0$ curve of Fig. 4) in order

to obtain these current expressions. If we were now to assume that $\Phi$ has

a continuous derivative at $r_s$, and in fact that $\underset{r \to r_s}{\text{Lim}} \Phi' = 0$ from the left

and from the right this would amount to requiring that, in the neighborhood

of $r_s$ the variation of $\Phi$ be as $(r - r_s)^n$, where $n > 1$. This contradicts

the gross-aspect requirement, used by Mott-Smith and Langmuir, that the

variation of $\Phi$ must approximate that of an inverse power less than 2.

More specifically, if one were to require that $\Phi' = 0$ at $r = r_s$,

this would in turn require that $\psi_s = mr_s^3 (d\Phi/dr)_{r=r_s} = 0$. For a finite

$r_s$, this is wholly inconsistent with the requirement illustrated by Fig.

7 that $\psi(r)$ be a monotonically increasing function of $r$ for $r_c \leq r < r_s$.

Therefore, as will be seen later, the current expressions obtained by

using $\Phi' = 0$ at $r = r_s$ are quite different from those of Mott-Smith and

Langmuir.

One may also note that in the finite sheath model, with $\underset{r \to r_s}{\text{Lim}}$

$\Phi' \neq 0$, a slight error in the estimation of $r_s$ can contribute a sig-

nificant error in the current calculation. This is so because the slope of Line (1) in Fig. 6 is inversely proportional to $r_s^2$.

## 3.6 ADMISSIBLE SPACE FOR THE ORBITAL-MOTION-LIMITED CONDITION IN THE MOTT-SMITH AND LANGMUIR THEORY

The case, where the sheath radius is large as compared with the probe radius, is of special interest in many applications. Following Langmuir, this is referred to as the orbital motion limited case. As $r_s$ increases, the slope of the function $E = M^2/2mr_s^2$ (see line 1 in Fig. 6) becomes small and in the limit of infinite sheath radius goes to zero. $\psi(r)$ becomes then a monotonically increasing function from $r = 0$ to $r = \infty$. Consequently, for every given $M^2$, Eqs. (27) are satisfied for some value of r. In other words, $\Phi_e(r_s) = \Phi_e(\infty) = 0$, and $\Phi_e(r)$ has a minimum for every $M^2$; this is illustrated in Fig. 8.

The corresponding admissible space is illustrated in Fig. 9, and is generated by the following expressions obtained as modifications of Eqs. (36-1) and (36-2):

$$0 \leq E < \infty, \text{ if } 0 \leq M^2 \leq M_s^2; \tag{45-1}$$

$$E \geq \frac{M^2}{2mr_c^2} + \Phi_c; \text{ if } M_s^2 < M^2 < \infty, \tag{45-2}$$

where $\boxed{r_s \to \infty \text{ in Eq. (35-1)}}$

$$M_s^2 = 2mr_c^2(-\Phi_c). \tag{45-3}$$

Note that the admissible space illustrated in Fig. 9 governs the Mott-Smith and Langmuir orbital-motion-limited condition.

43
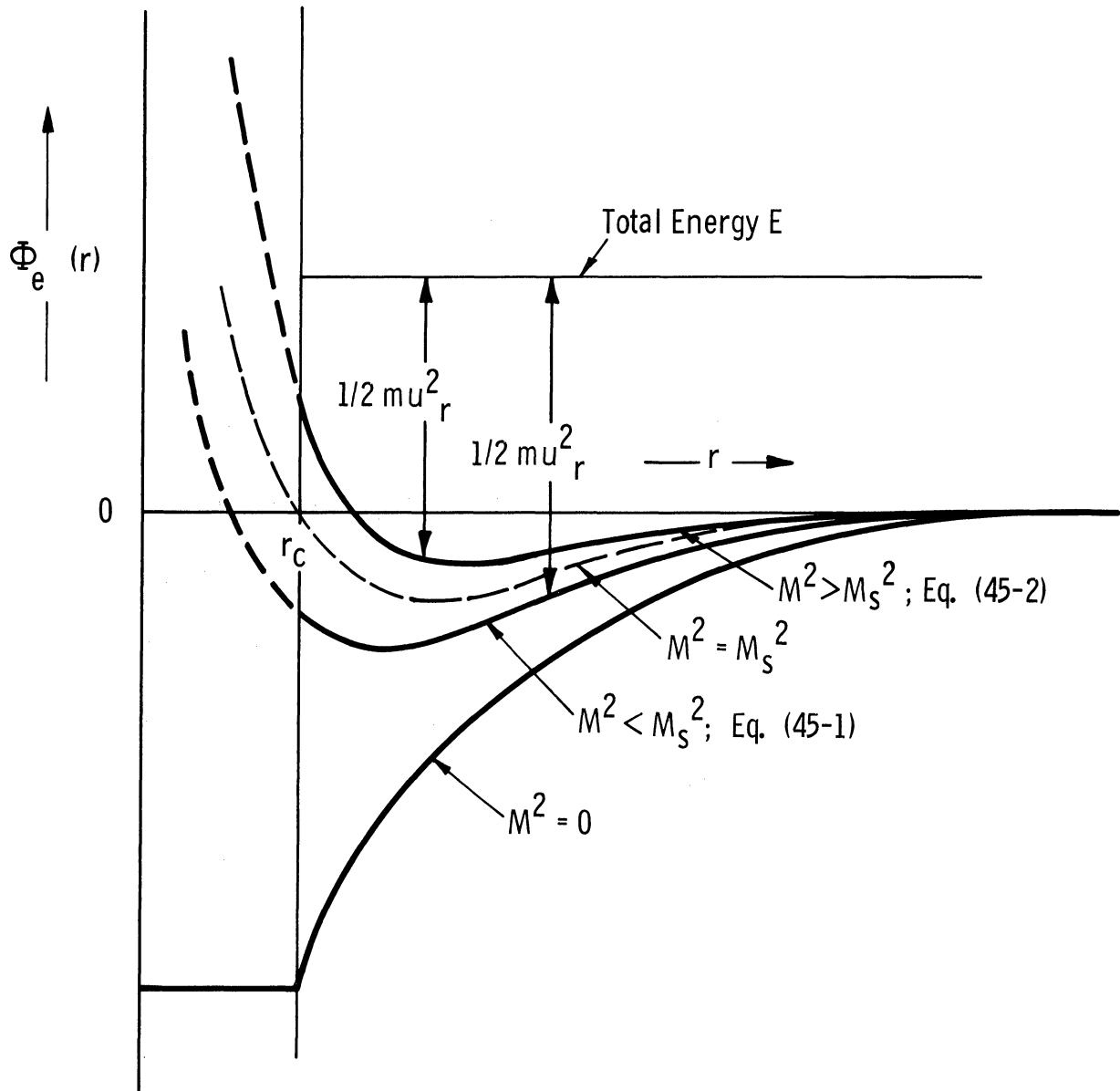
Fig. 8. Plots of the effective potential if $r_s \to \infty$, giving the Mott-Smith and Langmuir orbital-motion-limited condition. If $M^2 < M_s^2$, any positive E will result in collection, as expressed by Eq. (45-1), if $M^2 > M_s^2$, E must equal or exceed $\Phi_e(r_c)$ for collection to occur, as expressed by Eq. (45-2). See Fig. 9, for the corresponding admissible space.
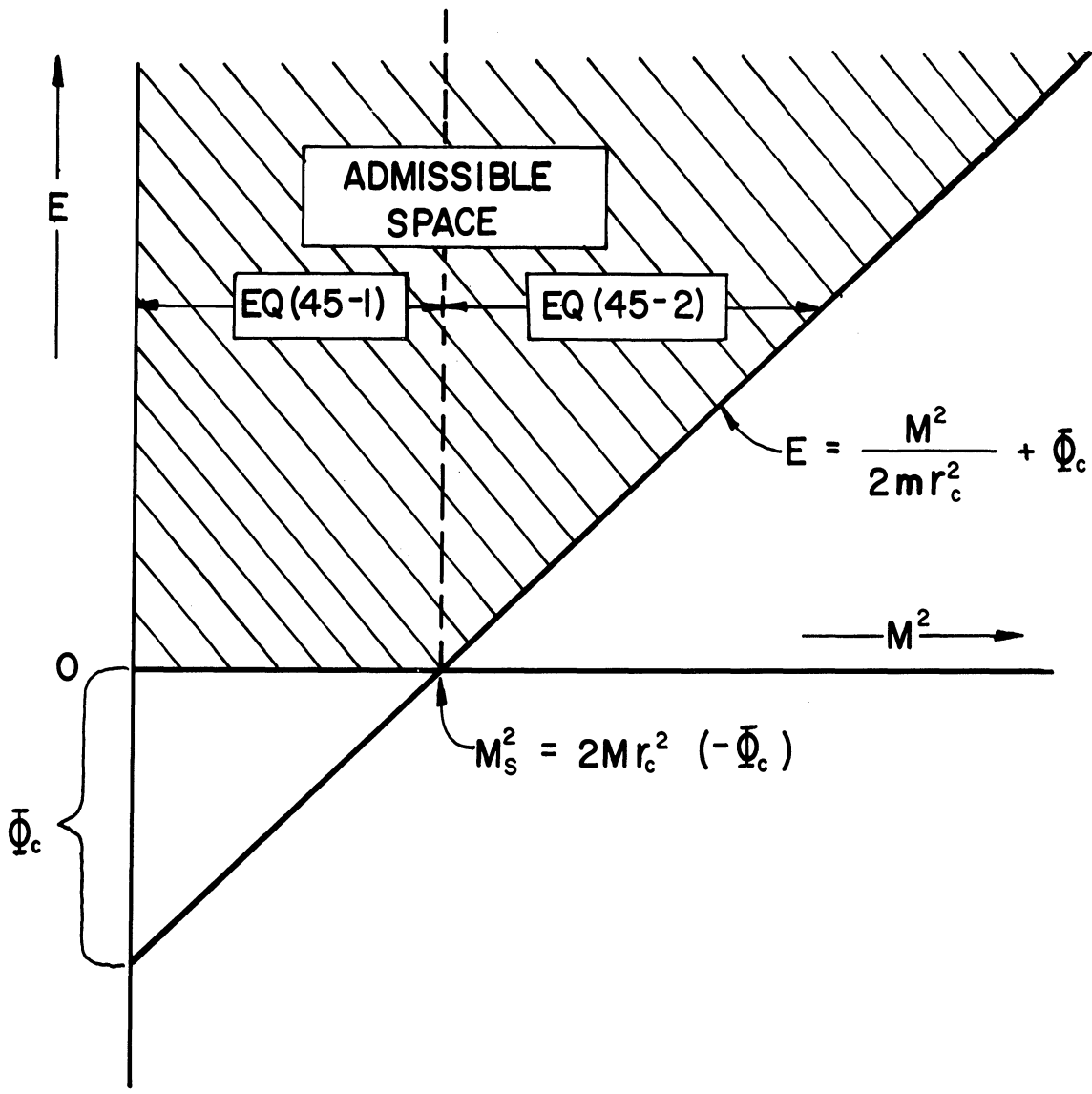
Fig. 9. "Admissible space" diagram, for the orbital-motion-limited condition, occurring for the Mott-Smith and Langmuir model when $r_s \to \infty$. The two shaded regions correspond respectively to the Fig. 8, curves for $M^2 < M_s^2$, as in Eq. (45-1), and for $M^2 > M_s^2$, as in Eq. (45-2).

## 3.7 A CLASS OF POTENTIAL FUNCTIONS, GIVING RISE TO BOTH A MAXIMUM AND A MINIMUM IN THE EFFECTIVE POTENTIAL

Next, we shall examine the effective potential $\Phi$ (r) for a class of

potential functions with the following properties: The associated $\psi$-function

increases montonically to a certain value of r denoted by $r_i$, where it reaches

a maximum, and then decreases montonically, as shown in Fig. 10. At r = 0,

$\psi(r)$ = 0. Consider for a time the condition $r_c < r_i$, and define $M_i$ so that

$\psi(r) = M_i^2$ at its maximum point $r = r_i$. Thus with this form of $\psi(r)$ we have

no solutions of Eq. (27-2) for $M > M_i^2$, which means that for these larger

values of $M^2$ the function $\Phi_e(r)$ monotonically decreases with increasing r,

for all $r < \infty$. Also, the curve for $\Phi_e(r,M_i^2)$ has an inflexion point at r = r .

For $M^2 < M_i^2$, Eq. (27-2) has two solutions corresponding to the values of r

where $\Phi_e$ has a maximum and a minimum.

Let $\Phi_e^*, r^*$, and $\Phi^*$ symbolize, respectively, the <u>maximum</u> value of $\Phi_e(r)$,

the radius at which it occurs, and the potential at that radius, all for

some given M . Evidently $r^* > r_i$. Thus we may

$$\Phi_e^* = \frac{M^2}{2mr^{*2}} + \Phi_e \qquad (46-1)$$

Of course $r^*$ is the solution of Eq. (27-2) which identifies the radius at

which this maximum occurs: $r^*$ is itself a function of $M^2$.

It is clear that in order to find the locus of the maxima of $\Phi_e$ one

must first know the form of $\Phi$. However, instead of restricting ourselves

to a particular form of $\Phi$, we shall consider a class of potential functions

for which the loci of the maxima of $\Phi$ (r) as a function of $\underline{M^2}$, are of the form

46

$$\Phi_e{}^* = K_\nu M^{2\nu} \qquad r^* > r_i \qquad\qquad (46\text{-}2)$$

Using the definition (26) of $\Phi_e$ we therefore obtain

$$\Phi_e{}^* = \frac{M^2}{2mr^{*2}} + \Phi^* = K_\nu M^{2\nu} \qquad\qquad (46\text{-}3)$$

$\Phi_e{}^*$ is said to be separable for a given potential $\Phi$ if it can be written in the form (46-2) such that $\nu$ and $K_\nu$ are independent of $M^2$. These parameters depend only on the probe geometry and potential. In Eqs. (46-2) and (46-3) one must always take $M^{2\nu}$ as $(M^2)^\nu$ for all values of $\nu$, in order to retain the symmetry $\Phi_e{}^*$ must have with respect to the angular momentum M.

Note particularly that Eqs. (46-2) and (46-3) describe only the behavior of $\Phi_e$ at the maxima, and do not restrict the location of the minima.

### 3.8 THE UNIQUE ANGULAR MOMENTUM $M_k$ FOR WHICH THE MAXIMUM VALUE OF EFFECTIVE POTENTIAL EQUALS THAT AT THE COLLECTOR SURFACE

We shall now study the relation of the maximum value $\Phi_e{}^*$ to the value $\Phi_e(r_c)$ of the effective potential at the probe surface for a $\psi$-function of the type illustrated in Fig. 10. Such a study leads to an evaluation of $K_\nu$ and $\nu$ for the particular class of potentials identified by Eqs. (46-2) and (46-3), but also of general interest as regards any potential function whose associated $\psi$-function varies as shown in Fig. 10.

For any particular potential function having two extrema in the expression for $\Phi_e(r)$, the probe radius $r_c$ may in principle be less than,
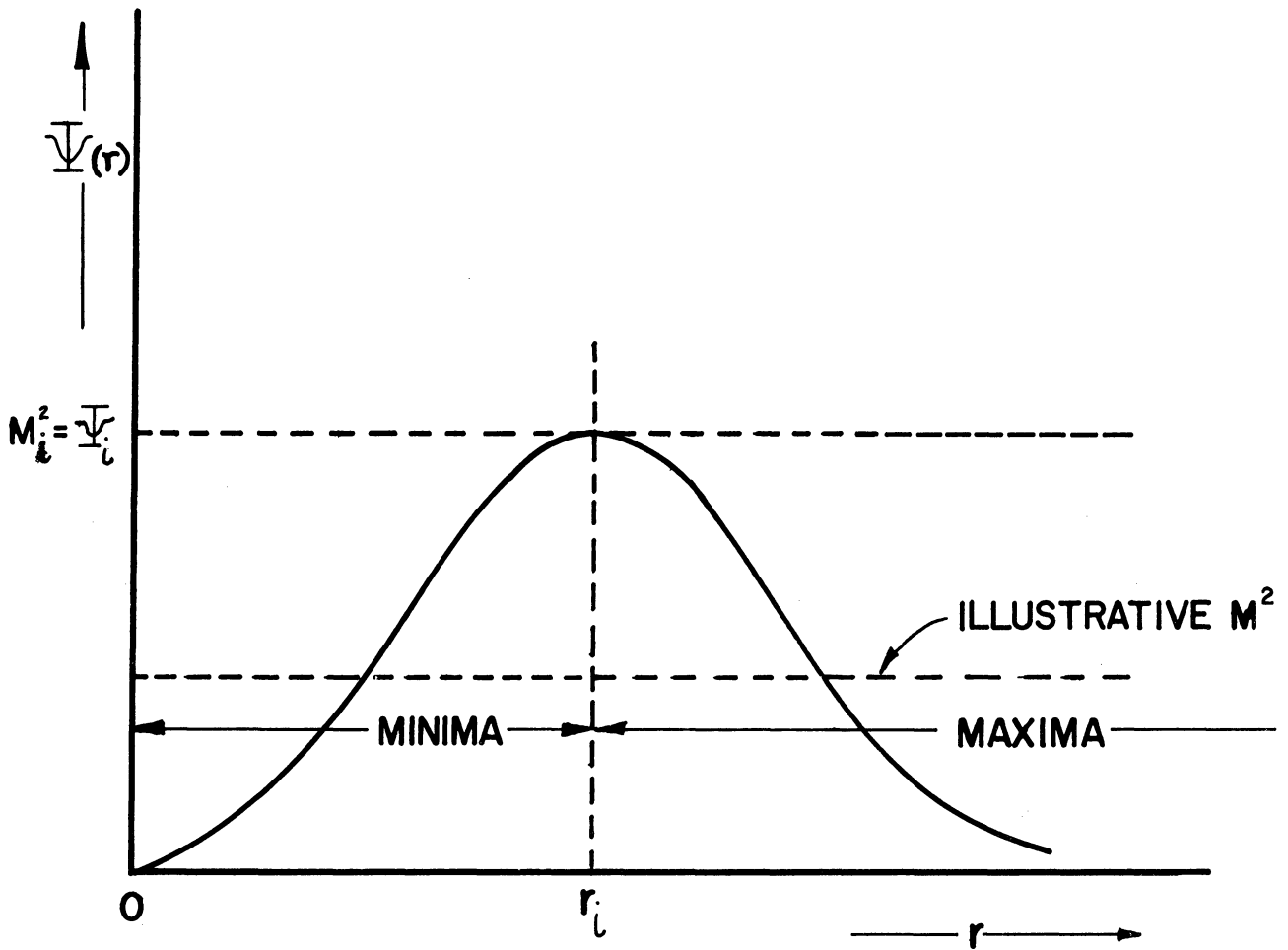
Fig. 10. Graph of a $\psi$-function, displaying a maximum inside the sheath. In this case the effective potential has: a minimum if $r < r_i$ and $M^2 < M_i{}^2$; a maximum if $r > r_i$ and $M^2 < M_i{}^2$; and inflection point if $r = r_i$ and $M^2 = M_i{}^2$; neither maximum nor minimum if $M^2 > M_i{}^2$.

equal to, or larger than $r_i$. This location of $r_c$ provides an important

basis for classification of the dynamic behavior. Of course, only the

region $r > r_c$ is of physical interest, wherever $r_c$ may lie relative to $r_i$.

For any relationship of $r_c$ to $r_i$, that is, for $r_c \gtrless r_i$, there can

exist a value of $M^2$, denoted by $M_k^2$, such that

$$\Phi_e(r_c, M_k^2) = \Phi_e^* (r_k, M_k^2), \tag{47}$$

i.e., when $M^2 = M_k^2$, $\Phi_e$ at the maximum equals that at the probe surface.

Use of Eqs. (26) and (46-1) gives:

$$\frac{M_k^2}{2mr_c^2} + \Phi_c = \frac{M_k^2}{2mr_k^2} + \Phi_k \quad . \tag{48}$$

This is also expressible as

$$M_k^2 = 2mr_c^2 r_k^2 \frac{\Phi_k - \Phi_c}{r_k^2 - r_c^2} \qquad r_k \neq r_c \tag{49}$$

Using Eq. (27-1) $M_k^2$ can also be expressed in the following way:

$$M_k^2 = mr_k^3 \Phi_k' \tag{50}$$

where $\Phi_k' = \Phi'(r_k)$. A relation between $r_k, \Phi_k$ and $\Phi_k'$ can be obtained

by eliminating $M_k^2$ between Eqs. (50) and (48). Useful forms of the

result are

$$\frac{r_k^3}{2r_c^2} \Phi_k' + \Phi_c = \frac{r_k}{2} \Phi_k' + \Phi_k \tag{51}$$

and

$$\Phi_k' \; \frac{r_k}{2} \; \left( \frac{r_k^2 - r_c^2}{r_k^2} \right) = \Phi_k - \Phi_c \qquad (52)$$

These equations apply to values of $r_c$ over the whole range $r_c \gtrless r_i$.

For a $\psi$-function of the type shown in Fig. 10 let

$$\psi_k = \psi(r_k), \qquad (53)$$

of course $\psi_k = M_k^2$. Thus, in Fig. 11, $\psi_k$ is some value of $\psi(r)$ that is less than $M_i^2$.

For the moment let us consider the case where $r_c < r_i$. It is clear from the concepts underlying Fig. 10 and Eq. (47), (without requiring that $\Phi_e^* = K_v M2^\nu$) that if $r_c < r_i$ the function $\Phi_e(r, M_k^2)$ will exhibit the following properties in the range $r_c \leq r \leq r_k$:

(a) A maximum at $r = r_k > r_i$ in accordance with the definition of $M_k^2$,

(b) a point of inflection at a radius between the two intersections of $M_k^2$ with $\psi(r)$,

(c) a minimum at some radius $r < r_i$ for which $\psi(r) = \psi_k = M_k^2$,

(d) a negative slope at $r = r_c$,

(e) $\Phi_e(r_k, M_k^2) = \Phi_e(r_c, M_k^2)$.

Figure 12b represents this behavior for a collector radius $r_c'$.

The case where $r_c > r_i$ is of special interest. An important aspect of it will be dealt with in the next section.
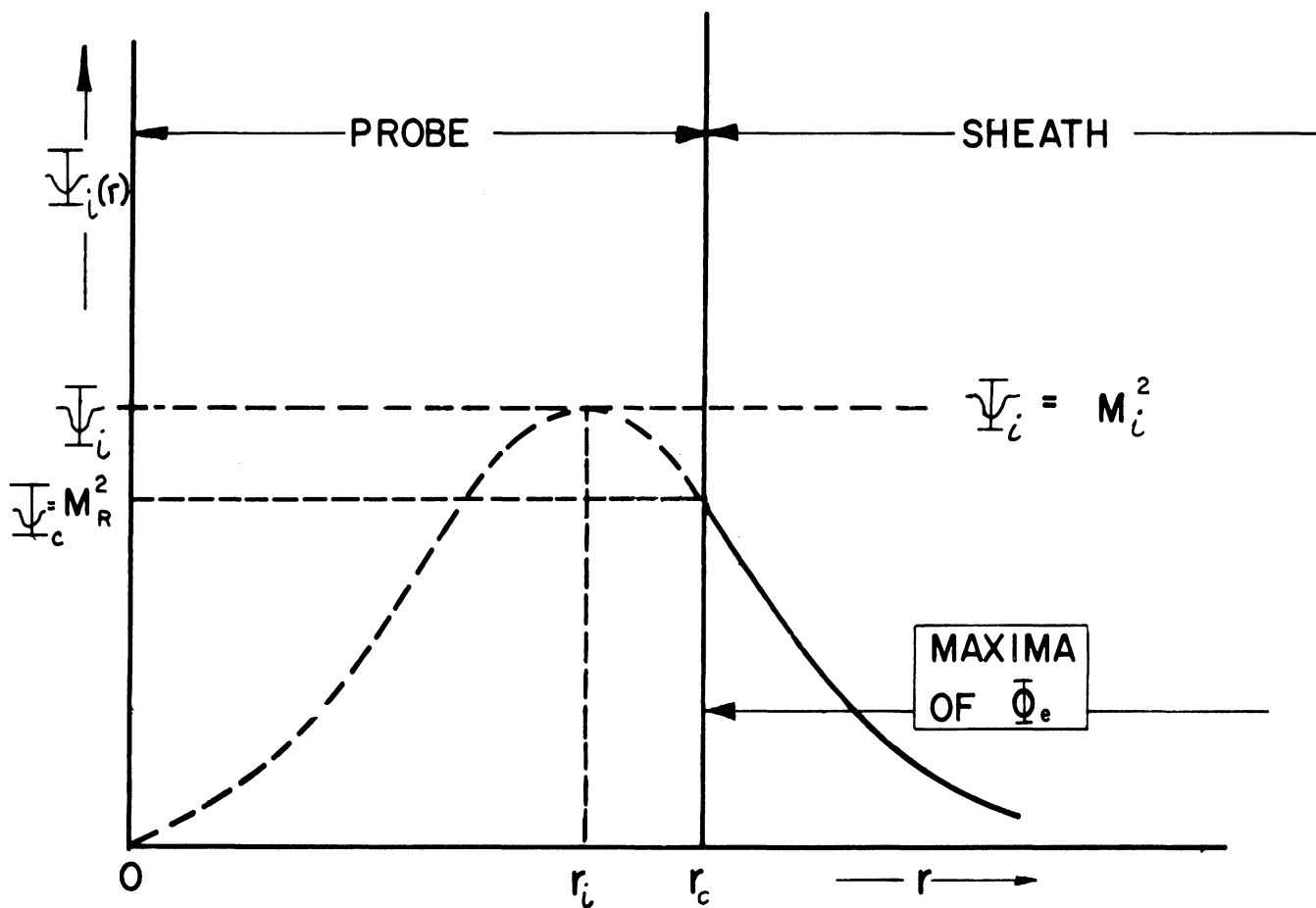
Fig. 11. Graph of a $\psi$-function for the case of a potential for which $r_i < r_c$.

Fig. 12. Graphs of $\Phi_e(r)$ showing in each of three cases the maximum $\Phi_e^*$ at $r = r^*$. Two possible sheath radii are shown, $r_c > r_i$ and $r_c' < r_i$.
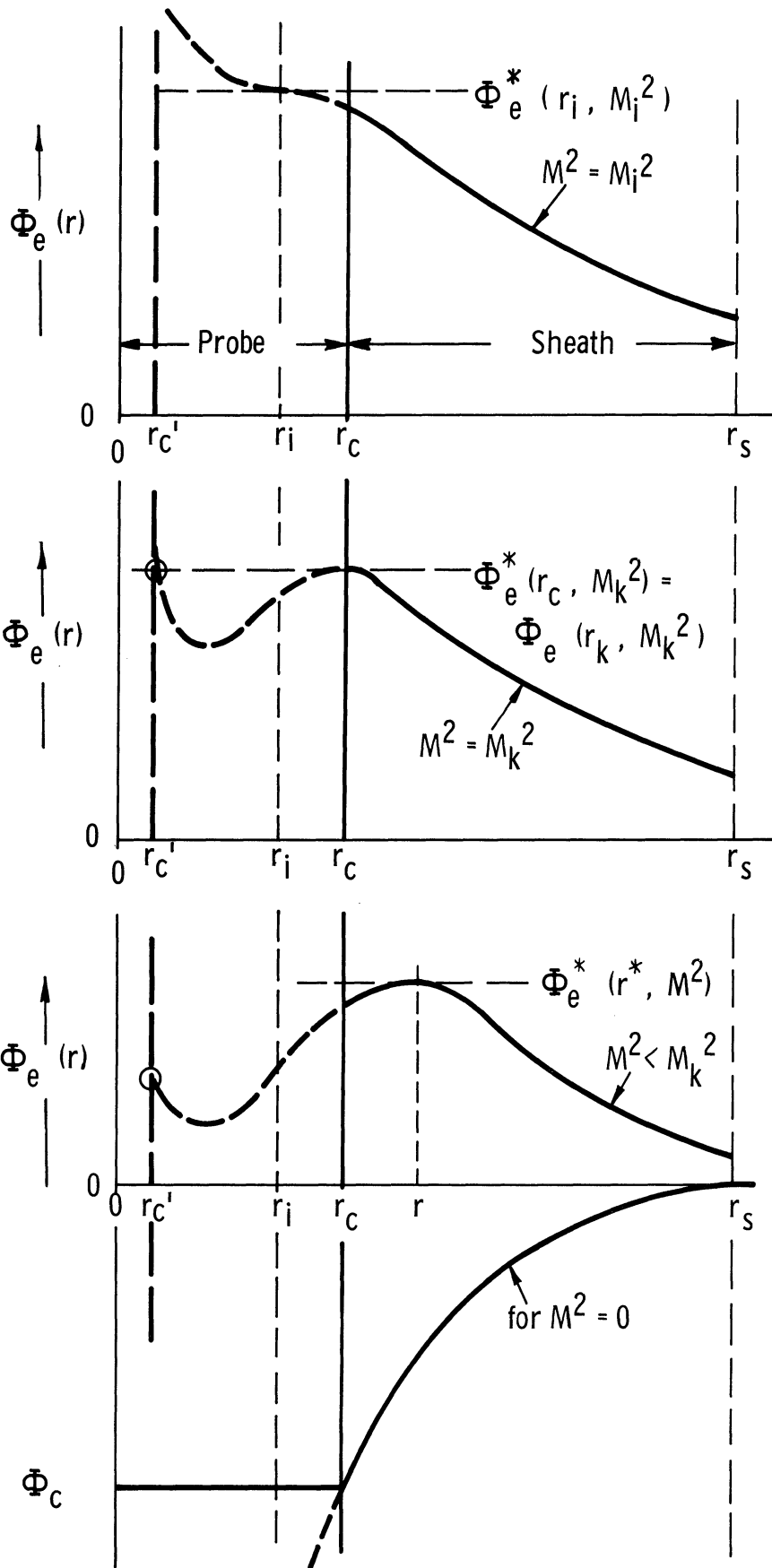
(a) For $M^2 = M_i^2$, $\Phi_e(r)$ has a zero-slope inflexion point at $r = r_i$.

(b) For $M^2 = M_k^2$, the maximum $\Phi_e^*(r_k, M_k^2)$ occurs at $r_k = r_c$.

(c) The general case, $M^2 < M_k^2$, with $\Phi_e^*$ occurring inside the sheath.

3.9 PROOF THAT FOR $r_c > r_i$ THE EFFECTIVE POTENTIAL MAXIMUM CAN EQUAL THE EFFECTIVE POTENTIAL AT THE PROBE SURFACE ONLY BY OCCURRING AT THE PROBE SURFACE: i.e., $r_k = r_c$ if $r_i < r_c$

The title of this section describes an important aspect of the behavior of $\Phi_e(r)$ for the conditions existing when $r_c > r_i$ (see Fig. 11).

It is intuitively evident that for $r_i < r_c$, $r_k$ must be equal to $r_c$. From Eq. (47) $r_k$ is the radius at which the maximum $\Phi_e*(r_k, M_k^2)$ equals the value $\Phi_e(r_k, M_k^2)$ at the probe surface. If the maximum $\Phi_e*(r_k, M_k^2)$ were to occur at a radius greater than $r_c$, then $\Phi_e(r_c, M_k^2)$ could equal $\Phi_e*(r_k, M_k^2)$ only if there were to exist a minimum of $\Phi_e(r, M_k^2)$ between $r_c$ and $r_k$. But according to the definition of $r_i$, the function $\Phi_e(r, M^2)$ has no minima in the range $r > r_i$ which includes the range $r > r_c$ since $r_c > r_i$.

Thus clearly $r_k = r_c$ if $r_c > r_i$; that is, the particular maximum $\Phi_e*(r_k, M_k^2)$ occurs at the surface of the probe, for the case $r_i < r_c$ presently under discussion. This is indicated in Fig. 11 and its significance and consequences clarified by Fig. 12. For an analytical proof that $r_k = r_c$ when $r_c > r_i$ we examine the identity

$$\Phi_e(r_k, M_k^2) - \Phi_e(r_c, M_k^2) = \int_{r_c}^{r_k} \frac{d\Phi_e}{dr} \, dr \qquad (54)$$

Let us assume that $r_c \neq r_k$. In that case $d\Phi_e/dr$ is positive in the range $r_c \leq r < r_k$ and zero at $r_k$, since $\Phi_e$ has a maximum at $r_k$ and no minimum for $r > r_c$ (since all the minima are located in the range $r < r_i$ and we consider now the case $r_c > r_i$). It follows that the integral on the right-hand side of Eq. (54) is positive definite. However, according to the definition of $r_k$ (Eq. (47)) the left-hand side of Eq. (54) vanishes. These two conclusions are contradictory. Therefore, the initial assumption that $r_c \neq r_k$ must be wrong, and we conclude that

$$r_k = r_c, \text{ if } r_i < r_c. \tag{55}$$

Consider for a moment the applicability of Eqs. (48) and (52) to Eq. (55). Obviously, $\Phi_k = \Phi_c$ when $r_k = r_c$. Therefore, both Eqs. (48) and (52) are identically satisfied when $r_k = r_c$.

### 3.10 EVALUATION OF $K_\nu$ AND $\nu$, FOR THE CLASS OF POTENTIAL FUNCTIONS DEFINED BY THE RELATION $\Phi_e^* = K_\nu M^{2\nu}$

In this section the properties of $\Phi_e(r, M_k^2)$ will be used to evaluate $K_\nu$ and $\nu$, first for arbitrary $r_i$ and then for the special case $r_i < r_c$. If $r_i$ is arbitrary, we can have $r_k \geq r_c$. By definition of $M_k^2$ in Eq. (47), the unique maximum $\Phi_e^*(r_k, M_k^2)$ has the same value as $\Phi_e(r_c, M_k^2)$. If $r_i > r_c$, then $r_k > r_c$. This is illustrated in Fig. 12b for a collector surface with radius $r_c'$.

Using Eq. (46-3), and its derivative with respect to $M^2$, both evaluated at $M^2 = M_k^2$, we can solve for $K_\nu$ and $\nu$ for arbitrary $r_i$. From Eqs. (46-3) and (47) we obtain, at $r = r_c$,

$$\Phi_e^*(r_k, M_k^2) = \Phi_e(r_c, M_k^2) = \frac{M_k^2}{2mr_c^2} + \Phi_c = K_\nu M_k^{2\nu}. \tag{56}$$

Solving this for $K_\nu$ gives

$$K_\nu = -\frac{\Phi_c + M_k^2/2mr_c^2}{M_k^{2\nu}} \tag{57}$$

In order to obtain an expression for $\nu$, we take the derivative of both sides of Eq. (46-3) with respect to $M^2$ and evaluate it at $M = M_k^2$. For the left-hand side of Eq. (46-3) we obtain

$$\frac{\partial \Phi_e^*(M^2)}{\partial (M^2)}\bigg|_{M_k^2} = \frac{\partial}{\partial (M^2)}\left(\frac{M^2}{2mr*^2} + \Phi*\right)\bigg|_{M_k^2} \qquad (58)$$

In carrying out the differentiation we must recall that r* is a function

of $M^2$, and that it becomes $r_k$ when $M^2 = M_k^2$. We then obtain

$$\frac{\partial \Phi_e^*(M^2)}{\partial (M^2)}\bigg|_{M_k^2} = -\frac{1}{2mr_k^2} - \frac{1}{mr_k^3}\left(M_k^2 - mr_k^3\Phi_k'\right)\frac{\partial r*}{\partial (M^2)}\bigg|_{M_k^2} \qquad (59)$$

In Eq. (59) we used the notation

$$\frac{\partial \Phi*}{\partial r*}\bigg|_{r_k} = -\frac{\partial \Phi}{\partial r}\bigg|_{r_k} = \Phi_k' \qquad (60)$$

Because of Eq. (50) the parenthesis in the second term on the right-hand

side of Eq. (59) vanishes, so that the slope of $\Phi_e^*(M^2)$ at $M_k^2$ is

$$\frac{\partial \Phi_e^*(M^2)}{\partial (M^2)}\bigg|_{M_k^2} = \frac{1}{2mr_k^2} \qquad (61)$$

Differentiating the right-hand side of Eq. (46-3) we obtain

$$\frac{\partial (K_\nu M^{2\nu})}{\partial (M^2)}\bigg|_{M_k^2} = \nu K_\nu M_k^{2\nu-2} \qquad (62)$$

On equating Eqs. (61) and (62) we get

$$\nu = \frac{M_k^2}{2mr_k^2 K_\nu M_k^{2\nu}} \qquad (63)$$

If Eq. (57) is substituted into Eq. (63) and $M_k^2$ is replaced by $\psi_k$, the

expression for $\nu$ becomes

$$\nu = \frac{\psi_k/2mr_k^2}{\Phi_c + \psi_k/2mr_c^2} \qquad (64)$$

which is correct for arbitrary values of $r_i$, i.e., $r_i \gtrless r_c$. It should

be pointed out that $\nu$ and $K_\nu$ are by definition independent of $M^2$. There-

fore, the evaluation of Eqs. (61) and (62) for $M^2 = M_k^2$ is merely a matter of

convenience. The expressions for $\nu$ and $K_\nu$ are valid for all values of $M$

for which $\Phi_e$ has a maximum. Equation (57) can be rewritten by setting

$M_k^2 = \psi_k$. This gives

$$K_\nu = \frac{\Phi_c + \psi_k/2mr_c^2}{\psi_k^\nu} \qquad (65)$$

where the exponent $\nu$ in the denominator is given by Eq. (64). Equations

(64) and (65) are the desired expressions for $\nu$ and $K_\nu$ for $r_i \gtrless r_c$. If

$r_i > r_c$, then the effective potential $\Phi_e(r, M_k^2)$ has both a maximum and a

minimum in the sheath region. In that case the value $\psi_k$, and thus also

the parameters $\nu$ and $K_\nu$ given by Eqs. (64) and (65), depend on the parti-

cular form of the potential function $\Phi(r)$.

If, however, $r_i < r_c$, then $r_k = r_c$, and Eq. (50) can take the form

$\psi_k = mr_c^3 \Phi_c'$. Using this in Eqs. (64) and (65) one obtains for $r_i < r_c$

$$K_\nu = \frac{2\Phi_c + r_c \Phi_c'}{2(mr_c^3 \Phi_c')^\nu} \qquad (66\text{-}1)$$

$$\nu = \frac{r_c \Phi_c'}{2\Phi_c + r_c \Phi_c'} \qquad (66\text{-}2)$$

It is clear that for the range of values $r_i < r_c$ once the potential

energy function $\Phi(r)$ is known, $K_\nu$ and $\nu$ can be found, provided $\Phi(r)$ be-

longs indeed to the class of functions defined by Eq. (46-2) in terms of the loci of the maxima of the effective potential $\Phi_e$.

3.11   THE ADMISSIBLE SPACE FOR THE CONDITION $r_i > r_c$

Next we examine the "admissible space," in the $(E, M^2)$ plane, for effective potentials satisfying the condition (46-2) and for the case $r_i > r_c$ which implies both a maximum and a minimum in $\Phi_e(r)$. (See Fig. 12   with probe radius $r_c'$.) From the definition of $M_k^2$ Eq. (47) it follows that any inward moving particle of angular momentum $M_k$ and energy $E > \Phi_e{}^*(r_k, M_k^2)$ will be able to reach the probe. For $M^2 < M_k^2$, a particle with energy $E > \Phi_e{}^*$ $(r^*, M^2)$ can reach the probe, because then $\Phi_e(r_c, M^2)$ will be lower than the maximum $\Phi_e{}^*(r^*, M^2)$. On the other hand, if $M^2 > M_k^2$, then $\Phi_e(r_c^2, M^2) > \Phi_e{}^*(r^*, M^2)$, as illustrated in Fig. 12. Therefore, in order for such a particle to be collected, it is not sufficient for its energy to be larger than the maximum $\Phi_e{}^*(r^*, M^2)$. Instead the requirement in this case is $E \geq \Phi_e(r_c^2, M^2)$. Thus, when $r_i > r_c$, the admissible space is generated by the following relations, illustrated in Fig. 13 (see Fig. 12 with collector radius at $r_c'$):

$$E \geq \Phi_e{}^* = K_\nu M^{2\nu}, \quad \text{if } 0 \leq M^2 \leq M_k^2 \tag{67-1}$$

$$E \geq \Phi_e(r_c) = \frac{M^2}{2mr_c^2} + \Phi_c, \quad \text{if } M_k^2 < M^2 < \infty \tag{67-2}$$

3.12   ABANDONMENT OF THE CONCEPT OF A WELL-DEFINED SHEATH OUTER
       BOUND IN FAVOR OF AN INFINITE SHEATH RADIUS

As discussed in the Introduction, and in Chapter III, there are
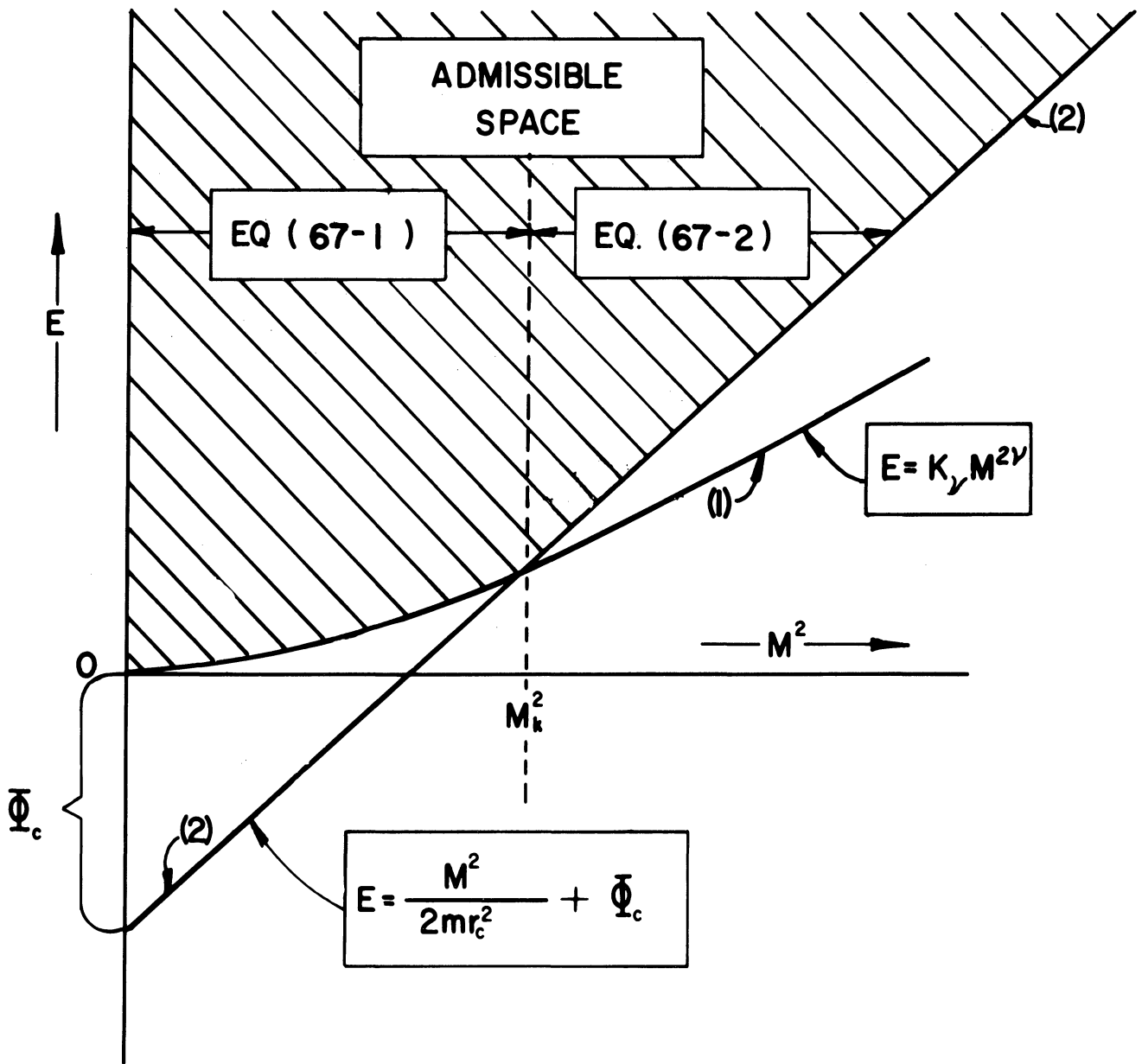
Fig. 13. Admissible space diagram from Eqs. (67-1), (67-2), for a $\psi$-function of the form illustrated in Fig. 10 with $r_i > r_c$.

serious logical inconsistencies in presuming that there is a well-defined

outer bound to the sheath. Realistically not only the potential energy

function but also all of its radial derivatives must be presumed to be

continuous through the sheath into the plasma. Such continuity demands

that the sheath potential approach the plasma potential asymptotically

with increasing radius; thus there can be no well-defined sheath radius.

There exists a range of values of the radius within which the merging

of the sheath into the plasma occurs. Any plasma will exhibit random

potential variations, and the sheath may be considered to have merged

into the plasma when the difference between the sheath potential and that

of the undisturbed plasma is small relative to the random spatial vari-

ations in plasma potential. In terms of experimental systems, this may

occur at a relatively small distance from the probe surface.

Mathematically the merging of the sheath into the plasma is pro-

vided for by letting the sheath radius become infinite $(r_s \to \infty)$ and requiring

that both the potential and the potential gradient be zero at infinite

radius. That is, $\Phi = 0$ and $\Phi' = 0$ at $r = r_s = \infty$.

Of course this makes the sheath include the region some authors have

described as the "potential well,"[6] a region that resembles the plasma in

having very nearly equal electron and ion concentrations, but resembling

the sheath in exhibiting a significant radial potential gradient and a

significant flow of charged particles of one sign or the other or both

toward the probe. The "potential well" concept represents a reasonably

good approximation to reality. It corresponds in general to the concept

of an ambipolar diffusion envelope around the probe, paralleling in some degree descriptions by Tonks[7] and others[8,9] of ambipolar diffusion in laboratory plasmas. Thus when, for purposes of orbital analysis, we extend the sheath radius to infinity, we must recognize that we are including in the sheath two types of regions having wholly different properties. Any self-consistent analysis of the sheath potential must be handled accordingly, as for example by using what has been called the "combined plasma-sheath equation."[7,8]

In the region close to the probe, particles of one or the other polarity dominate, so that space charge has a major effect on the potential distribution.

In the outer or transition region the positive ion and electron charge densities are undoubtedly very nearly, equal; particles of each polarity are themselves in thermal equilibrium, but may be at different temperatures. The potential gradient and net flux of particles to the probe are not zero. The flow of the heavy particles (ions) to the probe may either be governed by a "mobility" affected by collisions, or they might fall essentially freely without collisions.

## 3.13   ORBITAL BEHAVIOR AND ADMISSIBLE SPACE FOR AN INVERSE-POWER-LAW POTENTIAL FUNCTION

In this section the orbital behavior of particles moving in a potential of the form

$$\Phi = \Phi_c \left(\frac{r_c}{r}\right)^\alpha \tag{68-1}$$

will be discussed. Here $\alpha$ is some positive number and $\Phi_c$ is negative.

The sheath radius for such a potential is infinite, i.e., $\Phi \to 0$ and $\Phi' \to 0$

as $r \to \infty$. The gradient is

$$\Phi' = -(-\Phi_c)\alpha \, \frac{r_c^\alpha}{r^{\alpha + 1}} \qquad (68\text{-}2)$$

It is useful also to state the corresponding expression for the space-charge density, obtained by employing Eq. (68-1) in Poisson's equation. The results are:

For the infinite cylinder:

$$\rho = \epsilon_0 \left(\frac{-\Phi_c}{q}\right) \frac{\alpha^2 r_c^\alpha}{r^{\alpha + 2}} \qquad (68\text{-}3)$$

For the sphere

$$\rho = \epsilon_0 \left(\frac{-\Phi_c}{q}\right) \frac{\alpha(\alpha - 1)r_c^\alpha}{r^{\alpha + 2}} \qquad (68\text{-}4)$$

For the sphere the case $\alpha = 1$ corresponds to the space-charge-free situation; for the infinite cylinder the space-charge-free potential has a logarithmic variation and so is not included in the family of potential functions defined by Eq. (68-1). This zero-space-charge potential for an infinite cylinder has a zero gradient at infinite radius like the potentials of the form (68-1), but unlike them it becomes infinite at infinite radius.

We note the following aspects of the potential (68-1):

61

(a) The use of an arbitrarily assumed potential function cor-
responds to assuming a specific radial distribution of space-
charge density, as in this case described by Eqs. (68-3) and
(68-4). Note that for $\alpha > 2$ the space-charge density must
vary at $1/r^{\alpha+2}$.

(b) If $\alpha > 2$ in Eq. (68-1) then $\psi(r)$ of Eq. (28) is a monotonically
decreasing function of r, because $\psi(r)$ then has the form:

$$\psi(r) = m(-\Phi_c)\frac{\alpha r_c^{\alpha}}{r^{\alpha-2}} \qquad (69)$$

As discussed earlier, the locus of the extrema of the effective
potential $\Phi_e^*(r^*)$ is obtained by solving the equation $M^2 = \psi(r^*)$.
If $\psi'(r^*) > 0$ the extremum is a minimum, and if $\psi'(r^*) < 0$ it is
a maximum. Hence, the effective potentials associated with a po-
tential of the class (68-1) have only maxima if $\alpha > 2$. Conse-
quently, if $\alpha > 2$, the logic leading up to Eq. (55) applies
and requires that $r_k = r_c$; that is, the maximum of the function
$\Phi_e(r_k, M_k^2)$ must occur at the probe surface, $r = r_c$.

(c) For any non-negative value of $\alpha$ in the power-law potential (68-1)
the separability condition (46-2) is always satisfied; this will
shortly be shown for the case $\alpha > 2$.

For the moment, the treatment will be restricted to the case $\alpha > 2$. Then
$r_k = r_c$ as noted in (b) above. This situation is illustrated in Fig. 14
for $M^2 < M_k^2$, $M^2 = M_k^2$, and $M^2 > M_k^2$. We may then write Eq. (46-3) as
follows:

$$\frac{1}{2}r^*\Phi'^* + \Phi^* = K_\nu(mr^{*3}\Phi'^*)^\nu \tag{70}$$

where we have substituted $mr^{*3}\Phi'$ for $M^2$ from Eq. (27-1). Now, Eqs. (68-1) and (68-2) become at the maximum $\Phi_e^*$

$$\Phi'^* = (-\Phi_c)\frac{\alpha r_c^\alpha}{r^{*(\alpha + 1)}} \tag{71-1}$$

$$\Phi^* = -(-\Phi_c)\left(\frac{r_c}{r^*}\right)^\alpha \tag{71-2}$$

Introducing these into Eq. (70) yields the following equation

$$(-\Phi_c)\ r_c^\alpha(\frac{\alpha}{2} - 1) = \left[m\alpha(-\Phi_c)r_c^\alpha\right]K_\nu r^{*(2 - \alpha)\nu + \alpha} \tag{72}$$

As $r^*$ is a function of $M^2$, while none of the other quantities depends on $M^2$, this equation is satisfied only when the exponent of $r^*$ is zero. Therefore we find that

$$\nu = \frac{\alpha}{\alpha - 2} \tag{73}$$

According to Eq. (46-3) this value of $\nu$, together with the corresponding value of $K_\nu$ given below, determines the maximum $\Phi_e^*$ and its locus $r^*$, provided that the potential $\Phi(r)$ is of the form (68-1). These maxima have meaning only if $r^* \geq r_c$. Direct evaluation of $\nu$ from Eq. (66-2), confirms the value for $\nu$ given by Eq. (73).

The value of $K_\nu$ corresponding to the $\nu$ of Eq. (73) is,

$$K_\nu = \frac{(-\Phi_c)(\alpha - 2)}{2\left[\alpha mr_c^2(-\Phi_c)\right]^{\alpha/(\alpha-2)}}$$
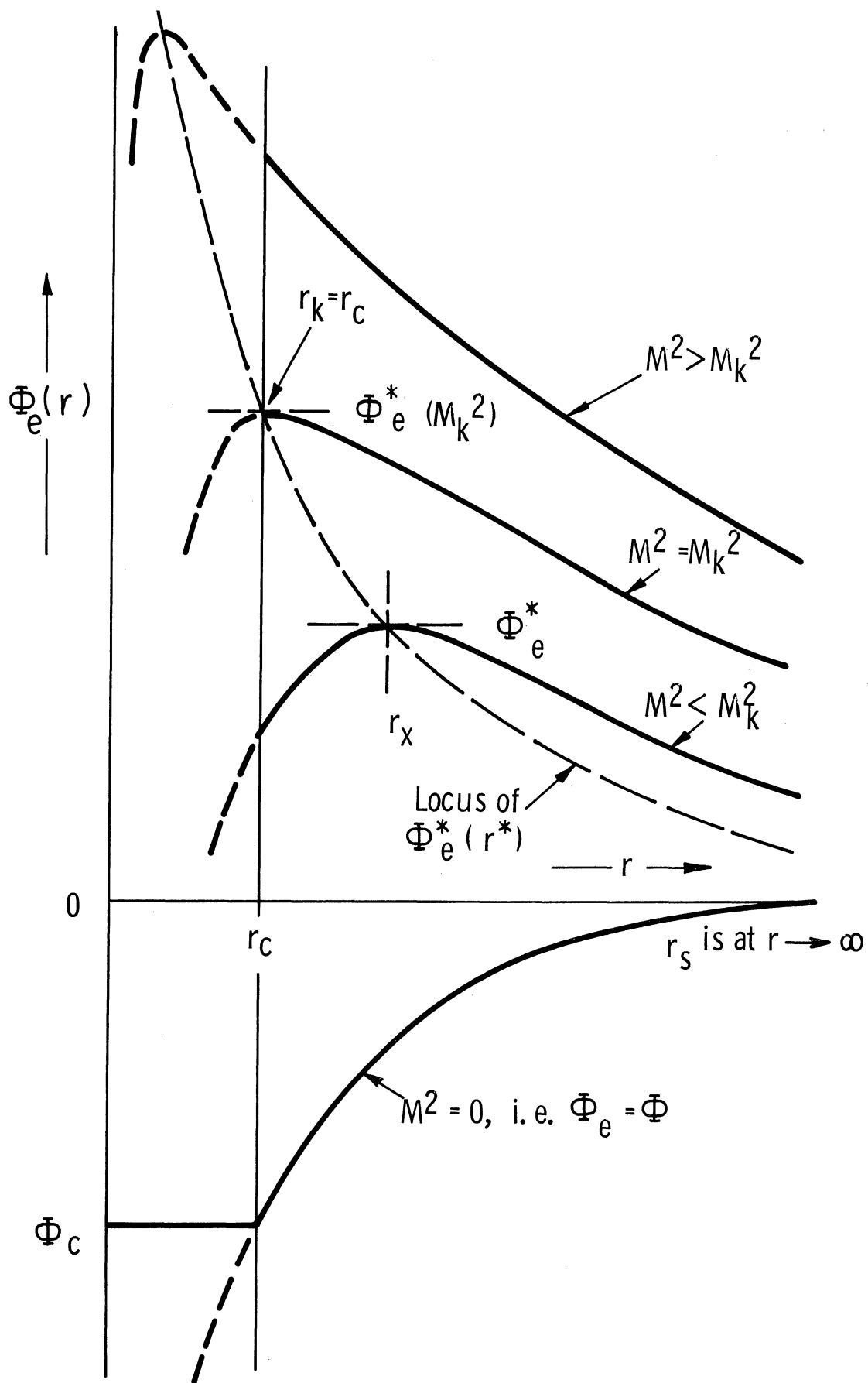
Fig. 14. Graph of the effective potentials, $\Phi_e(r)$ for an inverse-power-law potential function $\Phi = \Phi_c(r_c/r)^\alpha$ with $\alpha > 2$; also shown is the locus $\Phi_e^*(r^*)$.

For convenience Eq. (73) and an alternative form of Eq. (74) will be repeated in Eq. (75). These expressions evidently apply to the case $\alpha > 2$, and to some extent more broadly as discussed in a later section; they are valid for any $M^2$:

$$\nu \;=\; \frac{\alpha}{\alpha - 2} \tag{75-1}$$

$$K_\nu \;=-\; \frac{\alpha - 2}{2(-\Phi_c)^{2/(\alpha-2)}(m\alpha r_c^2)^{\alpha/(\alpha-2)}} \tag{75-2}$$

This last equation is precisely of the form that is directly obtainable from Eq. (66-1). Since Eq. (66-1) applies to the case of a monotonically decreasing $\psi(r)$, it is therefore valid in the range $\alpha > 2$ (see Eq. (69)).

The fact that Eqs. (75-1) and (75-2) are independent of $M^2$ shows that the separability condition (46-2) is satisfied in the case of the inverse-power-law potential (68-1) with $\alpha > 2$, as has been claimed above.

Substituting Eq. (71-1) into Eq. (27-1) with $r = r^* = r_k = r_c$ we obtain the following expression for $M_k 2$:

$$M_k^2 \;=\; \alpha m r_c^2 (-\Phi_c). \tag{76}$$

This expression is valid for potentials of the form (68-1) with $\alpha > 2$. It defines the angular momentum $M_k$ for which the corresponding effective potential $\Phi_e$ has its maximum at the probe radius.

Figure 14 illustrates the locus, $\Phi_e^*(r^*)$, of the maxima for the potential function $\Phi$ given by Eq. (68-1). The equation for the locus curve for the given model is obtained from Eq. (46-2) by using Eq. (27-1)

for $M^2$, with $\Phi'$ as in Eq. (68-2), and with Eqs. (75-1) and (75-2) used for $\nu$ and $K_\nu$. The locus equation so obtained is

$$\Phi_e{}^*(r^*) = -(-\Phi_c)\frac{\alpha-2}{2}\left(\frac{r_c}{r^*}\right)^\alpha \qquad (77)$$

The value of $r^*/r_c$ as a function of $M^2$ for any locus is obtained by eliminating $\Phi'^*$ between Eqs. (27-1) and (68-2), evaluated at $r^*$, and using Eq. (76). The result is

$$\frac{r^*}{r_c} = \left(\frac{M^2}{M_k{}^2}\right)^{1/(2-\alpha)} \qquad (78)$$

Combination of the last two equations give: $\Phi_e{}^*(r^*)$ as a function of $M^2$; thus

$$\Phi_e{}^*(M^2) = (-\Phi_c)\frac{\alpha-2}{2}\left(\frac{M^2}{M_k{}^2}\right)^{\alpha/(\alpha-2)} \qquad (79)$$

when Eq. (68-1) applies, and $\alpha > 2$.

Equation (78) can be rewritten in terms of the function $\psi(r)$ since at the maximum of $\Phi_e$ by definition $M^2 = \psi(r^*)$. Hence, one obtains,

$$\psi(r^*) = \psi_k\frac{1}{(r^*/r_c)^{\alpha-2}} \qquad (80)$$

This is illustrated by Fig. 15.

Figure 13, with $M_k{}^2$ given by Eq. (76), represents the admissible space for the dynamical system based on the inverse power law (68-1) with $\alpha > 2$, because this system satisfies Eq. (46-2), and Fig. 13 is adequate for any system that does so.
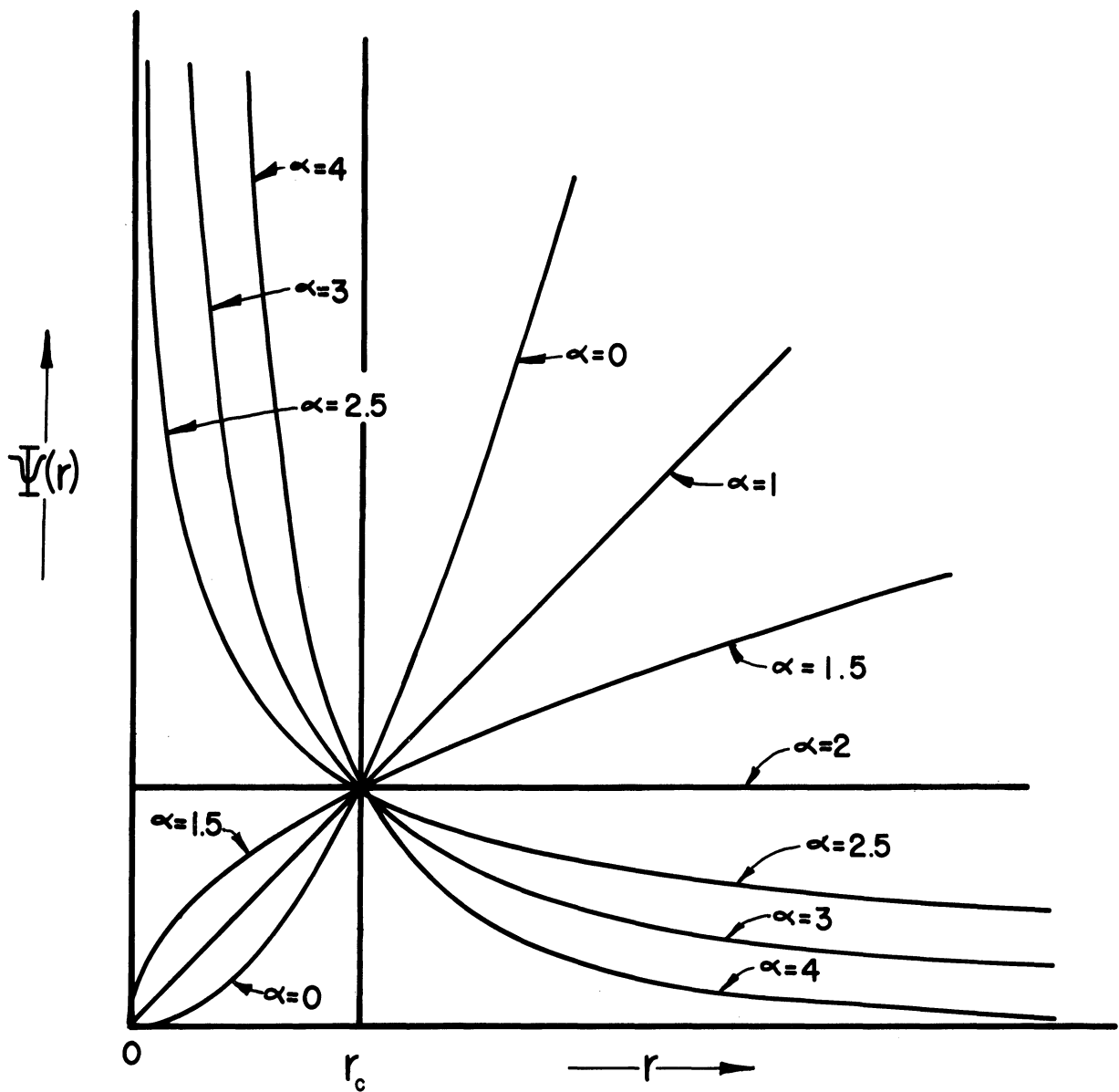
Fig. 15. Graphs of $\psi(r)$ for various values of $\alpha$ in the power-law-potential Eq. (68-1).

3.14 DISCUSSION OF POTENTIAL FUNCTIONS DIFFERENT FROM ANY INVERSE
POWER LAW, BUT WITH SEPARABLE LOCUS-OF-MAXIMA EQUATIONS

Illustrative potential functions different from Eq. (68-1) might

be postulated that would satisfy Eq. (46-2) or some equally useful separa-

bility condition, and at the same time have one or more of the following

properties not possessed by Eq. (68-1). Thus such functions might con-

ceivably

(a) be of forms giving the curve of $\psi(r)$ both increasing and de-

creasing portions as illustrated in Fig. 10, thus permitting

minima as well as maxima of $\Phi_e$, with the locus of the maxima

obeying Eq. (46-2) or some equally separable function.

(b) be of forms that permit the model to have a finite sheath

radius, with both $\Phi(r_s) = 0$ and $\Phi'(r_s) = 0$.

The model outlined in (b) has the weakness that it permits the

second, third, and higher derivatives of $\Phi$ to be discontinuous at the

sheath edge. It is intuitively reasonable to expect the true model to

exhibit continuity in all derivatives of the potential at all values of r.

One of the merits of Eq. (68-1) is that, by abandoning the concept of a

finite sheath radius, it does retain continuity of all derivatives of $\Phi$

for all values of the radius.

However, it is certain that the actual potential variation is much

more complex than Eq. (68-1), and that the loci of the maxima of the

effective potential do not obey Eq. (46-2), nor any similarly separable

function. Nature is not that kind to us. Yet one learns a great deal by

studying the model (68-1) for $\alpha > 2$, which satisfies the separability

property (46-2) and pushes $r_s$ out to infinity.

Undoubtedly one useful potential model would be the sum of two potentials, one corresponding to the space-charge-free potential variation, the other describing the potential due to the existing space-charge density, whatever it may be. For spherical geometry this would employ $\alpha = 1$ in Eq. (68-1) to describe the space-charge-free behavior with some other function describing the effect of the space charge. This second term would be of opposite sign to the first, because the charge causing it would be of opposite sign to that on the surface of the probe. For the cylindrical geometry, the space-charge-free term would have the form $\Phi = \Phi_c (\ln r/r_c + 1)$, which is obviously not of the form (68-1).

## 3.15  ADMISSIBLE SPACES FOR ARBITRARY POSITIVE VALUES OF THE EXPONENT IN THE INVERSE-POWER-LAW POTENTIAL (68-1)

It is desirable to discuss the properties of a model that uses the potential function (68-1) with arbitrary positive $\alpha$. Negative values of $\alpha$ are excluded because the purpose of introducing the potential function $\Phi = \Phi_e(r_c/r)^\alpha$ was to set up a model having an infinite sheath radius, i.e., to provide an asymptotic approach to $\Phi = 0$ as $r \to \infty$.

If we plot $v$ vs. $\alpha$ from Eq. (75-1) as is done in Fig. 16, we get a singularity at $\alpha = 2$, and we find that $v \to 1$ as $\alpha \to \infty$. Only non-negative values of $v$ are of interest because $\Phi_e{}^*$ in Eqs. (46-2) and (46-3) is identified with the <u>maxima</u> of $\Phi_e(r)$. In any realistic model the maximum value of the effective potential must of necessity be an increasing function of the angular momentum. This is a direct consequence of the definition of the effective potential Eq. (26). We note that for an arbitrary potential $\Phi(r)$ the effective potential $\Phi_e(r)$ increases with
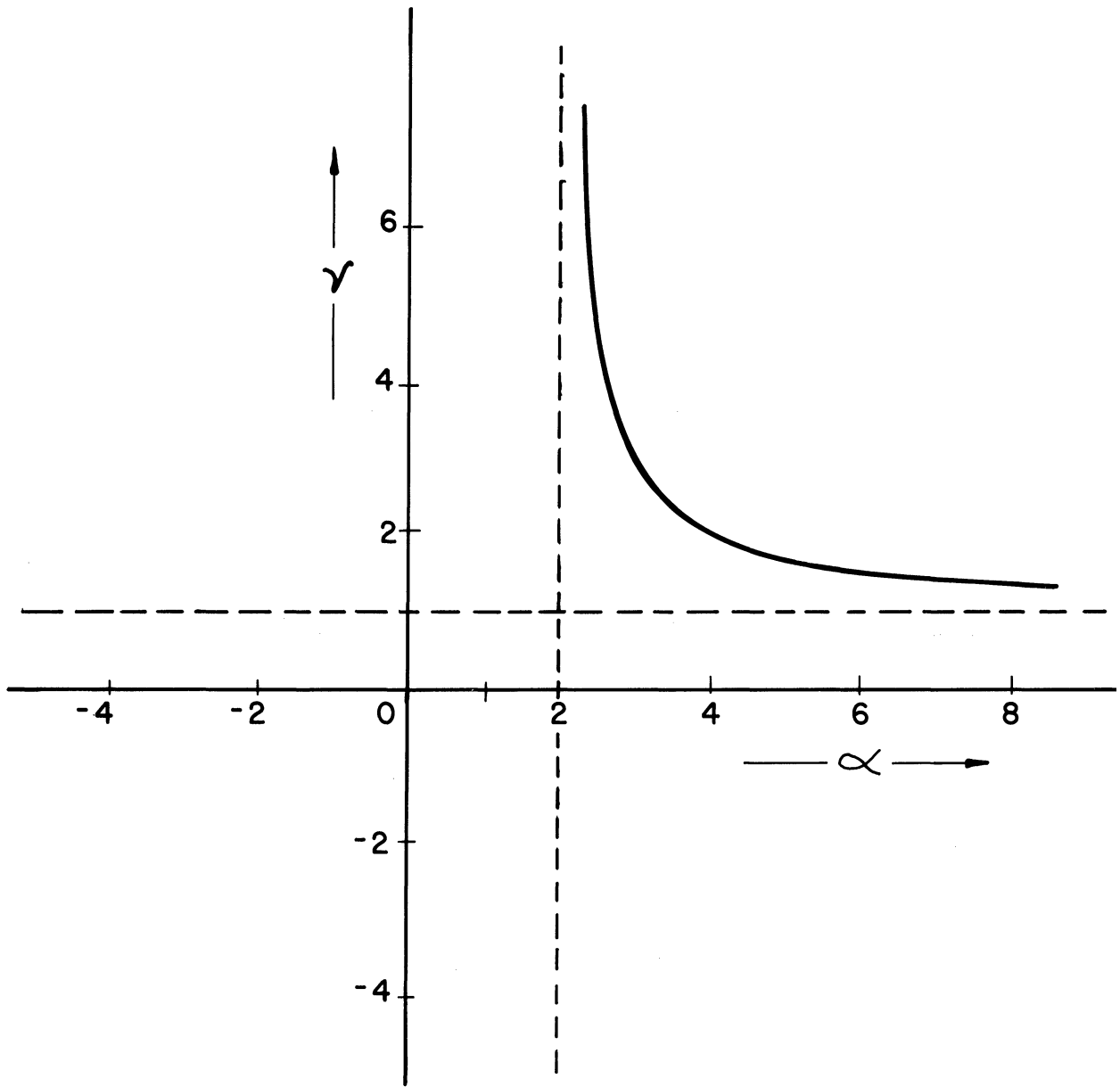
Fig. 16. Graph of $\nu$ versus $\alpha$ as given by Eq. (75-1) in the case of the power-law-potential given by Eq. (68-1).

$M^2$ for fixed values of $r$. Therefore the $\Phi_e(r)$ curves for different values

of the parameter $M^2$ (e.g., Fig. 4) cannot cross one another, and it follows

that the maximum value $\Phi_e{}^*(r_1{}^*, M_1{}^2)$ must exceed the maximum value $\Phi_e{}^*(r_2{}^*, M_2{}^2)$

if $M_1{}^2 > M_2{}^2$, i.e., $\Phi_e{}^*(r^*, M^2)$ is an increasing function of $M^2$, and therefore

negative values of $\nu$ have to be ruled out.

According to Eq. (73) $\alpha$ must be larger than 2 to assure positive values

of $\nu$. From Eq. (69), furthermore it can be seen that $\psi$ is a monotonically

increasing function of $r$ if $\alpha < 2$, and, as has been explained earlier, in

that case the effective potential $\Phi_e$ has no maxima, but only minima. Since

the parameters $\nu$ and $K_\nu$ have been defined in connection with the maxima of

$\Phi_e$, it follows that the separability property (46-2) is satisfied by in-

verse power potentials of the form (68-1) only if $\alpha > 2$.

Attention is next given to the special case $\alpha = 2$. In that case

$\nu$ is not defined by Eq. (73). In fact, the effective potential becomes

then

$$\Phi_e(r) \quad = \left( \frac{M^2}{2m} + \Phi_c r_c^2 \right) / r^2 \tag{81}$$

which has no extrema. Since this treatment is concerned with attractive

potentials (i.e., $\Phi_c < 0$), the effective potential vanishes for all values

of $r$ if

$$M^2 \quad = \quad -2mr_c{}^2\Phi_c. \tag{82}$$

This value of $M^2$ is easily seen to be the value of $M_k{}^2$ for $\alpha = 2$ (see

Eq. (76)). Figure 17 shows a set of curves of $\Phi_e(r)$ with $\alpha = 2$. It

should also be noted that the corresponding $\psi$-function is a constant, i.e.,

71
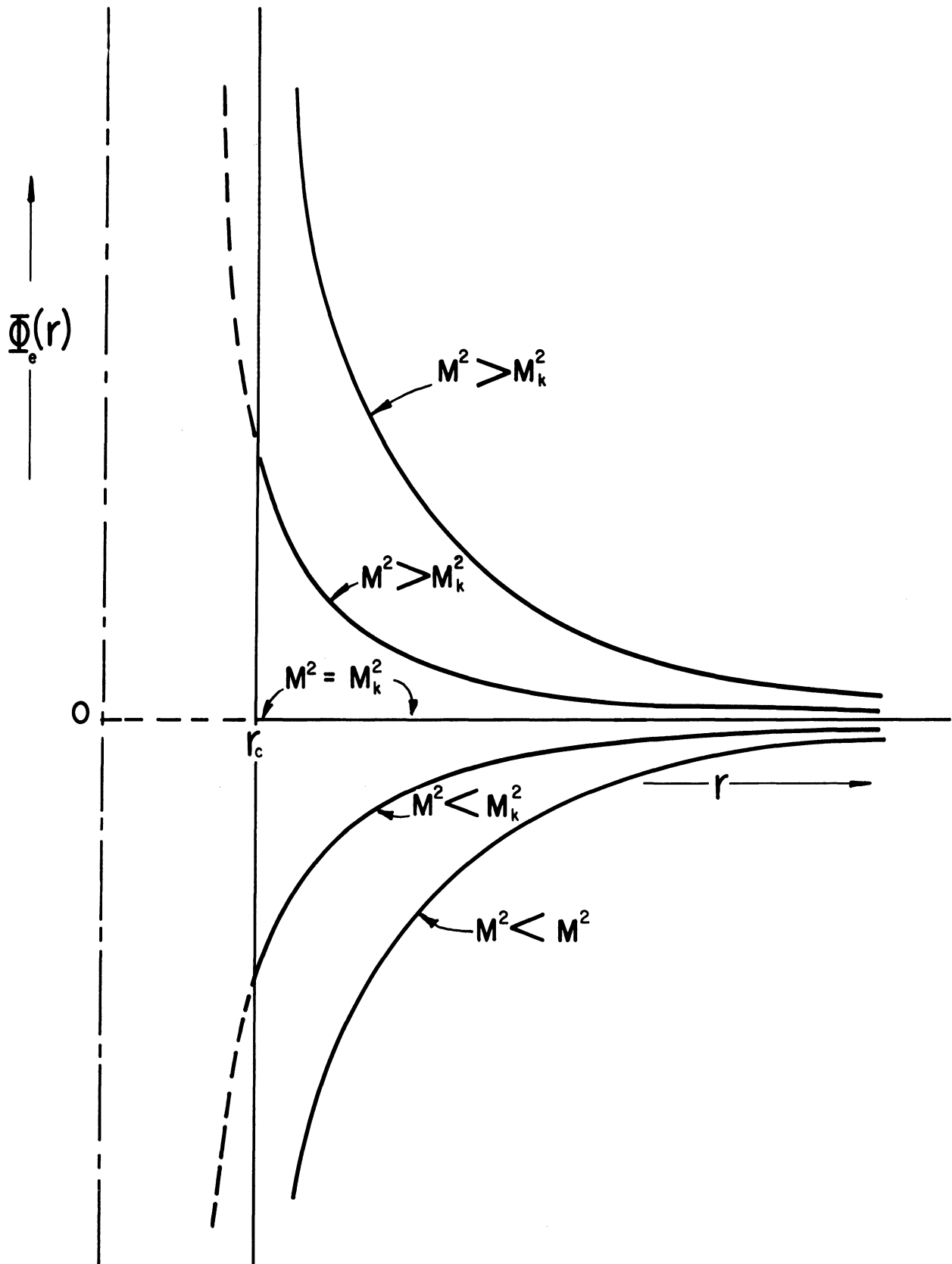
Fig. 17. Graphical representation of $\Phi_e$ when $\alpha = 2$ in the potential (68-1). These second-degree hyperbolas represent Eq. (81).

$$\psi = -2mr_c^2 \Phi_c . \tag{83}$$

Hence, there exists only one unique value of $M^2$ for which $M^2 = \psi$, the value given by Eqs. (82) and (83). Obviously this does not represent an extremum of the effective potential. The first derivative of $\Phi_e$ vanishes for this particular value of $M^2$ for all values of r simply because $\Phi_e$ itself is constant.

It has been discussed in Section 3.4 that any potential with a non-decreasing $\psi$-function satisfies the conditions for applicability of Langmuir's equations. This also includes the case of constant $\psi$. In particular it has been shown that the inverse square potential is the orbital-motion-limited case for the set of potentials having constant $\psi$ functions. Therefore, the admissible space for potentials of the form (68-1) with $\alpha = 2$ is given by Eqs. (45-1) and (45-2).

Considering next the case $0 < \alpha < 2$ we note that the $\psi$-function is now monotonically increasing as illustrated in Fig. 15. The effective potentials corresponding to this range of $\alpha$ have minima, as shown in Fig. 8. This leads again to the admissible space described by Eqs. (45-1) and (45-2). As has been explained in Section 2.4, the range $\alpha < 1$ is physically meaningless in the case of a spherical probe. We conclude therefore that potentials of the form (68-1) give rise to the orbital-motion-limited current-voltage characteristics derived by Langmuir, if $0 < \alpha \le 2$ in the case of a cylindrical probe or $1 \le \alpha \le 2$ in the case of a spherical probe.

For very large values of $\alpha$ the sheath thickness becomes small and the collection is no longer determined by the orbital motions. In the

limit $\alpha \to \infty$, the potential $\Phi(r)$ vanishes for all values $r > r_c$ and equals $\Phi_c$ at the collector surface, $r = r_c$. Hence, the potential gradient is zero for $r > r_c$ and becomes infinite at $r = r_c$. The collected current should approach the random current in the limit $\alpha \to \infty$. In order to verify this statement, we note first that the maximum $\Phi_e$ can be expressed by substituting Eq. (76) into Eq. (79) to obtain

$$\Phi_e^*(M^2) = (-\Phi_c) \frac{\alpha - 2}{2} \left[ \frac{M^2}{\alpha m r_c^2 (-\Phi_c)} \right]^{\alpha/(\alpha-2)} \tag{79-1}$$

It is easy to show that

$$\lim_{\alpha \to \infty} \Phi_e^*(M^2) = \frac{M^2}{2mr_c^2}, \quad \text{for } 0 \le M^2 < \infty. \tag{79-2}$$

From Eq. (78) it follows furthermore that

$$\lim_{\alpha \to \infty} r^* = r_c$$

Hence, since $\Phi_e$ has its maximum value at the collector surface, the requirement for collection is that $E \ge \Phi_e(r_c)$ for all values of $M^2$, which means in view of Eq. (79-2),

$$E \ge \frac{M^2}{2mr_c^2} \quad \text{for } 0 \le M^2 < \infty.$$

The admissible space defined by this expression is illustrated in Fig. 18. By integation of Eq. (97) below it can be easily verified that this admissible space leads to the random current as has been claimed above.
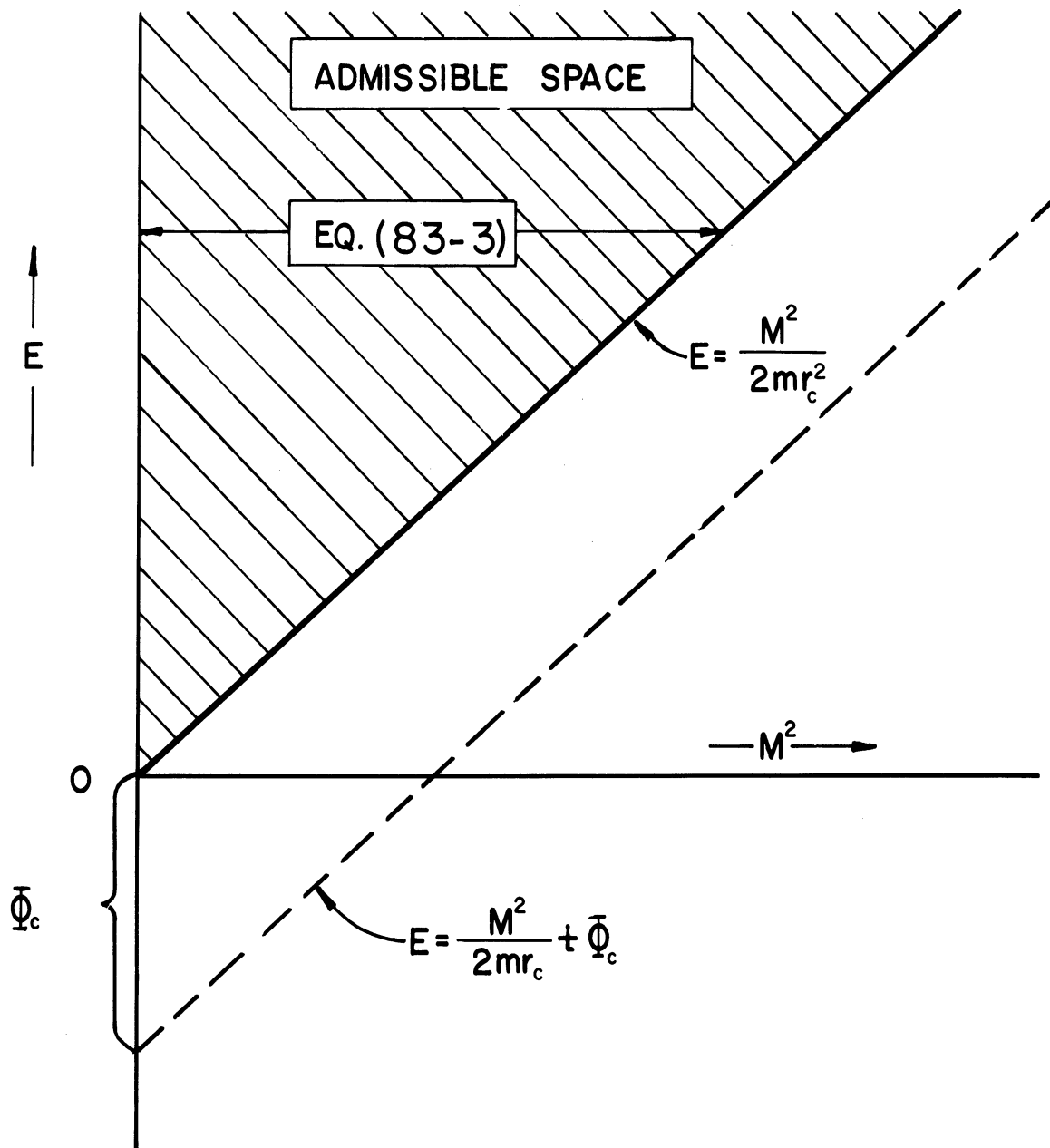
Fig. 18. Admissible space diagram, from Eq. (83-3), for the infinitely thin sheath around an electron accelerating probe described by letting $\alpha \to \infty$ in the potential function (68-1).

# IV. THE VOLT-AMPERE EQUATIONS

## 4.1 GENERAL EXPRESSIONS FOR THE CURRENT

In this final chapter the expressions for the current collected by an accelerating probe will be set up in general form and then integrated between the limits of integration described by appropriate admissible spaces.

Let $f(\bar{u})$ be the velocity distribution of the particles, and $\bar{u}$ the velocity vector of a particle at any instant. The flux density $J_r$ of electric current carried toward the probe by the particles crossing a particular closed surface at which the velocity distribution is known is given by:

$$J_r = q\int d\bar{u}\ \bar{u}\ .\ \hat{n}\ f(\bar{u}) \tag{84}$$

where $q$ is the electric charge carried by each particle and $n$ is the inward-pointing normal unit vector. The integration is to be carried out only over inward-bound particles and, among them, only those destined to arrive at the probe. Thus "admissible space" criteria govern the integration limits. $\bar{u}\ .\ \hat{n}$ is taken positive when pointing in the direction of the center of the force field. The closed surface chosen for this integration can be the outer radius $r_s$ of the sheath, or it might be a "sheath edge" surface as introduced earlier in Section 2.1. Because the inward orbital motion involves loss of radial energy to angular energy, the orbital behavior in the accelerating field causes marked departures of directions of motion from an initial random distribution. Therefore, the closed surface at which the integration is to take place should be far enough so that this effect of the probe

on the velocity distribution is as yet insignificant.

If the known initial velocity distribution is the Maxwell-Boltzmann distribution function, then for a cylindrical probe Eq. (84) may be written as:

$$J_r = \frac{N_o q}{(\pi c^2)^{3/2}} \int \int \int du_z \, du_t \, du_r \, u_r \exp\left[ - \frac{u_z^2 + u_t^2 + u_r^2 + (2\Phi/m)}{c^2} \right]$$

(85)

where, as earlier in this paper, $u_z$, $u_t$, $u_r$ are the velocity components in the axial, tangential, and radial directions, respectively, $c = \sqrt{2kT/m}$ the most probable velocity, k is Boltzmann's constant, T the temperature, and $\Phi(r)$ the potential energy of the particle at the radial distance r.

For a cylinder of infinite length, which is the model used here, the admissible values of $u_z$, are from $-\infty$ to $+\infty$, and $u_z$ is independent of $u_r$ and $u_t$. Therefore Eq. (85) may immediately be integrated with respect to $u_z$ and rewritten for the cylinder as

$$J_r = \frac{N_o q}{\pi c^2} \int \int du_t \, du_r u_r \exp\left[ -\frac{1}{c^2} \left( u_r^2 + u_t^2 + \frac{2}{m}\Phi \right) \right]$$

(86)

For a spherical probe we define $u_r$, $u_\theta$, $u_\phi$ to be the components of $\overline{u}$ along the radial, polar, and azimuthal directions, respectively. Since the motion of a particle in a centrally symmetric field is planar, the components $u_\theta$ and $u_\phi$ may be reduced to one tangential component $u_t$ by introducing polar coordinates as follows:

$$u_\theta = u_t \cos \gamma$$

(87-1)

77

$$u_\phi = u_t \sin \gamma \qquad (87\text{-}2)$$

where $\gamma$ is the angle between the plane of motion and the plane containing $u_\theta$ and the polar axis. With this change of variables Eq. (84) may be written for the sphere as

$$J_r = \frac{N_0 q}{(\pi c^2)^{3/2}} \int \int \int du_t \, du_r \, d\gamma \, u_r \, u_t \, \exp\left[-\frac{1}{c^2}\left(u_r^2 + u_t^2 + \frac{2\Phi}{m}\right)\right] \qquad (88)$$

where, once again, the integration is to be carried out over the inward-bound particles and with limits established by admissible space criteria. Since all planes of motion are equivalent we integrate Eq. (88) with respect to $\gamma$ from 0 to $2\pi$ and write for the sphere

$$J_r = \frac{2N_0 q}{\pi^{1/2} c^3} \int_{u_r u_t} \int du_t \, u_t \, du_r \, u_r \, \exp\left[-\frac{1}{c^2}\left(u_t^2 + u_r^2 + \frac{2}{m}\Phi\right)\right] \qquad (89)$$

We may now transform the variables of integration of both Eq. (86) and Eq. (89) from the velocity space $(u_r, u_t)$ to $(M,E)$ space, as follows:

$$E = \frac{1}{2} m(u_t^2 + u_r^2) + \Phi \qquad (90\text{-}1)$$

$$M = mru_t. \qquad (90\text{-}2)$$

The second of these equations can be used to eliminate $u_t^2$ from the first resulting in explicit equations for the velocities in terms of M and E,

$$u_r^2 = -\frac{M^2}{m^2 r} + \frac{2}{m}(E - \Phi), \qquad (91\text{-}1)$$

$$u_t = \frac{M}{mr}. \qquad (91\text{-}2)$$

The transformation of the $(du_t \, du_r)$ area element in $(u_r, u_t)$ space to the

(dE dM) area element in (M, E) space takes the form

$$du_r \, du_t = \frac{\partial(u_r, u_t)}{\partial(E, M)} \, dE \, dM. \tag{92}$$

By the use of Eqs. (91-1) and (91-2) the Jacobian[10] is found to be

$$\frac{\partial(u_r, u_t)}{\partial(E, M)} = \frac{1}{m^2 r u_r} \tag{93}$$

Therefore,

$$du_r \, du_t = \frac{1}{m^2 r u_r} \, dE \, dM \tag{94}$$

The variable r in Eqs. (90), (91), (93), and (94) is of course the radius of the surface at which the velocity distribution is known. But the current density is that at the probe surface, denoted by $J_c$. The two current densities are related by the equations

$$J_c = J_r \frac{r}{r_c} \qquad \text{(cylindrical geometry)} \tag{95-1}$$

$$J_c = J_r \frac{r^2}{r_c^2} \qquad \text{(spherical geometry)} \tag{95-2}$$

Applying the transformation (91-1), (91-2) to the integrals in Eqs. (86) and (89) and using the relations (95-1) and (95-2), one obtains the following expressions for the current densities at the probe surface.

For cylindrical geometry:

$$J_c = \frac{N_o q}{\pi c^2 m^2 r_c} \int_M \int_E dE dM \, \exp(-\frac{E}{kT}). \tag{96-1}$$

For spherical geometry:

$$J_c = \left( \frac{2N_0 q}{\pi^{1/2} c^3 m^3 r_c^2} \right) \int_M \int_E dE \, dM \, M \exp\left( -\frac{E}{kT} \right). \qquad (96\text{-}2)$$

The last two equations may jointly be written in the form

$$J_c = J_0 \, h_\delta \int_M \int_E dE \, dM \, M^\delta \exp\left( -\frac{E}{kT} \right) \qquad (97)$$

where $\delta = 0$ for the cylinder, $\delta = 1$ for the sphere, and

$$J_0 = N_0 q \sqrt{\frac{kT}{2m\pi}}, \qquad (98)$$

$$h_\delta = \frac{2^\delta}{kT(2mr_c^2 kT)^{(\delta+1)/2} \Gamma (\delta+1)/2} \qquad (99)$$

For $\delta = 0$ and $\delta = 1$, respectively, $h_\delta$ reduces to:

$$h_0 = \frac{1}{(kT)^{3/2} \sqrt{2\pi m r_c^2}} \qquad \text{(cylindrical geometry)} \qquad (100\text{-}1)$$

$$h_1 = \frac{1}{m r_c^2 (kT)^2} \qquad \text{(spherical geometry)} \qquad (100\text{-}2)$$

## 4.2 INTEGRATION OF THE GENERAL EXPRESSION FOR THE CURRENT

The limits of integration are determined by the assumed potential model. Various potential models have been discussed in earlier sections. For example, the admissible space defined by Eqs. (67-1) and (67-2) applies to effective potentials which have the property (46-2). This property is quite general and includes the case of effective potentials which have both a minimum and a maximum, as has been discussed in Section 3.11.

In Eq. (97), we may set $M^2 = x$, and write

$$J_c = J_o \frac{h\delta}{2^\delta} \left[ \int_{x=0}^{x=M_k^2} \int_{E=K_\nu x^\nu}^{E=\infty} dE\ dx\ x^{(\delta-1)/2} \exp(-E/kT) \right.$$

$$\left. + \int_{x=M_k^2}^{x=\infty} \int_{E=\frac{x}{2mr_c^2}+\Phi_c}^{E=\infty} dE\ dx\ x^{(\delta-1)/2} \exp(-E/kT) \right] \tag{101}$$

The integration with respect to E is straightforward, leading to

$$J_c = J_o \frac{h\delta kT}{2^\delta} \left[ \int_{x=0}^{x=M_k^2} dx\ x^{(\delta-1)/2} \exp\left(-\frac{K_\nu x^\nu}{kT}\right) \right.$$

$$\left. + \exp\left(-\frac{\Phi_c}{kT}\right) \int_{M_k^2}^{\infty} dx\ x^{(\delta-1)/2} \exp\left(-\frac{x}{2mr_c^2 kT}\right) \right] \tag{102}$$

This can be rearranged to yield the following expression:

$$J_c = J_o \frac{h\delta kT}{2^\delta} \left[ \left(\frac{kT}{K_\nu}\right)^{(\delta+1)/2\nu} \int_{y=0}^{y=M_k^2(K_\nu/kT)^{1/2}} dy\ y^{(\delta-1)/2} \exp(-y^\nu) \right.$$

$$\left. + \exp\left(-\frac{\Phi_c}{kT}\right) (2mr_c^2 kT)^{\frac{\delta+1}{2}} \int_{y=M_k^2/2mr_c^2 kT}^{y=\infty} dy\ y^{(\delta-1)/2} \exp(-y) \right] \tag{103-1}$$

where the variables of integration have been changed by using

$y = (K_\nu/kT)^{1/\nu} x$ in the first integral, and $y = x/2mr_c^2 kT$ in the second

integral. Now let $y^\nu = z$ in the first integral, to convert the expression into the following:

$$J_c = J_o \frac{h\delta kT}{2^\delta} \left[ \left(\frac{kT}{K_\nu}\right)^{(\delta+1)/2\nu} \nu^{-1} \int_{z=0}^{z=K_\nu M_k^{2\nu}/kT} dz\ z^{(\delta+1)/2\nu} \exp(-z) \right.$$

$$+ \exp\left(-\frac{\Phi_c}{kT}\right)(2mr_c^2kT)^{(\delta+1)/2}\int_{y=M_k^2/2mr_c^2kT}^{y=\infty} dy \; y^{-1+(\delta+1)/2} \exp(-y)\Bigg]$$

<div align="right">(103-2)</div>

This may be expressed as

$$J_c = \frac{J_o}{\Gamma\left(\frac{\delta+1}{2}\right)}\left[\left(\frac{kT}{K_\nu}\right)^{(\delta+1)/2}(2mr_c^2kT)^{-(\delta+1)/2}\nu^{-1}\gamma\left(\frac{\delta+1}{2\nu}, \frac{K_\nu M_k^{2\nu}}{kT}\right)\right.$$
$$\left. + \exp\left(-\frac{\Phi_c}{kT}\right)\Gamma\left(\frac{\delta+1}{2}, \frac{M_k^2}{2mr_c^2kT}\right)\right]$$

<div align="right">(104)</div>

where the incomplete gamma function $\gamma(\xi,x)$ is defined as

$$\gamma(\xi,x) \equiv \int_{t=o}^{t=x} dt \; t^{\xi-1} \exp(-t)$$

<div align="right">(105-1)</div>

and we recognize that

$$\Gamma(\xi,x) \equiv \int_{t=x}^{t=\infty} dt \; t^{\xi-1} \exp(-t) = \Gamma(\xi) - \gamma(\xi,x)$$

<div align="right">(105-2)</div>

Equation (104) represents the accelerated-particle current to the probe, with $\delta = 0$ corresponding to the cylindrical model and $\delta = 1$ to the spherical model. The radius of the probe is arbitrary, so that Eq. (104) applies to a $\psi$-function of the general shape shown in Fig. 10, whether $r_c > r_c$, or $r_i < r_c$, but satisfying condition (46-2) on the maxima of $\Phi_e(r)$.

However, the case of special interest to us is the one where $r_i < r_c$ (see Fig. 11), where in the range $r > r_c$ there exists either no extremum in $\Phi_e$ or only a maximum as illustrated in Fig. 14. In that case $r_k = r_c$ according to Eq. (55) that is, the maximum value of $\Phi_e^*(r^*)$ equals its value $\Phi_e(r_c)$ at the probe surface only if the maximum occurs at the probe

surface. For the class of potential functions, which have the property (46-2) and for which $r_i < r_c$, the coefficients $K_\nu$ and $\nu$ are given by Eqs. (66-1) and (66-2), i.e.,

$$K_\nu = \frac{2\Phi_c + r_c \Phi'_c}{2mr_c^3 \Phi'_c} \tag{106-1}$$

$$\nu = \frac{r_c \Phi'_c}{2\Phi_c + r_c \Phi'_c} \tag{106-2}$$

This is the condition for which

$$M_k^2 = \psi_k = \psi_c = mr_c^3 \Phi'_c \tag{107}$$

## 4.3 COLLECTED CURRENT EXPRESSIONS FOR THE INVERSE-POWER-LAW POTENTIAL

For an inverse-power-law potential function, as given by Eq. (68-1) we obtained expressions (75-1) and (75-2) for $\nu$ and $K_\nu$, which can be written in the following forms:

$$\nu = \frac{\alpha}{\alpha - 2} \tag{108-1}$$

$$K_\nu = \frac{(-\Phi_c)(\frac{\alpha}{2}-1)}{[\alpha mr_c^2(-\Phi_c)]^{\alpha/(\alpha-2)}} \tag{108-2}$$

where

$$M_k^2 = \psi_c = \alpha mr_c^2(-\Phi_c).$$

Now by substituting these expressions for $\nu$, $K_\nu$, and $M_k^2$ into Eq. (104), we obtain

$$J_c = \frac{J_o}{\Gamma\left(\frac{\delta+1}{2}\right)}\left[\left(\frac{-\Phi_c}{2kT}\right)^{(\delta+1)/\alpha}(\alpha-2)^{1-(\delta+1)(\alpha-2)/2\alpha}\,\alpha^{(\delta-1)/2}\right.$$
$$\cdot\,\gamma\left(\frac{(\delta+1)(\alpha-2)}{2\alpha},\ (\alpha-2)\left(\frac{-\Phi_c}{kT}\right)\right)$$
$$\left.+\ \exp\left(-\frac{\Phi_c}{kT}\right)\Gamma\left(\frac{\delta+1}{2},\ \alpha\left(\frac{-\Phi_c}{kT}\right)\right)\right]\ . \tag{109}$$

Equation (109) represents the accelerated current collected by a probe for the inverse-power-law potential (68-1). The mode of orbital-limited current collection is obtained by setting $\alpha = 2$. Denoting the orbital-motion-limited current density at the probe surface by $J_{oml}$, Eq. (109) becomes for the case $\alpha = 2$;

$$J_{oml} = \frac{J_o}{\Gamma\left(\frac{\delta+1}{2}\right)}\left[\frac{2}{\delta+1}\left(\frac{-\Phi_c}{kT}\right)^{(\delta+1)/2} + \exp\left(\frac{-\Phi_c}{kT}\right)\Gamma\left(\frac{\delta+1}{2},\ \frac{-\Phi_c}{kT}\right)\right] \tag{110}$$

For $\delta = 0$ and $\delta = 1$, corresponding to the cylindrical and spherical geometries respectively, Eq. (110) takes the familiar forms given by Eq. (A-13) and Eq. (A-14) in the Appendix.

For $\alpha = \infty$, the right-hand side of Eq. (109) reduces to $J_o$. Consequently, in this mode of collection the probe collects the random current, as was anticipated in comments in the last paragraph of Section 3.15.

## 4.4 CURRENT COLLECTION FOR A POWER-LAW APPROXIMATION TO THE DEBYE POTENTIAL DISTRIBUTION FOR A LARGE SPHERE

As a final example we will consider the Debye potential distribution for a large spherical probe $(\lambda_D < r_i \ll r_c)$, and find a power law which approximates it. The new notation is as follows:

$$\Phi_D(r) \quad = \quad \text{The Debye potential function}$$

$$\lambda_D \quad = \quad \text{The Debye length.}$$

Thus

$$\Phi_D \quad = \quad \Phi_c \; \frac{r_c}{r} \; \exp\left(-\frac{r-r_c}{\lambda_D}\right) \tag{111}$$

By using this potential in Eq. (106) we get

$$\nu \quad = \quad \frac{r_c + \lambda_D}{r_c - \lambda_D} \; . \tag{112}$$

We are now looking for a particular potential of the form (68-1) which has the property that the exponent $\nu$, given by Eq. (108-1) is equal to the expression of $\nu$ (112) for a Debye potential. The two values of $\nu$ are equal if

$$\alpha \quad = \quad \frac{r_c + \lambda_D}{\lambda_D} \tag{113}$$

Hence, the desired potential is

$$\Phi \quad = \quad \Phi_c \left(\frac{r_c}{r}\right)^{(r_c + \lambda_D)/\lambda_D} \tag{114}$$

It can be shown that for values of $r$ close to $r_c$ the potential (114) is approximately equal to the Debye potential if $r_c/\lambda_D \gg 1$ In order to show this we let $r = r_c + \delta r$ with $\delta r / r_c \ll 1$. Then Eq. (114) can be rewritten in the following form,

$$\Phi \quad = \quad \Phi_c \; \frac{r_c/r}{(r/r_c)^{r_c/\lambda_D}} \tag{115}$$

$$\Phi \;=\; \Phi_c \frac{r_c/r}{\left(1+\frac{\delta r}{r_c}\right)^{r_c/\lambda_D}} \tag{116}$$

$$\Phi \;\cong\; \Phi_c \frac{r_c}{r}\left(1-\frac{\delta r}{\lambda_D}\right) \;\text{if}\; \frac{\delta r}{r_c} \ll 1$$

$$\Phi \;\cong\; \Phi_c \frac{r_c}{r}\exp\left(-\frac{\delta r}{\lambda_D}\right) \;\text{if}\; \frac{\delta r}{\lambda_D} \ll 1. \tag{117}$$

Hence, the volt-ampere relation for a spherical probe of large radius for

the case of a Debye potential can be obtained by using the expression (113)

for $\alpha$ and $\delta = 1$ in Eq. (109). The result is

$$J_c \;=\; J_0 \left[\left(\frac{-\Phi_c}{kT}\frac{\chi-1}{2}\right)^{2/(\chi+1)}\gamma\left(\frac{\chi-1}{\chi+1},\;\frac{-\Phi_c}{kT}\frac{\chi-1}{2}\right)\right.$$
$$\left. +\exp\left(-\frac{\Phi_c}{kT}\frac{\chi-1}{2}\right)\right] \tag{118}$$

where $\chi \equiv r_c/\lambda_D$.

## 4.5 DISCUSSION OF THE VOLT-AMPERE RELATIONS

The accelerated current density at the collector (cylindrical or

spherical), for a power law potential, is given by Eq. (109). For the

cylindrical geometry we set $\delta = 0$ and obtain,

$$J_{co} \;=\; J_0\left[\left(\frac{-\Phi_{oc}}{2}\right)^{1/\alpha}\frac{(\alpha-2)^{(\alpha+2)/2\alpha}}{\sqrt{\pi\alpha}}\gamma\left(\frac{\alpha-2}{2\alpha},\;-\Phi_{oc}(\alpha-2)\right)\right.$$
$$\left. +\exp(-\Phi_{oc})\cdot\operatorname{erfc}(\sqrt{-\Phi_{oc}\alpha})\right] \tag{109-1}$$

where $\Phi_{oc} = \Phi_c/kT < 0$ is the dimensionless potential energy at the col-

lector surface.

If we plot $J_{co}/J_0$ against $(-\Phi_{oc})$ for fixed values of $\alpha$ we would an-

ticipate that for increasing $\alpha$ the ratio $J_{co}/J_o$ would uniformly decrease

i.e., if $\alpha_1 > \alpha_2$ then $J_{co}(\alpha_1) < J_{co}(\alpha_2)$ for all values of $(-\Phi_{oc})$. In other

words, the larger the values of $\alpha$ the smaller is the current density at

the probe. The plot of $J_{co}/J_o$ against $(-\Phi_{oc})$ for various values of $\alpha$ is shown

in Fig. 19. The first curve for $\alpha = 2$ is the oribital-motion-limited form

of Eq. (109-1). The rest of the curves are for higher values of $\alpha$ as shown.

One observes that for $\alpha > 2$ the saturation region is attained progressively

faster. The decreasing character of $J_{co}/J_o$ for increasing $\alpha$ is illustrated

in Fig. 20. These curves also show that in the range $0 \leq \alpha \leq 2$ the current

is independent of $\alpha$, which is not surprising since Langmuir's theory applies

in this range and his volt-ampere characteristics are independent of the de-

tailed structure of the potential. Table I lists the values of $J_{co}/J_o$ for

different $\alpha$ and $\Phi_{oc}$ calculated from Eq. (109-1).

For the spherical probe ($\delta = 1$) Eq. (109) reduces to,

$$J_{c1} = J_o\left[\left(\frac{-\Phi_{oc}}{2}\right)^{2/\alpha} (\alpha-2)^{2/\alpha} \gamma\left(\frac{\alpha-2}{\alpha}, -\Phi_{oc}(\alpha-2)\right) + \exp\left(-\Phi_{oc}(1-\alpha)\right)\right] \tag{109-2}$$

where $\Phi_{oc}$ again is the dimensionless potential energy $(\Phi_c/kT)$ at the col-

lector surface, and for attracting potential it is negative.

Figure 21 illustrates the behavior of $J_{c1}/J_o$ as a function of $(-\Phi_{oc})$

(Eq.(109-2)) for various values of $\alpha$. For any fixed value of $(-\Phi_{oc})$ the

decreasing character of $J_{c1}/J_o$ for increasing $\alpha$ is evident. Figure 22

illustrates that behavior for some representative values of $(-\Phi_{oc})$. These

curves have been drawn for the range $\alpha \geq 1$ since the case $\alpha < 1$ is

physically meaningless as has been discussed in Section 2.4. Table II

TABLE I

ATTRACTING CYLINDRICAL COLLECTOR

POWER POTENTIAL, $\Phi = \Phi_c(r_c/r)^\alpha$

COMPUTED VALUES OF THE DIMENSIONLESS CURRENT AS A FUNCTION OF THE DIMENSIONLESS COLLECTOR POTENTIAL WITH ALPHA PARAMETERIZED.

DELTA = .000

| PHI | ALPHA 3.0 | ALPHA 3.5 | ALPHA 4.0 | ALPHA 4.5 | ALPHA 5.0 | ALPHA 6.0 | ALPHA 7.0 | ALPHA 8.0 | ALPHA 9.0 | ALPHA 10.0 |
|---|---|---|---|---|---|---|---|---|---|---|
| .0 | 1.0000E 00 | 1.0000E 00 | 1.0000E 00 | 1.0000E 00 | 1.0000E 00 | 1.0000E 00 | 1.0000E 00 | 1.0000E 00 | 1.0000E 00 | 1.0000E 00 |
| .5 | 1.3084E 00 | 1.2987E 00 | 1.2889E 00 | 1.2793E 00 | 1.2702E 00 | 1.2532E 00 | 1.2382E 00 | 1.2248E 00 | 1.2128E 00 | 1.2021E 00 |
| 1.0 | 1.5215E 00 | 1.4965E 00 | 1.4719E 00 | 1.4486E 00 | 1.4270E 00 | 1.3889E 00 | 1.3567E 00 | 1.3294E 00 | 1.3061E 00 | 1.2859E 00 |
| 1.5 | 1.6943E 00 | 1.6519E 00 | 1.6113E 00 | 1.5741E 00 | 1.5405E 00 | 1.4829E 00 | 1.4362E 00 | 1.3979E 00 | 1.3659E 00 | 1.3390E 00 |
| 2.0 | 1.8417E 00 | 1.7812E 00 | 1.7249E 00 | 1.6744E 00 | 1.6296E 00 | 1.5551E 00 | 1.4962E 00 | 1.4490E 00 | 1.4103E 00 | 1.3780E 00 |
| 2.5 | 1.9713E 00 | 1.8926E 00 | 1.8211E 00 | 1.7582E 00 | 1.7033E 00 | 1.6138E 00 | 1.5447E 00 | 1.4898E 00 | 1.4457E 00 | 1.4092E 00 |
| 3.0 | 2.0874E 00 | 1.9908E 00 | 1.9047E 00 | 1.8303E 00 | 1.7664E 00 | 1.6636E 00 | 1.5853E 00 | 1.5243E 00 | 1.4753E 00 | 1.4351E 00 |
| 3.5 | 2.1929E 00 | 2.0788E 00 | 1.9790E 00 | 1.8939E 00 | 1.8216E 00 | 1.7067E 00 | 1.6207E 00 | 1.5539E 00 | 1.5007E 00 | 1.4574E 00 |
| 4.0 | 2.2898E 00 | 2.1587E 00 | 2.0458E 00 | 1.9508E 00 | 1.8704E 00 | 1.7452E 00 | 1.6519E 00 | 1.5801E 00 | 1.5232E 00 | 1.4770E 00 |
| 4.5 | 2.3796E 00 | 2.2321E 00 | 2.1069E 00 | 2.0019E 00 | 1.9152E 00 | 1.7798E 00 | 1.6799E 00 | 1.6035E 00 | 1.5432E 00 | 1.4945E 00 |
| 5.0 | 2.4634E 00 | 2.3000E 00 | 2.1618E 00 | 2.0496E 00 | 1.9561E 00 | 1.8114E 00 | 1.7054E 00 | 1.6248E 00 | 1.5614E 00 | 1.5103E 00 |
| 5.5 | 2.5421E 00 | 2.3634E 00 | 2.2144E 00 | 2.0936E 00 | 1.9938E 00 | 1.8404E 00 | 1.7288E 00 | 1.6443E 00 | 1.5780E 00 | 1.5248E 00 |
| 6.0 | 2.6164E 00 | 2.4208E 00 | 2.2634E 00 | 2.1346E 00 | 2.0288E 00 | 1.8673E 00 | 1.7504E 00 | 1.6622E 00 | 1.5934E 00 | 1.5381E 00 |
| 6.5 | 2.6868E 00 | 2.4774E 00 | 2.3093E 00 | 2.1729E 00 | 2.0616E 00 | 1.8923E 00 | 1.7705E 00 | 1.6790E 00 | 1.6076E 00 | 1.5505E 00 |
| 7.0 | 2.7485E 00 | 2.5308E 00 | 2.3526E 00 | 2.2090E 00 | 2.0924E 00 | 1.9159E 00 | 1.7894E 00 | 1.6946E 00 | 1.6209E 00 | 1.5620E 00 |
| 8.0 | 2.8756E 00 | 2.6297E 00 | 2.4325E 00 | 2.2756E 00 | 2.1490E 00 | 1.9590E 00 | 1.8239E 00 | 1.7231E 00 | 1.6451E 00 | 1.5830E 00 |
| 9.0 | 2.9920E 00 | 2.7199E 00 | 2.5052E 00 | 2.3359E 00 | 2.2002E 00 | 1.9978E 00 | 1.8548E 00 | 1.7487E 00 | 1.6668E 00 | 1.6017E 00 |
| 10.0 | 3.0996E 00 | 2.8031E 00 | 2.5721E 00 | 2.3912E 00 | 2.2471E 00 | 2.0332E 00 | 1.8829E 00 | 1.7718E 00 | 1.6864E 00 | 1.6187E 00 |
| 11.0 | 3.2000E 00 | 2.8805E 00 | 2.6341E 00 | 2.4424E 00 | 2.2903E 00 | 2.0658E 00 | 1.9087E 00 | 1.7931E 00 | 1.7044E 00 | 1.6342E 00 |
| 12.0 | 3.2944E 00 | 2.9530E 00 | 2.6921E 00 | 2.4901E 00 | 2.3305E 00 | 2.0959E 00 | 1.9326E 00 | 1.8127E 00 | 1.7209E 00 | 1.6485E 00 |
| 13.0 | 3.3836E 00 | 3.0213E 00 | 2.7465E 00 | 2.5348E 00 | 2.3681E 00 | 2.1241E 00 | 1.9548E 00 | 1.8309E 00 | 1.7363E 00 | 1.6617E 00 |
| 14.0 | 3.4683E 00 | 3.0860E 00 | 2.7978E 00 | 2.5769E 00 | 2.4035E 00 | 2.1505E 00 | 1.9756E 00 | 1.8479E 00 | 1.7507E 00 | 1.6741E 00 |
| 15.0 | 3.5490E 00 | 3.1474E 00 | 2.8465E 00 | 2.6167E 00 | 2.4369E 00 | 2.1753E 00 | 1.9952E 00 | 1.8640E 00 | 1.7641E 00 | 1.6857E 00 |
| 16.0 | 3.6263E 00 | 3.2060E 00 | 2.8928E 00 | 2.6545E 00 | 2.4685E 00 | 2.1989E 00 | 2.0137E 00 | 1.8791E 00 | 1.7768E 00 | 1.6966E 00 |
| 17.0 | 3.7003E 00 | 3.2620E 00 | 2.9370E 00 | 2.6905E 00 | 2.4987E 00 | 2.2212E 00 | 2.0312E 00 | 1.8933E 00 | 1.7888E 00 | 1.7069E 00 |
| 18.0 | 3.7715E 00 | 3.3157E 00 | 2.9793E 00 | 2.7249E 00 | 2.5274E 00 | 2.2425E 00 | 2.0479E 00 | 1.9069E 00 | 1.8002E 00 | 1.7167E 00 |
| 19.0 | 3.8401E 00 | 3.3674E 00 | 3.0198E 00 | 2.7578E 00 | 2.5549E 00 | 2.2628E 00 | 2.0637E 00 | 1.9199E 00 | 1.8111E 00 | 1.7260E 00 |
| 20.0 | 3.9063E 00 | 3.4171E 00 | 3.0588E 00 | 2.7895E 00 | 2.5812E 00 | 2.2822E 00 | 2.0789E 00 | 1.9322E 00 | 1.8214E 00 | 1.7349E 00 |

## TABLE II

### ATTRACTING SPHERICAL COLLECTOR

### POWER POTENTIAL, $\Phi = \Phi_c(r_c/r)^\alpha$

COMPUTED VALUES OF THE DIMENSIONLESS CURRENT
AS A FUNCTION OF THE DIMENSIONLESS COLLECTOR
POTENTIAL WITH ALPHA PARAMETERIZED.

DELTA = 1.000

| PHI | ALPHA 3.0 | ALPHA 3.5 | ALPHA 4.0 | ALPHA 4.5 | ALPHA 5.0 | ALPHA 6.0 | ALPHA 7.0 | ALPHA 8.0 | ALPHA 9.0 | ALPHA 10.0 |
|---|---|---|---|---|---|---|---|---|---|---|
| .0 | 1.0000E 00 | 1.0000E 00 | 1.0000E 00 | 1.0000E 00 | 1.0000E 00 | 1.0000E 00 | 1.0000E 00 | 1.0000E 00 | 1.0000E 00 | 1.0000E 00 |
| .5 | 1.4851E 00 | 1.4738E 00 | 1.4622E 00 | 1.4505E 00 | 1.4392E 00 | 1.4176E 00 | 1.3975E 00 | 1.3791E 00 | 1.3622E 00 | 1.3466E 00 |
| 1.0 | 1.9430E 00 | 1.9021E 00 | 1.8615E 00 | 1.8228E 00 | 1.7864E 00 | 1.7209E 00 | 1.6645E 00 | 1.6158E 00 | 1.5737E 00 | 1.5369E 00 |
| 1.5 | 2.3771E 00 | 2.2933E 00 | 2.2132E 00 | 2.1394E 00 | 2.0723E 00 | 1.9570E 00 | 1.8629E 00 | 1.7853E 00 | 1.7206E 00 | 1.6660E 00 |
| 2.0 | 2.7904E 00 | 2.6540E 00 | 2.5279E 00 | 2.4153E 00 | 2.3158E 00 | 2.1507E 00 | 2.0213E 00 | 1.9180E 00 | 1.8340E 00 | 1.7643E 00 |
| 2.5 | 3.1854E 00 | 2.9893E 00 | 2.8135E 00 | 2.6606E 00 | 2.5287E 00 | 2.3159E 00 | 2.1541E 00 | 2.0274E 00 | 1.9271E 00 | 1.8451E 00 |
| 3.0 | 3.5641E 00 | 3.3034E 00 | 3.0759E 00 | 2.8824E 00 | 2.7187E 00 | 2.4607E 00 | 2.2686E 00 | 2.1224E 00 | 2.0069E 00 | 1.9137E 00 |
| 3.5 | 3.9284E 00 | 3.5994E 00 | 3.3191E 00 | 3.0856E 00 | 2.8911E 00 | 2.5895E 00 | 2.3712E 00 | 2.2058E 00 | 2.0769E 00 | 1.9736E 00 |
| 4.0 | 4.2797E 00 | 3.8800E 00 | 3.5466E 00 | 3.2737E 00 | 3.0470E 00 | 2.7079E 00 | 2.4635E 00 | 2.2808E 00 | 2.1394E 00 | 2.0270E 00 |
| 4.5 | 4.6195E 00 | 4.1472E 00 | 3.7609E 00 | 3.4457E 00 | 3.1954E 00 | 2.8166E 00 | 2.5479E 00 | 2.3489E 00 | 2.1962E 00 | 2.0754E 00 |
| 5.0 | 4.9489E 00 | 4.4028E 00 | 3.9571E 00 | 3.6126E 00 | 3.3335E 00 | 2.9173E 00 | 2.6257E 00 | 2.4116E 00 | 2.2482E 00 | 2.1196E 00 |
| 5.5 | 5.2688E 00 | 4.6482E 00 | 4.1530E 00 | 3.7698E 00 | 3.4644E 00 | 3.0115E 00 | 2.6982E 00 | 2.4698E 00 | 2.2963E 00 | 2.1603E 00 |
| 6.0 | 5.5801E 00 | 4.8733E 00 | 4.3393E 00 | 3.9190E 00 | 3.5862E 00 | 3.1001E 00 | 2.7661E 00 | 2.5241E 00 | 2.3411E 00 | 2.1983E 00 |
| 6.5 | 5.8836E 00 | 5.1049E 00 | 4.5175E 00 | 4.0612E 00 | 3.7029E 00 | 3.1840E 00 | 2.8301E 00 | 2.5751E 00 | 2.3832E 00 | 2.2337E 00 |
| 7.0 | 6.1494E 00 | 5.3282E 00 | 4.6886E 00 | 4.1973E 00 | 3.8144E 00 | 3.2636E 00 | 2.8907E 00 | 2.6232E 00 | 2.4227E 00 | 2.2671E 00 |
| 8.0 | 6.7344E 00 | 5.7535E 00 | 5.0129E 00 | 4.4540E 00 | 4.0237E 00 | 3.4122E 00 | 3.0031E 00 | 2.7123E 00 | 2.4957E 00 | 2.3285E 00 |
| 9.0 | 7.2921E 00 | 6.1554E 00 | 5.3172E 00 | 4.6934E 00 | 4.2178E 00 | 3.5488E 00 | 3.1059E 00 | 2.7933E 00 | 2.5619E 00 | 2.3840E 00 |
| 10.0 | 7.8272E 00 | 6.5381E 00 | 5.6049E 00 | 4.9185E 00 | 4.3993E 00 | 3.6756E 00 | 3.2008E 00 | 2.8679E 00 | 2.6226E 00 | 2.4347E 00 |
| 11.0 | 8.3434E 00 | 6.9043E 00 | 5.8785E 00 | 5.1313E 00 | 4.5703E 00 | 3.7943E 00 | 3.2892E 00 | 2.9371E 00 | 2.6787E 00 | 2.4816E 00 |
| 12.0 | 8.8434E 00 | 7.2564E 00 | 6.1400E 00 | 5.3336E 00 | 4.7322E 00 | 3.9060E 00 | 3.3720E 00 | 3.0016E 00 | 2.7310E 00 | 2.5251E 00 |
| 13.0 | 9.3291E 00 | 7.5961E 00 | 6.3907E 00 | 5.5268E 00 | 4.8861E 00 | 4.0116E 00 | 3.4500E 00 | 3.0623E 00 | 2.7800E 00 | 2.5659E 00 |
| 14.0 | 9.8022E 00 | 7.9247E 00 | 6.6319E 00 | 5.7118E 00 | 5.0331E 00 | 4.1119E 00 | 3.5238E 00 | 3.1196E 00 | 2.8262E 00 | 2.6042E 00 |
| 15.0 | 1.0264E 01 | 8.2434E 00 | 6.8647E 00 | 5.8897E 00 | 5.1740E 00 | 4.2076E 00 | 3.5939E 00 | 3.1739E 00 | 2.8699E 00 | 2.6404E 00 |
| 16.0 | 1.0715E 01 | 8.5531E 00 | 7.0898E 00 | 6.0611E 00 | 5.3093E 00 | 4.2991E 00 | 3.6608E 00 | 3.2255E 00 | 2.9113E 00 | 2.6747E 00 |
| 17.0 | 1.1158E 01 | 8.8546E 00 | 7.3080E 00 | 6.2266E 00 | 5.4396E 00 | 4.3868E 00 | 3.7248E 00 | 3.2747E 00 | 2.9508E 00 | 2.7073E 00 |
| 18.0 | 1.1591E 01 | 9.1486E 00 | 7.5199E 00 | 6.3868E 00 | 5.5654E 00 | 4.4712E 00 | 3.7861E 00 | 3.3219E 00 | 2.9885E 00 | 2.7384E 00 |
| 19.0 | 1.2016E 01 | 9.4356E 00 | 7.7259E 00 | 6.5421E 00 | 5.6871E 00 | 4.5525E 00 | 3.8451E 00 | 3.3671E 00 | 3.0246E 00 | 2.7682E 00 |
| 20.0 | 1.2434E 01 | 9.7163E 00 | 7.9267E 00 | 6.6930E 00 | 5.8050E 00 | 4.6310E 00 | 3.9018E 00 | 3.4105E 00 | 3.0593E 00 | 2.7968E 00 |
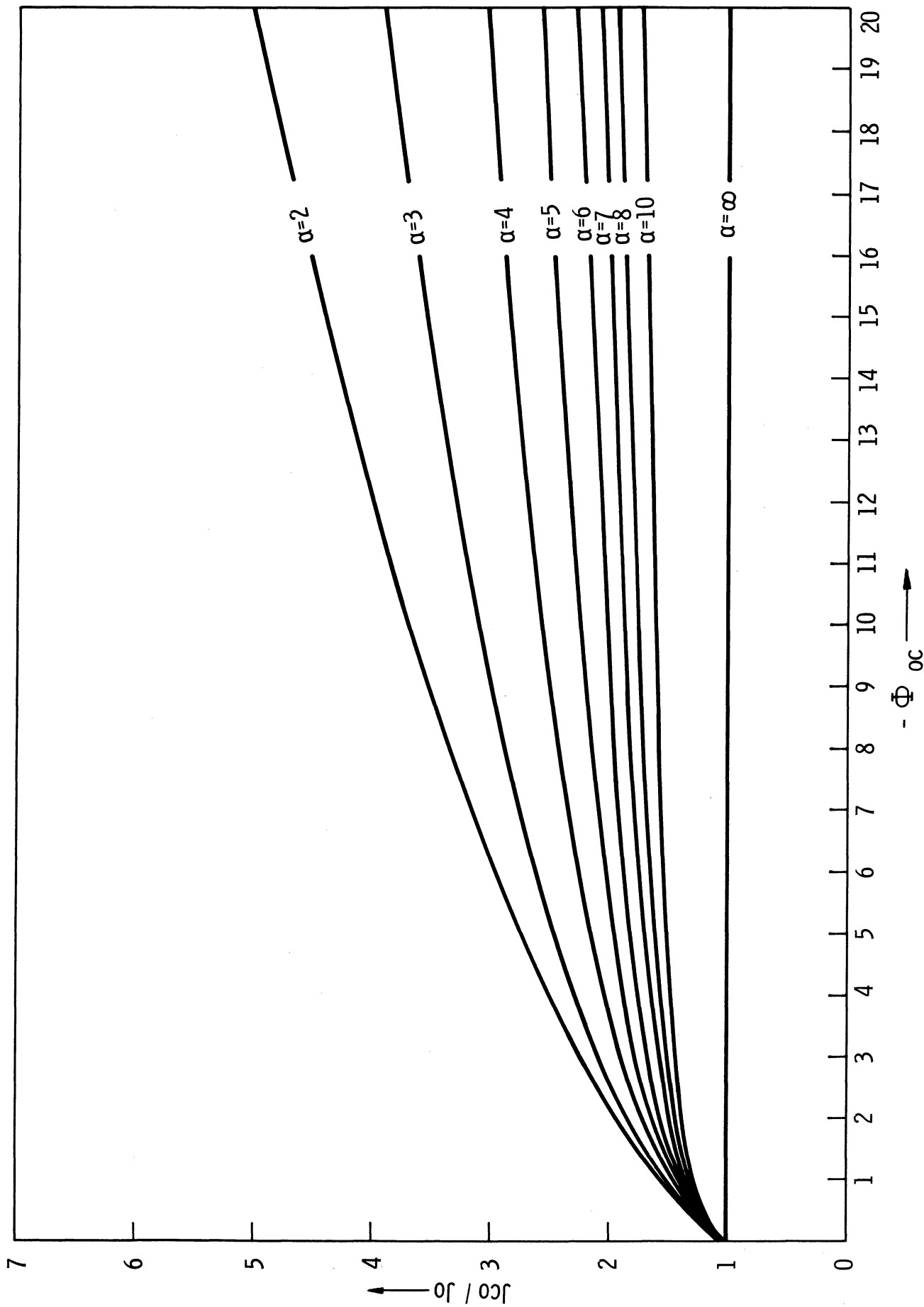
Fig. 19. Cylindrical probe ($\delta=0$). Plot of the dimensionless current density ($J_{CO}/J_O$) vs. dimensionless voltage ($-\Phi_{OC}$) for various values of $\alpha$.

90
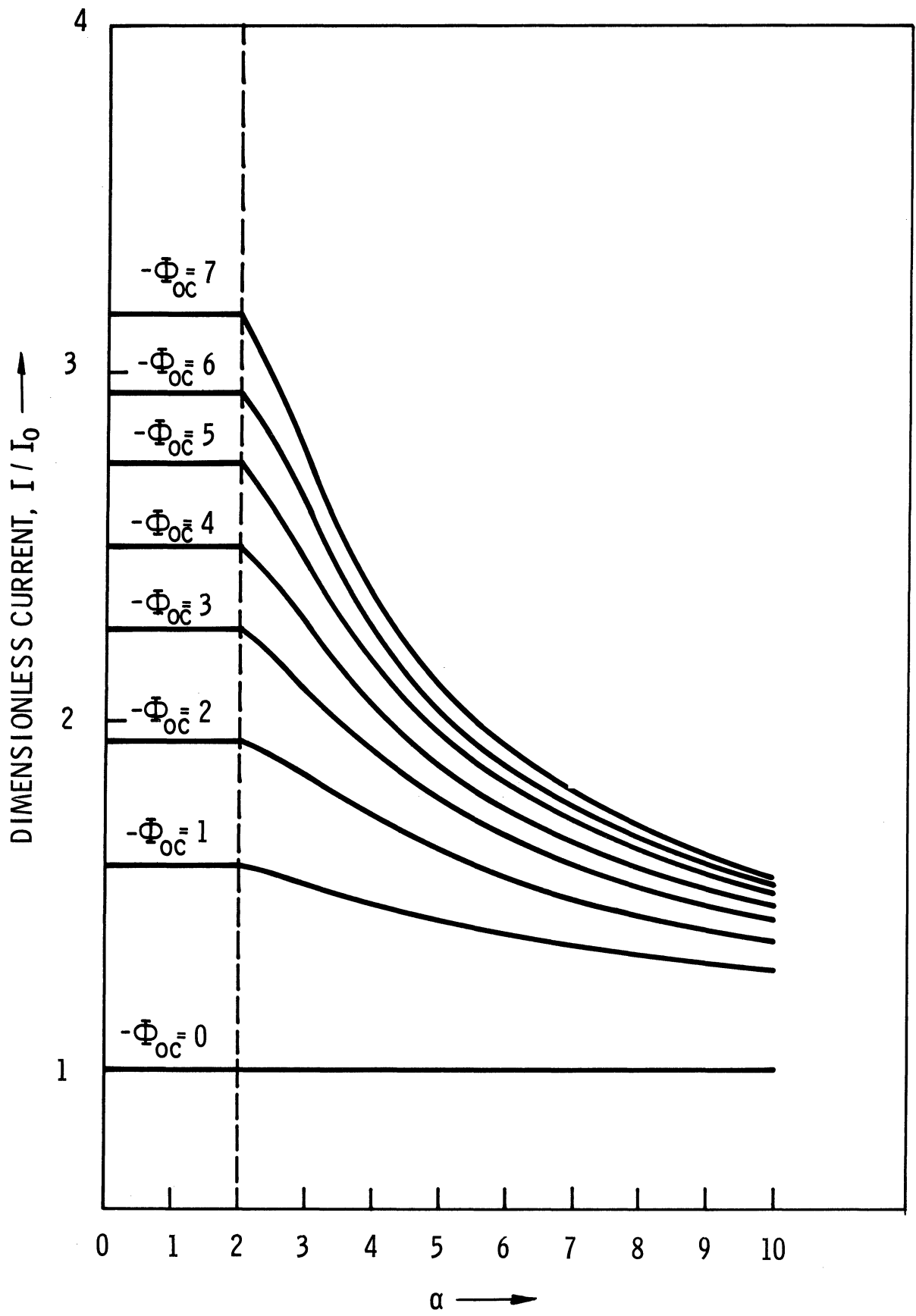
Fig. 20. Cylindrical probe ($\delta=0$). Dimensionless accelerated current density ($J_{co}/J_o$) vs. $\alpha$ for various values of ($-\Phi_{oc}$).

Fig. 21. Spherical probe ($\delta=1$). Plot of the dimensionless accelerated current density ($J_{cl}/J_o$) vs. the dimensionless potential ($-\Phi_{oc}$) for various values of $\alpha$.
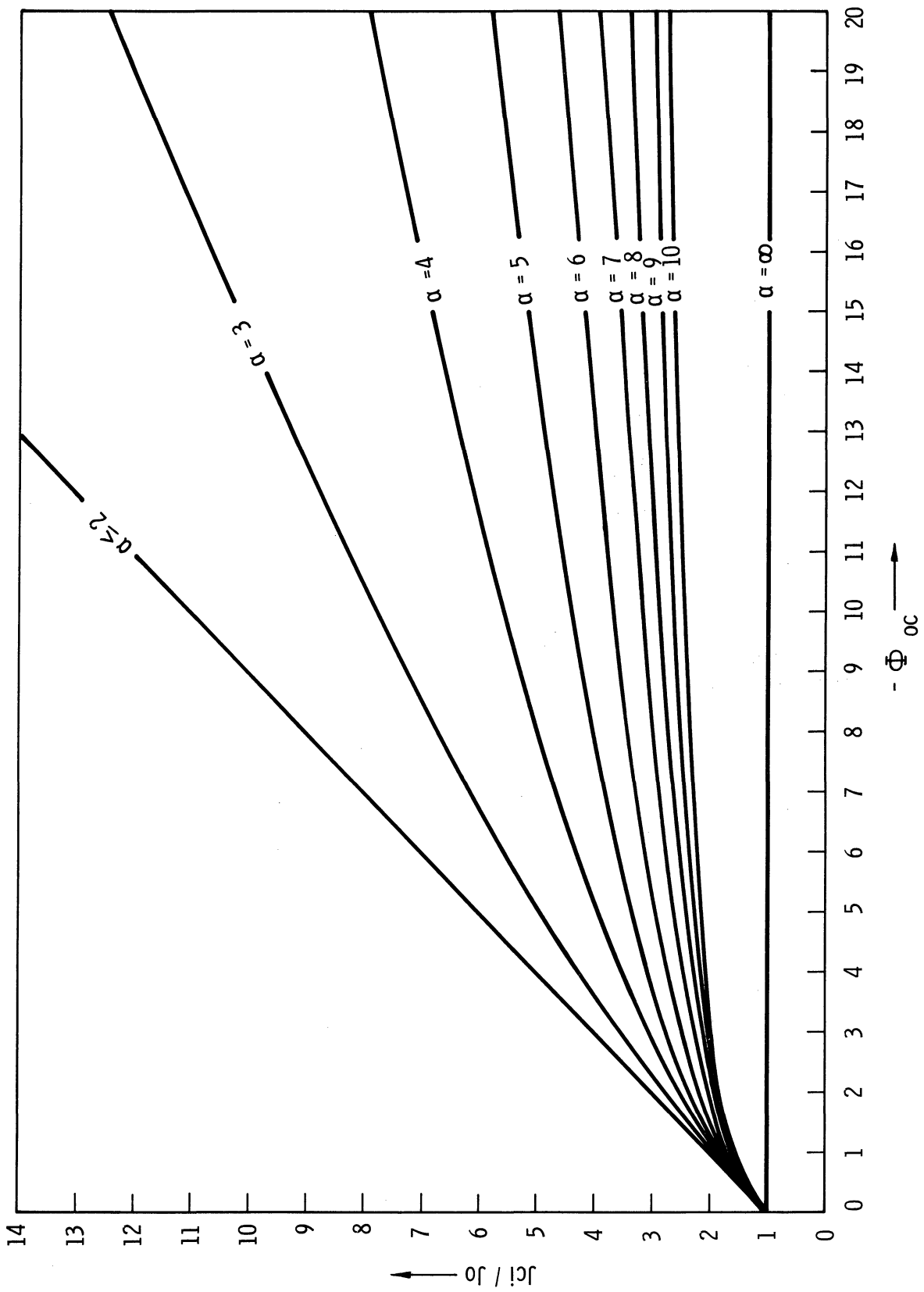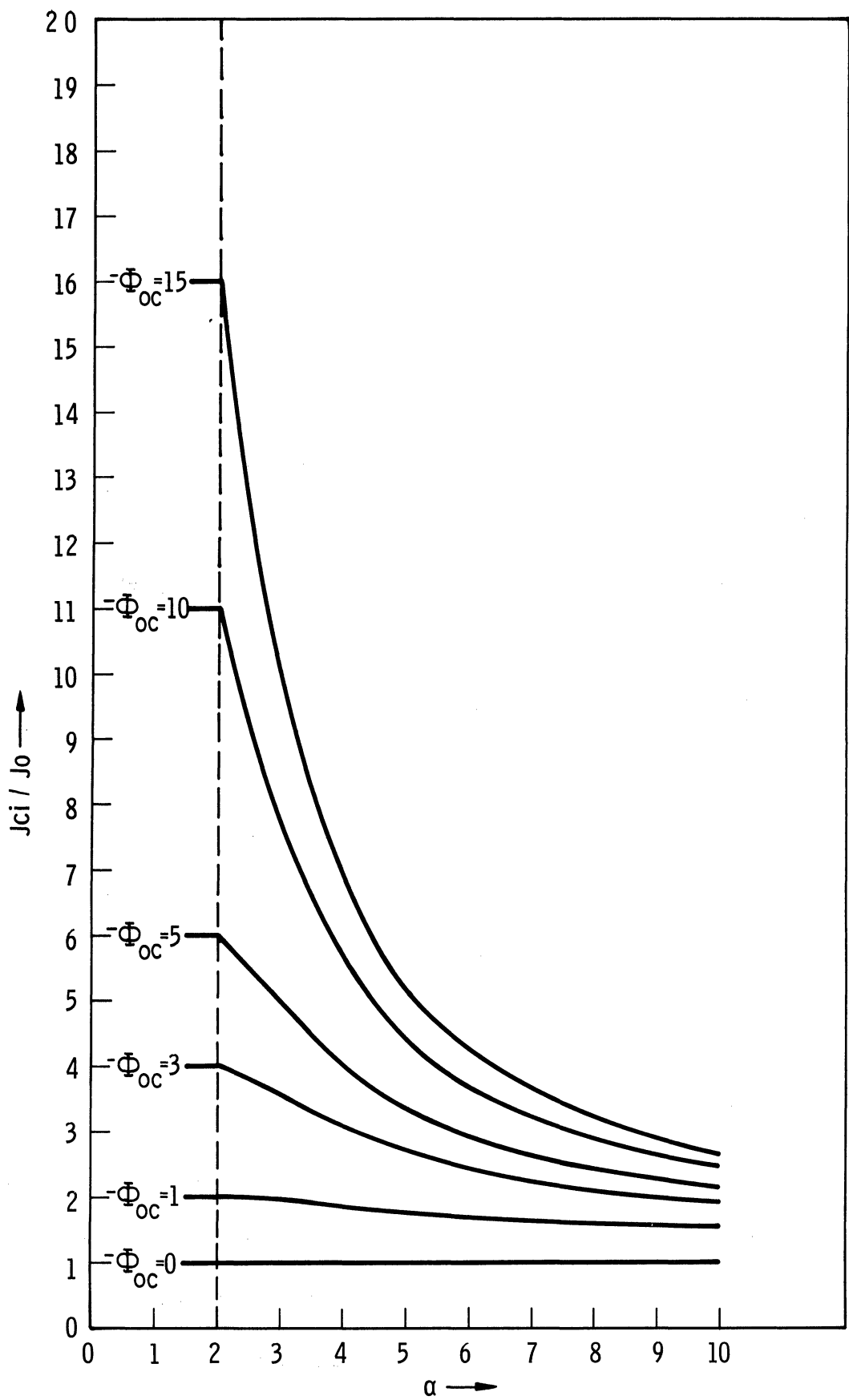
Fig. 22. Spherical probe ($\delta=1$). Plot of the dimensionless accelerated current density ($J_{cl}/J_o$) vs. $\alpha$ for various values of ($-\Phi_{oc}$).

lists the values of $J_{cl}/J_o$ for different values of $\alpha$ and $\Phi_{oc}$ calculated from Eq. (109-2).

In the volt-ampere characteristics of cylindrical and spherical probes (Figs. 19 and 21) the values of the parameter $\alpha$ were considered independent of $\Phi_{oc}$ and $\chi$, where $\chi$ is the ratio of the probe radius $r_c$ to the Debye length $\lambda_D$. If one represents the potential distribution in the sheath by an inverse power law of the form (68-1), the exponent $\alpha$ will of course depend on the probe potential $\Phi_{oc}$ and the parameter $\chi$. This is merely a consequence of the fact that the rate at which the potential disturbance decreases radially (which is controlled by $\alpha$) depends on the probe potential and on the electron temperature and density. In a realistic sheath model, as pointed out earlier, the potential function must be determined in a self-consistent way together with the charge density. In the following section the relation between $\alpha$, $\Phi_{oc}$, and $\chi$, will be obtained numerically by comparison of Eqs. (109-1) and (109-2) with the volt-ampere relations obtained by a self-consistent treatment of the problem.

## 4.6 COMPARISON WITH THE RESULTS OF A SELF-CONSISTENT ANALYSIS

Using numerical methods Laframboise[2] has recently carried out a self-consistent field analysis of the potential and volt-ampere current relations for cylindrical and spherical probes. Tables III and IV contain his calculated values for the respective probes and Figs. 23 and 24 show the corresponding characteristic curves. For the determination of $\alpha$ as a function of $\Phi_{oc}$ and $\chi$ we took the values of the current from Tables III and IV, inserted them in Eqs. (109-1) and (109-2) respectively, and in-

## TABLE III

### CYLINDRICAL PROBE

Computed Values of Attracted-Species Current Density Ratio $(J_{co}/J_o)$ for $T_{ion}/T_{electron} = 1$

(Both Species Maxwellian)

| $-\Phi_{oc}$ | \( $\chi = r_c/\lambda_D$ \) 0 | 1 | 1.5 | 2 | 2.5 | 3 | 4 | 5 | 10 | 20 | 30 | 40 | 50 | 100 |
|---|---|---|---|---|---|---|---|---|---|---|---|---|---|---|
| 0    | 1.0    | 1.0    | 1.0    | 1.0    | 1.0    | 1.0    | 1.0    | 1.0    | 1.0    | 1.0    |       |       | 1.0   | 1.0   |
| 0.1  | 1.0804 | 1.0804 | 1.0804 | 1.0804 | 1.0804 | 1.0804 | 1.0804 | 1.0804 | 1.0803 | 1.0803 |       |       |       |       |
| 0.3  | 1.2101 | 1.2101 | 1.2101 | 1.2101 | 1.2101 | 1.2101 | 1.2101 | 1.2100 | 1.208  | 1.205  |       |       | 1.198 | 1.194 |
| 0.6  | 1.3721 | 1.3721 | 1.3721 | 1.3721 | 1.3721 | 1.3721 | 1.3721 | 1.371  | 1.362  | 1.348  |       |       | 1.327 | 1.314 |
| 1.0  | 1.5560 | 1.5560 | 1.5560 | 1.5560 | 1.5560 | 1.5560 | 1.554  | 1.549  | 1.523  | 1.486  |       |       | 1.439 | 1.409 |
| 1.5  | 1.7551 | 1.7551 | 1.7551 | 1.7551 | 1.7551 | 1.7551 | 1.747  | 1.735  | 1.677  | 1.605  |       |       | 1.523 | 1.478 |
| 2.0  | 1.9320 | 1.9320 | 1.9320 | 1.9320 | 1.9320 | 1.928  | 1.913  | 1.893  | 1.798  | 1.689  |       |       | 1.576 | 1.518 |
| 3.0  | 2.2417 | 2.2417 | 2.2417 | 2.2417 | 2.237  | 2.226  | 2.192  | 2.151  | 1.98   | 1.801  |       |       | 1.638 | 1.561 |
| 5.0  | 2.7555 | 2.7555 | 2.7555 | 2.750  | 2.731  | 2.701  | 2.626  | 2.544  | 2.22   | 1.940  |       |       | 1.703 | 1.599 |
| 7.5  | 3.2846 | 3.2846 | 3.2846 | 3.266  | 3.227  | 3.174  | 3.050  | 2.920  | 2.442  | 2.060  |       |       | 1.756 | 1.628 |
| 10.0 | 3.7388 | 3.7388 | 3.735  | 3.703  | 3.645  | 3.567  | 3.402  | 3.231  | 2.622  | 2.157  |       |       | 1.798 | 1.650 |
| 15.0 | 4.5114 | 4.5114 | 4.493  | 4.439  | 4.342  | 4.235  | 3.990  | 3.749  | 2.919  | 2.319  | 2.082 |       | 1.868 | 1.686 |
| 20.0 | 5.1695 | 5.1695 | 5.141  | 5.060  | 4.936  | 4.789  | 4.489  | 4.183  | 3.166  | 2.455  | 2.177 | 2.025 | 1.929 | 1.719 |
| 25.0 | 5.7526 | 5.7525 | 5.711  | 5.607  | 5.462  | 5.291  | 4.926  | 4.565  | 3.384  | 2.576  | 2.262 | 2.092 | 1.983 | 1.747 |

## TABLE IV

### SPHERICAL PROBE ( δ = 1 )

Computed Values of Attracted-Species Current Density Ratio ($J_{cl}/J_o$) for $T_{ion}/T_{electron} = 1$
(Both Species Maxwellian)

$$\chi = r_c/\lambda_D$$

| $-\Phi_{oc}$ | 0 | 0.2 | 0.3 | 0.5 | 1 | 2 | 3 | 5 | 7.5 | 10 | 15 | 20 | 50 | 100 |
|---|---|---|---|---|---|---|---|---|---|---|---|---|---|---|
| 0 | 1.0 | 1.0 | 1.0 | 1.0 | 1.0 | 1.0 | 1.0 | 1.0 | 1.0 | | | | | 1.0 |
| 0.1 | 1.1 | 1.1 | 1.1 | 1.1 | 1.0999 | 1.0999 | 1.0999 | 1.099 | 1.099 | 1.098 | | 1.097 | 1.095 | 1.094 |
| 0.3 | 1.3 | 1.3 | 1.3 | 1.3 | 1.299 | 1.299 | 1.293 | 1.288 | 1.288 | 1.280 | | 1.269 | 1.255 | 1.245 |
| 0.6 | 1.6 | 1.6 | 1.6 | 1.6 | 1.595 | 1.584 | 1.572 | 1.552 | 1.552 | 1.518 | | 1.481 | 1.433 | 1.402 |
| 1.0 | 2.0 | 2.0 | 2.0 | 2.0 | 1.987 | 1.955 | 1.922 | 1.869 | 1.869 | 1.783 | | 1.694 | 1.592 | 1.534 |
| 1.5 | 2.5 | 2.5 | 2.5 | 2.493 | 2.469 | 2.399 | 2.329 | 2.219 | 2.219 | 2.050 | | 1.887 | 1.719 | 1.632 |
| 2.0 | 3.0 | 3.0 | 3.0 | 2.987 | 2.945 | 2.824 | 2.709 | 2.529 | 2.529 | 2.266 | | 2.030 | 1.803 | 1.694 |
| 3.0 | 4.0 | 4.0 | 4.0 | 3.970 | 3.878 | 3.632 | 3.406 | 3.068 | 3.068 | 2.609 | | 2.235 | 1.910 | 1.762 |
| 5.0 | 6.0 | 6.0 | 6.0 | 5.917 | 5.687 | 5.126 | 4.640 | 3.957 | 3.957 | 3.119 | | 2.516 | 2.037 | 1.833 |
| 7.5 | 8.5 | 8.5 | 8.5 | 8.324 | 7.871 | 6.847 | 6.007 | 4.887 | 4.094 | 3.620 | | 2.779 | 2.148 | 1.891 |
| 10.0 | 11.0 | 11.0 | 11.0 | 10.704 | 9.990 | 8.460 | 7.258 | 5.710 | 4.658 | 4.050 | | 3.002 | 2.241* | 1.938* |
| 15.0 | 16.0 | 16.0 | 16.0 | 15.403 | 14.085 | 11.482 | 9.542 | 7.167 | 5.645 | 4.796 | | 3.383 | 2.397 | 2.022 |
| 20.0 | 21.0 | 21.0 | 21.0 | 20.031 | 18.041 | 14.314 | 11.636 | 8.473 | 6.518 | 5.453 | 4.318 | 3.716 | 2.532* | 2.097* |
| 25.0 | 26.0 | 25.763 | 25.462 | 24.607 | 21.895 | 17.018 | 13.603 | 9.676 | 7.318 | 6.053 | 4.719 | 4.018 | 2.658 | 2.166 |

*Obtained by Graphical Interpolation.
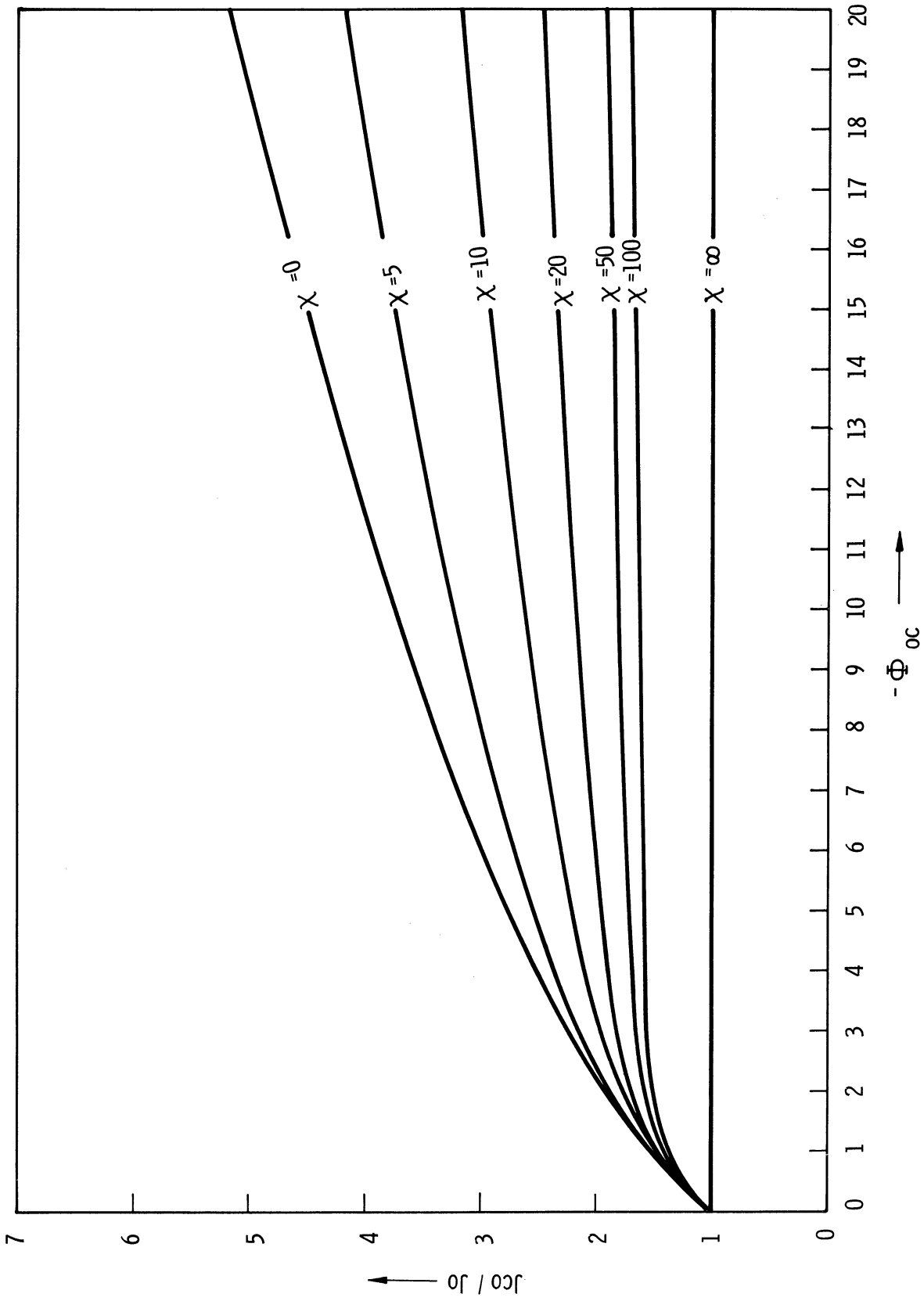
Fig. 23. Cylindrical probe ($\delta=0$). Plot of accelerated dimensionless current density ($J_{co}/J_o$) vs. ($-\Phi_{oc}$) for various values of $\alpha$. Temperature ratio $T_{ion}/T_{electron} = 1$. The plotted curves are from Laframboise's Table III.
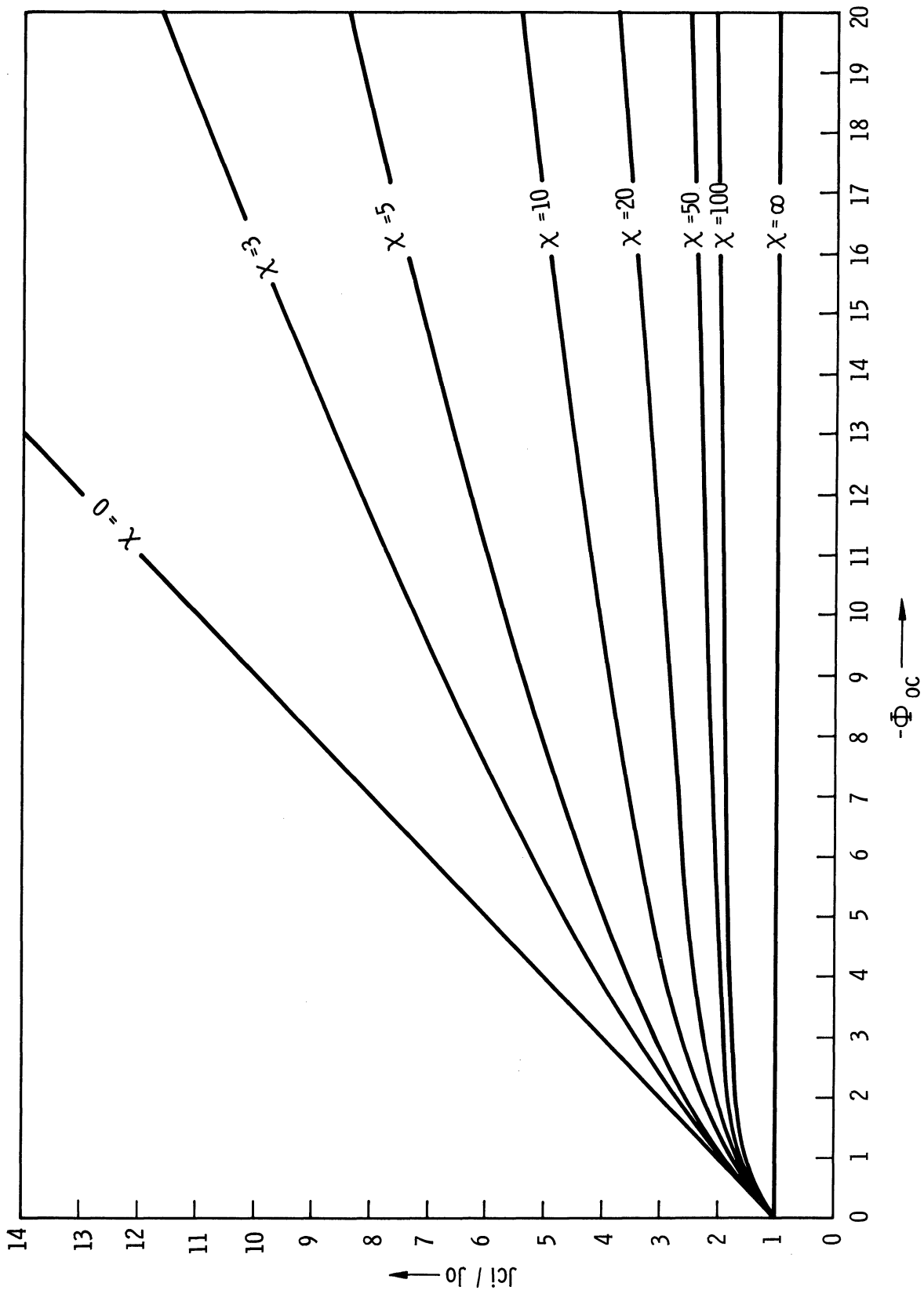
Fig. 24. Spherical probe ($\delta=1$).

verted these expressions numerically to obtain the corresponding values of $\alpha$ for given values of $\Phi_{OC}$ and $\chi$. Figure 25 illustrates $\alpha$, for the cylindrical probe as a function of $(-\Phi_{OC})$ for various values of $\chi$ and for the temperature ratio $T_{ion}/T_{elec} = 1$. Figure 26 shows $\alpha$, for the cylindrical probe, as a function of $\chi$ for various values of $(-\Phi_{OC})$. Table V contains these calculated values.

Similarly, for the spherical probe, Fig. 27 illustrates $\alpha$ as a function of $(-\Phi_{OC})$ for various values of $\chi$, and Fig. 28 shows $\alpha$ as a function of $\chi$ for various values of $(-\Phi_{OC})$. The temperature ratio for all cases is unity. Table VI contains these calculated values.

In order for an inverse-power-law potential to be realistic, the exponent $\alpha$ should not depend on the probe potential $\Phi_{OC}$. Figures 25 and 27 show that $\alpha$ is fairly insensitive to changes in the probe potential $\Phi_{OC}$ for values of $\chi$ less than about 5, except in the immediate neighborhood of the plasma potential. In the range $\chi \leq 5$, $\alpha$ is essentially constant for $(-\Phi_{OC}) > 4$. For a plasma of $2000°K$ and a value of $(-\Phi_{OC}) = 4$ the probe potential is about 0.7 volt. Electron density data are generally obtained at higher voltages, where $\alpha$ does not change anymore with probe potential. From Fig. 25 it is seen that $\alpha = 2.8$ if $\chi = 5$ and $\Phi_{OC} \geq 4$. If one compares the $\chi = 5$ curve of Fig. 27 with the $\alpha = 2.8$ curve obtained by interpolation from Fig. 19, one finds that the two curves are practically identical for all values of $\Phi_{OC}$ (even for $|\Phi_{OC}| < 4$). For $\chi < 5$ the agreement improves of course.

In the case of cylindrical probes used for ionospheric measurements

TABLE V

CYLINDRICAL PROBE ($\delta$ = 0)

Temperature ratio $T_{ion}/T_{electron}$ = 1. Values of $\alpha$ as a function of $(-\Phi_{oc})$, for various values of $\chi$ = $r_c/\lambda_D$, derived from Laframboise's Table III of volt-ampere characteristics.

| $-\Phi_{oc}$ | $\chi=5$ $\alpha$ | $\chi=10$ $\alpha$ | $\chi=20$ $\alpha$ | $\chi=50$ $\alpha$ | $\chi=100$ $\alpha$ |
|---|---|---|---|---|---|
| 0.0 | 2.00 | 2.00 | 2.00 | 2.00 | 2.00 |
| 0.1 | | 2.235 | 2.236 | | |
| 0.3 | | 2.508 | 2.892 | 3.648 | 4.070 |
| 0.6 | 2.195 | 2.719 | 3.304 | 4.141 | 4.679 |
| 1.0 | 2.365 | 2.696 | 3.710 | 4.717 | 5.450 |
| 1.5 | 2.483 | 3.203 | 4.082 | 5.281 | 6.093 |
| 2.0 | 2.564 | 3.359 | 4.349 | 5.693 | 6.596 |
| 3.0 | 2.680 | 3.559 | 4.720 | 6.299 | 7.367 |
| 5.0 | 2.774 | 3.780 | 5.10 | 7.026 | 8.382 |
| 7.5 | 2.793 | 3.860 | 5.295 | 7.488 | 9.071 |
| 10.0 | 2.809 | 3.881 | 5.375 | 7.738 | 9.507 |
| 15.0 | 2.795 | 3.866 | 5.401 | 7.964 | 10.001 |
| 20.0 | 2.774 | 3.834 | 5.371 | 8.025 | 10.203 |
| 25.0 | 2.754 | 3.797 | 5.323 | 8.028 | 10.337 |

## TABLE VI

### SPHERICAL PROBE ($\delta = 1$)

Temperature ratio $T_{ion}/T_{electron} = 1$. Values of $\alpha$ as a function of $(-\Phi_{oc})$, for various values of $\chi = r_c/\lambda_D$, derived from Laframboise's Table IV of volt-ampere characteristics.

| $\Phi_{oc}$ | $\chi=5$ $\alpha$ | $\chi=10$ $\alpha$ | $\chi=20$ $\alpha$ | $\chi=50$ $\alpha$ | $\chi=100$ $\alpha$ |
|---|---|---|---|---|---|
| 0.0 | 2.00 | 2.00 | 2.00 | 2.00 | 2.00 |
| 0.1 | 3.397 | 4.336 | 5.242 | 7.054 | 7.956 |
| 0.3 | 3.767 | 4.644 | 5.893 | 7.570 | 8.860 |
| 0.6 | 3.831 | 4.893 | 6.157 | 8.053 | 9.503 |
| 1.0 | 3.909 | 5.053 | 6.451 | 8.553 | 10.092 |
| 1.5 | 3.956 | 5.178 | 6.720 | 9.031 | 10.711 |
| 2.0 | 3.993 | 5.278 | 6.915 | 9.422 | 11.226 |
| 3.0 | 4.018 | 5.397 | 7.210 | 10.044 | 12.177 |
| 5.0 | 4.006 | 5.459 | 7.481 | 10.773 | 13.398 |
| 7.5 | 3.968 | 5.468 | 7.568 | 11.189 | 14.209 |
| 10.0 | 3.931 | 5.431 | 7.556 | 11.348 | 14.648 |
| 15.0 | 3.878 | 5.340 | 7.465 | 11.419 | 14.976 |
| 20.0 | 3.829 | 5.243 | 7.331 | 11.356 | 15.023 |
| 25.0 | 3.789 | 5.172 | 7.218 | 11.219 | 14.961 |
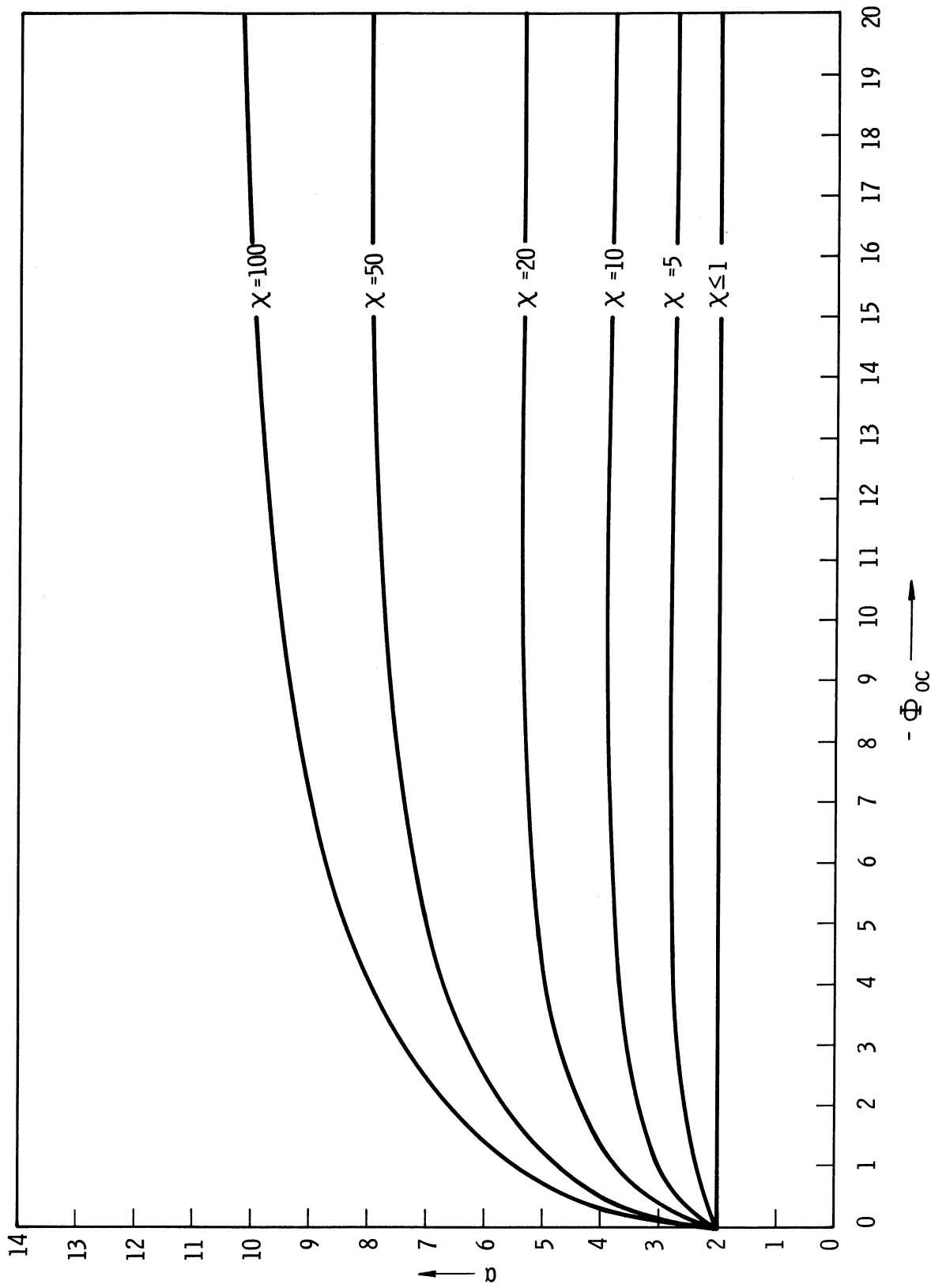
Fig. 25. Cylindrical probe. Plot of $\alpha$ vs. $(-\Phi_{oc})$ with $\chi = r_c/\lambda_D$ parameterized. $\alpha$ is the exponent in the power-law-potential $\Phi = \Phi_c(r_c/r)^\alpha$. $\Phi_{oc} = qV/kT$ is the dimensionless collector potential. $\lambda_D$ is the Debye length. Temperature ratio $T_{ion}/T_{electron} = 1$.
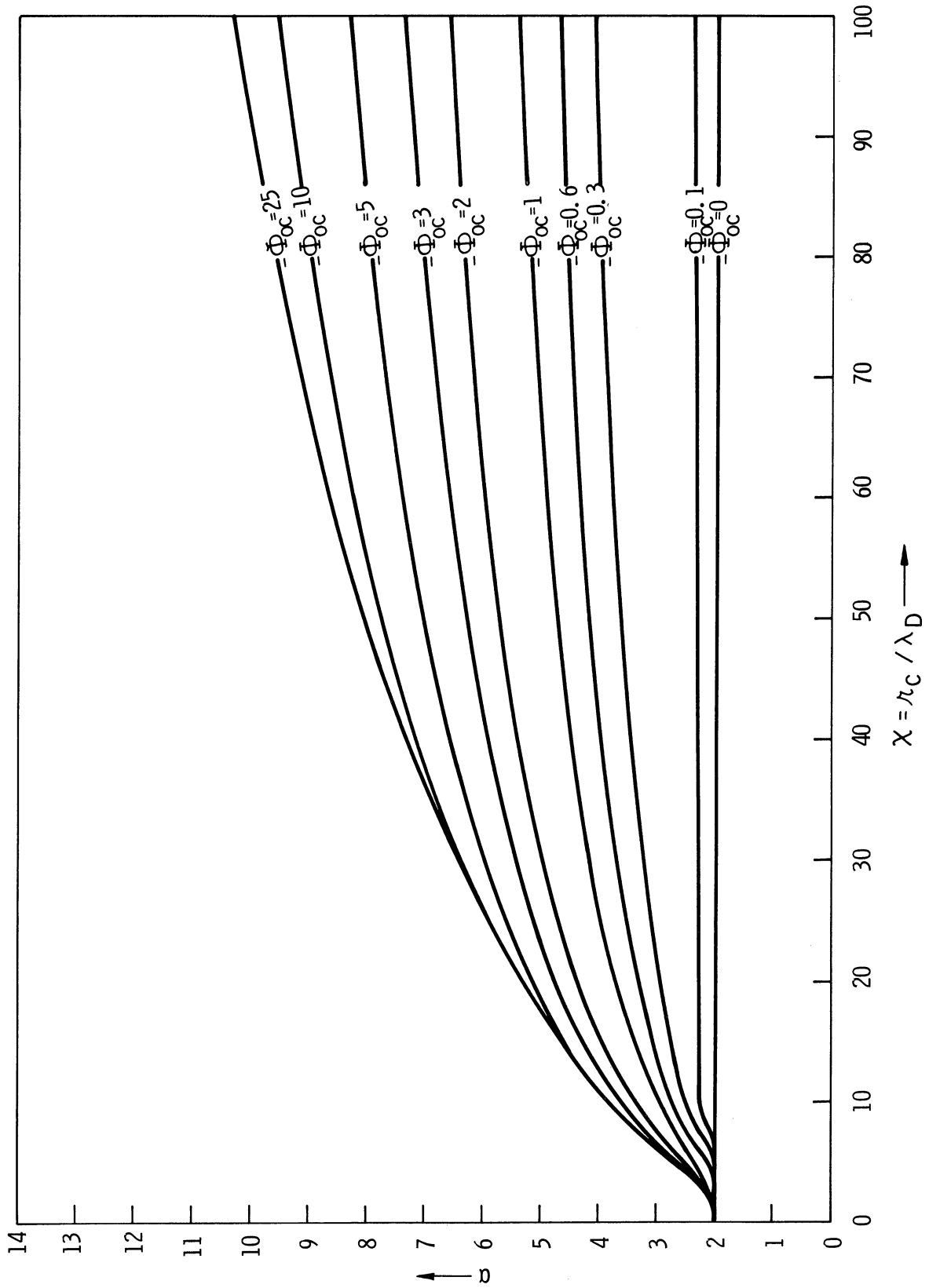
Fig. 26. Cylindrical probe ($\delta=0$). Plot of $\alpha$ vs. $\chi$ for various values of $(-\Phi_{oc})$. Temperature ratio $T_{ion}/T_{electron} = 1$.

$$\chi = r_c / \lambda_D \longrightarrow$$

$-\Phi_{oc}=25$
$-\Phi_{oc}=10$
$-\Phi_{oc}=5$
$-\Phi_{oc}=3$
$-\Phi_{oc}=2$
$-\Phi_{oc}=1$
$-\Phi_{oc}=0.6$
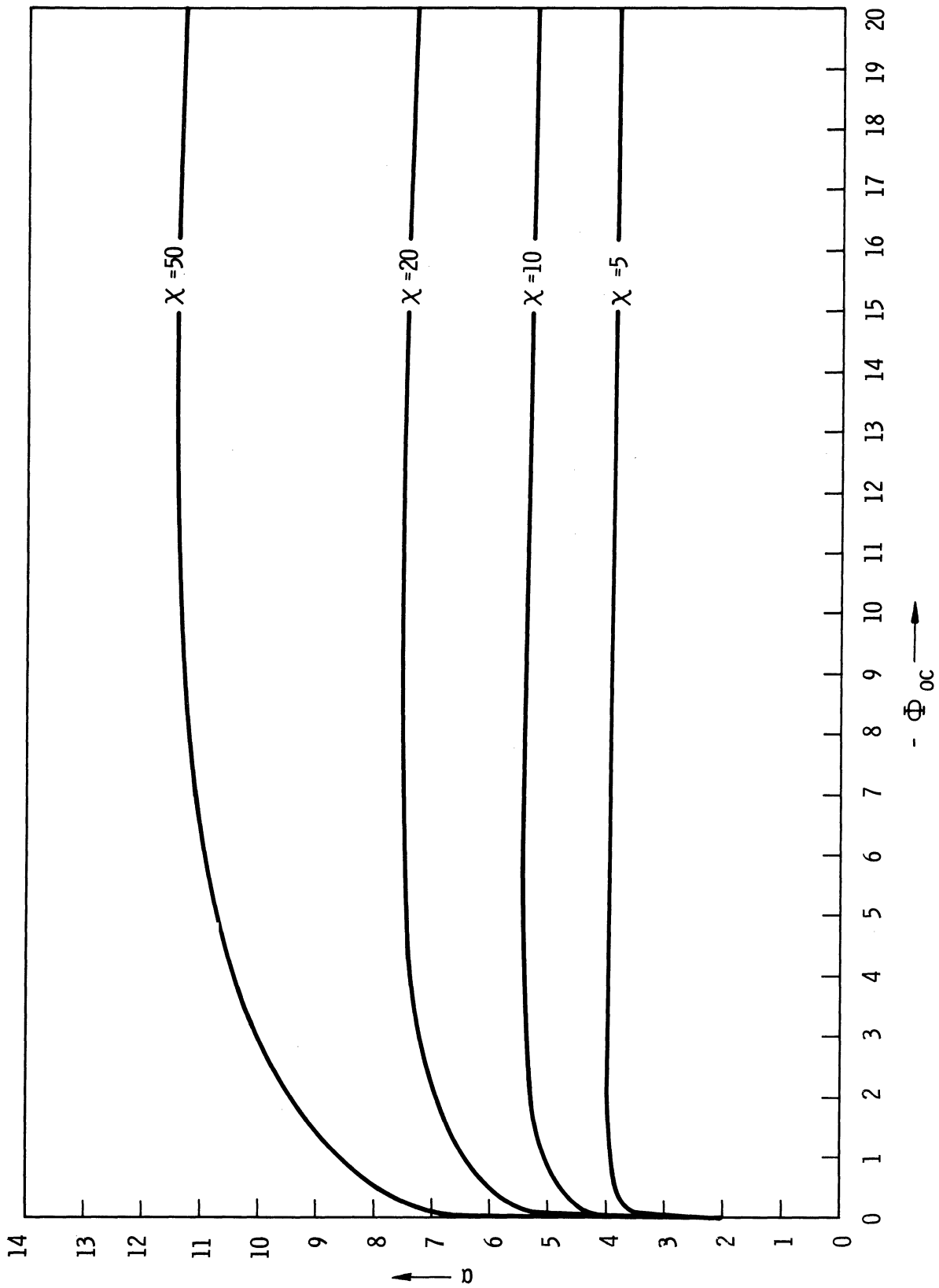$-\Phi_{oc}=0.3$
$-\Phi_{oc}=0.1$
$-\Phi_{oc}=0$

Fig. 27. Spherical probe. ($\delta=1$). Plot $\alpha$ vs. ($-\Phi_{oc}$) with $\chi = r_c/\lambda_D$ parameterized. Temperature ratio $T_{ion}/T_{electron} = 1$.
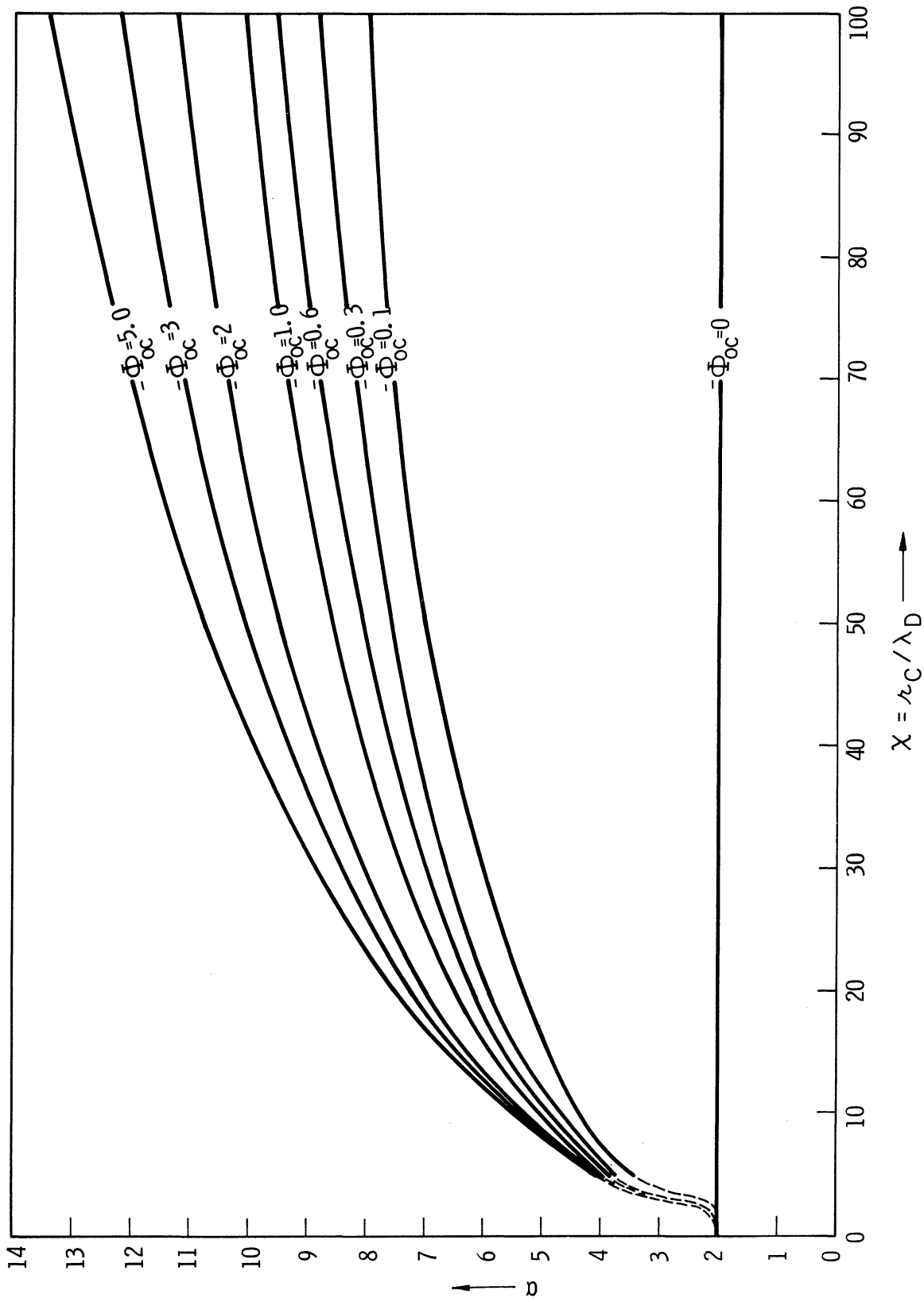
Fig. 28. Spherical probe ($\delta=1$). Plot of $\alpha$ vs. $\chi$ for various values of $(-\Phi_{oc})$. Temperature ratio $T_{ion}/T_{electron} = 1$.

105

$\chi$ is usually considerably less than unity so that $\alpha = 2$, and Langmuir's

volt-ampere characteristics correctly give the collected current.

# V. CONCLUSION

Experimental data of excellent quality are now being obtained from electrostatic probes both in the ionosphere and in laboratory plasmas. The detailed shapes of the measured volt-ampere curves obtained would give valuable information about plasma properties if the theory of these curves were better understood. This requires the use of realistic models of the potential structure in the sheath region. The need for such realistic, yet mathematically tractable, potential models provided the stimulation for undertaking this study.

This report illustrates the artificial nature of any probe theory based on the use of potential functions that exhibit discontinuities of the potential gradient, or of higher radial derivatives of the potential at any specified sheath radius. Discontinuity of the gradient presumes a surface charge suspended in space; discontinuity of the second derivative presumes a step function in space-charge density; neither of these corresponds to any physical reality. Thus a model might be considered in which the potential and its first and second derivatives are all matched at a "sheath edge" surface interior to the outer bound of the sheath.[1] In this case the region outside the sheath edge would be a low-space-charge transition region[6,7,8,9] between the plasma and the high-space-charge steep-gradient sheath region.

One of the most interesting aspects of the material presented is the comparison between the results of the self-consistent field analysis by Laframboise[2] and the results of our calculations based on the inverse-

power-law potential (68-1). In particular our results show that in the range of parameters of interest in ionospheric applications our probe characteristics agree very well with those of Laframboise.

Of course the "infinite" sheath radius should not literally be taken to be infinite. It means merely that the sheath potential approaches the plasma potential asymptotically. At a range of radius values in which the difference between the sheath potential and the plasma potential has become small relative to the inherent random variations in plasma potential, one is outside the sheath. Thus the "infinite radius" of the sheath can in fact be a very short distance. One ought to think in terms of some mean value radius, as one thinks of a time constant of an asymptotically decaying circuit transient.

In summary, this study emphasizes the need for recognizing that, to be reasonably in accord with reality, one must indeed use a sheath model in which the sheath potential approaches the plasma potential asymptotically.

It appears from the present work that it is feasible to devise a simple potential function model that serves these purposes well. Of course other equally good or better models may be found, but the inverse-power-law function proposed here seems to provide a good compromise between the need for representing reality and the need for mathematical tractability.

# APPENDIX

## DERIVATIONS OF THE MOTT-SMITH AND LANGMUIR EQUATIONS
## FOR CURRENT TO CYLINDRICAL OR SPHERICAL PROBES FOR FINITE SHEATH MODELS

This derivation is carried out by using the domain of integration shown shaded in Fig. 6 of the text, described as follows in accordance with Eqs. (36-1) and (36-2) of the text:

$$E \geq \frac{M^2}{2mr_s^2}, \quad \text{if } 0 \leq M^2 \leq M_s^2 \tag{A-1}$$

$$E \geq \frac{M^2}{2mr_c^2} + \Phi_c, \quad \text{if } M_s^2 < M^2 < \infty \tag{A-2}$$

where

$$M_s^2 = \frac{2mr_s^2 r_c^2(-\Phi_c)}{(r_s^2 - r_c^2)} \tag{A-3}$$

To obtain the current density $J_c$ to a cylindrical or spherical probe for a sheath of finite radius $r_s$ we apply the above Eqs. (A-1),(A-2) and (A-3) in Eq. (107) of the text, with symbolism as therein, and using $M^2 = x$; the result is:

$$J_c = J_0 \frac{h_\delta}{2^\delta} \left[ \int_{x=0}^{x=M_s^2} \int_{E=\frac{x}{2mr_s^2}}^{E=\infty} dE \, dx \, x^{(\delta-1)/2} \exp\left(-\frac{E}{kT}\right) \right.$$

$$\left. + \int_{x=M_s^2}^{x=\infty} \int_{E=\frac{x}{2mr_c^2}+\Phi_c}^{E=\infty} dE \, dx \, x^{(\delta-1)/2} \exp\left(-\frac{E}{kT}\right) \right] \tag{A-4}$$

Integration with respect to E gives:

$$J_c = \frac{h_\delta kT}{2^\delta} \left[ \int_{x=0}^{x=M_s^2} dx \; x^{\frac{\delta+1}{2}-1} \exp\left(-\frac{x}{2mkTr_s^2}\right) \right.$$

$$\left. + \exp\left(\frac{-\Phi_c}{kT}\right) \int_{x=M_s^2}^{x=\infty} dx \; x^{\frac{\delta+1}{2}-1} \exp\left(-\frac{x}{2mkTr_c^2}\right) \right] \qquad \text{(A-5)}$$

Use of new variables of integration $y = x/2mkTr_s^2$ in the first integral, and $y = x/2mkTr_c^2$ in the second converts this to:

$$J_c = \frac{h_\delta kT}{2^\delta} \left[ (2mkTr_s^2)^{(\delta+1)/2} \int_{y=0}^{y=M_s^2/2mkTr_s^2} dy \; y^{\frac{\delta+1}{2}-1} \exp(-y) \right.$$

$$\left. + (2mkTr_c^2)^{(\delta+1)/2} \exp\left(-\frac{\Phi_c}{kT}\right) \int_{y=M_s^2/2mkTr_c^2}^{y=\infty} dy \; y^{\frac{\delta+1}{2}-1} \exp(-y) \right] \qquad \text{(A-6)}$$

Now substitute for $h_\delta$ from Eq. (109) in the text, and for $M_s^2$ from Eq. (A-3), and express the integrals in terms of incomplete gamma functions as in Eqs. (115-1) and (115-2), to get

$$J_c = \frac{J_o}{\Gamma\left(\frac{\delta+1}{2}\right)} \left[ \left(\frac{r_s}{r_c}\right)^{\delta+1} \gamma\left(\frac{\delta+1}{2}, \frac{-\Phi_c}{kT} \frac{r_c^2}{r_s^2 - r_c^2}\right) \right.$$

$$\left. + \exp\left(\frac{-\Phi_c}{kT}\right) \Gamma\left(\frac{\delta+1}{2}, \frac{-\Phi_c}{kT} \frac{r_s^2}{r_s^2 - r_c^2}\right) \right] \qquad \text{(A-7)}$$

For cylindrical geometry $\delta = 0$. The incomplete gamma functions then become

$$\gamma\left(\frac{1}{2}, \frac{-\Phi_c}{kT} \frac{r_c^2}{r_s^2 - r_c^2}\right) = \int_{t=0}^{t=\frac{-\Phi_c}{kT} \frac{r_c^2}{r_s^2 - r_c^2}} dt \; t^{-1/2} \exp(-t)$$

$$= \sqrt{\pi} \; \text{erf}\left(\sqrt{\frac{-\Phi_c}{kT} \frac{r_c^2}{r_s^2 - r_c^2}}\right) \qquad \text{(A-8)}$$

110

and

$$\Gamma\left(\frac{1}{2}, \frac{-\Phi_c}{kT} \frac{r_s^2}{r_s^2 - r_c^2}\right) = -\sqrt{\pi}\ \text{erfc}\left(\sqrt{\frac{-\Phi_c}{kT} \frac{r_s^2}{r_s^2 - r_c^2}}\right) \quad (A\text{-}9)$$

Thus the expression for the current collection to the inwardly-accelerating

infinite-cylinder probe may be written as

$$J_c = -J_o\left[\frac{r_s}{r_c}\ \text{erf}\left(\sqrt{\frac{-\Phi_c}{kT} \frac{r_c^2}{r_s^2 - r_c^2}}\right) + \exp\left(\frac{-\Phi_c}{kT}\right)\text{erfc}\left(\sqrt{\frac{-\Phi_c}{kT} \frac{r_s^2}{r_s^2 - r_c^2}}\right)\right]$$

$$(A\text{-}10)$$

For the spherical probe, we obtain by a similar procedure after using

$\delta = 1$ in Eq. (A-7):

$$J_c = J_o\left[\frac{r_s^2}{r_c^2} - \left(\frac{r_s^2 - r_c^2}{r_c^2}\right)\exp\left(\frac{\Phi_c}{kT} \frac{r_c^2}{r_s^2 - r_c^2}\right)\right] \quad (A\text{-}11)$$

These Eqs. (A-10) and (A-11) for the current were originally derived by

Mott-Smith and Langmuir using the velocity space domain.

In the orbital-motion-limited mode of collection, $r_s/r_c \to \infty$ and Eq.

(A-7) becomes

$$J_{oml} = \frac{J_o}{\Gamma\left(\frac{\delta+1}{2}\right)}\left[\frac{2}{\delta+1}\left(\frac{-\Phi_c}{kT}\right)^{(\delta+1)/2} + \exp\left(-\frac{\Phi_c}{kT}\right)\Gamma\left(\frac{\delta+1}{2}, \frac{-\Phi_c}{kT}\right)\right] \quad (A\text{-}12)$$

For the infinite cylinder, $\delta = 0$, we get

$$J_{oml} = J_o\left[\frac{2}{\sqrt{\pi}}\ \sqrt{\frac{-\Phi_c}{kT}} + \exp\left(\frac{-\Phi_c}{kT}\right)\text{erfc}\left(\sqrt{\frac{-\Phi_c}{kT}}\right)\right] \quad (A\text{-}13)$$

For the sphere, $\delta = 1$ we get

$$J_{oml} = J_o\left(1 - \frac{\Phi_c}{kT}\right) \quad (A\text{-}14)$$

Equations (A-13) and (A-14) are the well known orbital motion limited volt-ampere equations of Mott-Smith and Langmuir.

# REFERENCES

1. Mott-Smith, H. M. and I. Langmuir, "The Theory of Collectors in Gaseous Discharges." Phys. Rev. 28, 727 (1926). (In Eq. (28a) the factor exp. 7 should appear in the last term.)

2. Laframboise, J. G., "Theory of Spherical and Cylindrical Langmuir Probes in a Collisionless, Maxwellian Plasma at Rest." UTIAS Report No. 100, University of Toronto, 1966.

3. Langmuir, I. and K. T. Compton, "Electrical Discharges in Gases, Part II, Fundamental Phenomena in Gaseous Discharges." Rev. Modern Physics, 3, 191 (April 1931).

4. Bernstein, I. B. and I. N. Rabinowitz, "Theory of Electrostatic Probes in a Low-Density Plasma." Physics of Fluids, 2, 112 (1959).

5. Gurevitch, A. V., "The Distribution of Particles in a Centrally Symmetric Field." Geomagnetism and Aeronomy, 2, 151 (1963).

6. Hok, Gunnar, N. W. Spencer, A. Reifman, and W. G. Dow, "Dynamic Probe Measurements in the Ionosphere," Scientific Report No. FS-3, The University of Michigan Research Institute, Space Physics Research Laboratory, Electrical Engineering Department, November, 1958. Issued under Contract No. AF 19(604)-1843, being a reprint of the original issue in August 1951 under Contract No. AF 19(122)-55, both contracts with the Geophysics Division.

7. Tonks, Lewi and I. Langmuir, "A General Theory of the Plasma of an Arc." Phys. Rev., 34, 876 (September 1929).

8. Cobine, J. D., pp. 321, 236, Gaseous Conductors. McGraw-Hill Book Co., New York, 1941, reprinted in paperback circa 1955.

9. v. Engel, A. and M. Steenbeck, Elektrische Gasentladungen, ihre Physilc u. Technik, Vol. 2, pp. 83-92, Julius Springer, 1934.

10. Kaplan, Wilfred, Advanced Calculus, pp. 94, 200, 289, Addison-Wesley Publishing Co., Reading, Mass., 1952.